



UNIVERSIDADE FEDERAL DE SANTA CATARINA
CENTRO TECNOLÓGICO
PROGRAMA DE PÓS-GRADUAÇÃO EM ENGENHARIA ELÉTRICA

Arliones Stevert Hoeller Junior

Performance Analysis and Optimization of Low-Power Wide-Area Networks

Florianópolis
2021

Arliones Stevert Hoeller Junior

Performance Analysis and Optimization of Low-Power Wide-Area Networks

Thesis submitted to the Electrical Engineering Graduate Program of the Federal University of Santa Catarina as a requirement for the title of doctor in Electrical Engineering.

Supervisor: Prof. Richard Demo Souza, Dr.

Co-supervisor: Prof. Hirley Alves, Dr.

Florianópolis

2021

Ficha de identificação da obra elaborada pelo autor,
através do Programa de Geração Automática da Biblioteca Universitária da UFSC.

Hoeller Junior, Arliones Stevert
Performance Analysis and Optimization of Low-Power Wide
Area Networks / Arliones Stevert Hoeller Junior ;
orientador, Richard Demo Souza, coorientador, Hirley
Alves, 2021.
91 p.

Tese (doutorado) - Universidade Federal de Santa
Catarina, Centro Tecnológico, Programa de Pós-Graduação em
Engenharia Elétrica, Florianópolis, 2021.

Inclui referências.

1. Engenharia Elétrica. 2. Sistemas de Comunicação Sem
Fios. 3. Machine-Type Communications. 4. Internet das
Coisas. I. Souza, Richard Demo. II. Alves, Hirley. III.
Universidade Federal de Santa Catarina. Programa de Pós
Graduação em Engenharia Elétrica. IV. Título.

Arliones Stevert Hoeller Junior

Performance Analysis and Optimization of Low-Power Wide-Area Networks

O presente trabalho em nível de doutorado foi avaliado e aprovado por banca examinadora composta pelos seguintes membros:

Prof. Marcelo Eduardo Pellenz, Dr.
Pontifícia Universidade Católica do Paraná, Brasil
Programa de Pós-Graduação em Informática

Prof. Glauber Gomes de Oliveira Brante, Dr.
Universidade Tecnológica Federal do Paraná, Brasil
Departamento de Eletrotécnica

Prof. Pedro Henrique Juliano Nardelli, Dr.
Lappeenranta-Lahti University of Technology, Finlândia
School of Energy Systems

Certificamos que esta é a **versão original e final** do trabalho de conclusão que foi julgado adequado para obtenção do título de doutor em Engenharia Elétrica.

Coordenação do Programa de
Pós-Graduação

Prof. Richard Demo Souza, Dr.
Orientador

Florianópolis, 2021.

To Ana.

ACKNOWLEDGEMENTS

Although a doctoral thesis is an individual work, the truth is that finishing a doctorate requires the collaboration of several people. From academic supervision to family and friends to funding, I certainly would not have finished this thesis without adequate support. As a token of my appreciation for all the help I received, I try my best to address all collaborators in their native language.

Eu sou muito grato ao meu orientador, Richard, pela orientação ímpar que recebi e pelo modo humano como trabalha. O Richard me acolheu como aluno anos após eu concluir o mestrado, e me ajudou a recuperar a minha “auto-estima acadêmica”. Além de todo ensinamento técnico-científico que recebi, levarei para sempre o que ele ensina silenciosamente, através de exemplos, sobre a essência de ser um grande Professor e Pesquisador. Sou muito feliz em poder evoluir agora da relação aluno-orientador para a relação de colegas e amigos.

Também agradeço enormemente ao meu coorientador, Hirley, pela acolhida e direcionamentos ao longo deste doutorado. O Hirley não mediu esforços para alavancar a nossa colaboração internacional. O acolhimento que recebemos do Hirley e da Priscila nas duas passagens que tivemos por Oulu foram essenciais para o sucesso deste trabalho. Do Hirley fica um exemplo de determinação, foco e trabalho duro que também levarei comigo, além da amizade.

Não poderia deixar de agradecer muito àqueles que colaboraram nos momentos difíceis desta jornada. Sou muito grato ao meu amigo e colega de IFSC Mário de Noronha Neto por ter me apresentado ao Richard e me motivado a buscar este título. Sem sua ajuda e motivação, isto nunca teria acontecido.

Agradezco mucho a Onel Luis Alcaraz López su amistad y colaboración en varios momentos a lo largo de este trabajo. Sin la cooperación que tuvimos, este viaje hubiera sido mucho más arduo. También estoy muy agradecido por el apoyo recibido de Samuel Montejo Sánchez para las diversas conversaciones y colaboraciones.

Sou muito grato aos colegas e professores por suas amizades, aulas, lições, discussões, e colaborações. Jean de Souza Sant’Ana, Glauber Brante, Marcelo Pellenz, Carlos Montez, Gabriel Jesus, Bartolomeu Uchoa Filho, Carlos Morais de Lima, Matti Latva-Aho, Juho Markkula, Konstantin Mikhaylov, Mohammad Shehab, Muhammad Asad-Ullah, Junnaid Iqbal e, certamente, muitos outros:

Seu suporte foi muito importante para que eu chegasse até aqui.

Tukesi oli minulle erittäin tärkeää päästä tänne.

Your support was very important for me to get here.

E claro, sou muito grato a todos os familiares que, fora do ambiente acadêmico, me deram o suporte emocional necessário para viver uma vida plena. Agradeço aos meus pais, Arliones e Elisabete, pelo seu amor incondicional e por estarem sempre ao

meu lado nos momentos bons e não tão bons. Agradeço ao meu irmão Alexandre e à minha cunhada Fernanda pela sua amizade e apoio, e às minhas sobrinhas Maria Júlia e Maria Alice por trazer a leveza da infância para o nosso cotidiano. Agradeço à minha sogra Mirian por ter me acolhido como um filho, e dado a mim e à Ana toda a ajuda que precisamos. E sou muito grato aos meus avós, tios, primos e toda minha família pelo convívio ao longo destes quase 40 anos. Eu sou a combinação do que aprendi com vocês. Há pedaço de cada um de vocês neste trabalho.

Aos meus amigos, obrigado por tornar meus dias mais alegres, seja pessoalmente aqui no Brasil ou na Finlândia, ou mesmo em uma video-conferência durante nosso isolamento em tempos de pandemia. Aos meus amigos da *midnight* (Carlucci, Petrúcio, Capin, Pelotas, Iomani, Ivanrs, Cabeça, Zé, Pretin, Bokão, Frango, Ghost, Fedro, Camina), obrigado por me fazer perder tempo falando besteira. Poder ter happy hours filosóficos com vocês é um privilégio. Aos Amendoins (Cancian, Maiara, Márcio, Eva, Tiago, Fran), obrigado pela amizade e parceria. Ao pessoal do Bar do Tomé (Tomé, Jean, Henrique, Eduardo, Lucas, Rafaela), aos colegas de CWC e familiares (Hirley, Pricila, Onel, Lisi, Shehab), e aos novos amigos (Jarmo, Lina, Mari, Solange) obrigado pela amizade, companhia e apoio durante o longo inverno finlandês. Aos meus amigos e colegas do IFSC-SJE, especialmente à chefia (Saul, Tiago, Odilson), obrigado pelo apoio e por acreditar neste projeto de tese.

E por fim, justamente por ser mais importante, sou muito grato à minha amada esposa Ana. Eu não teria conseguido sem ter você ao meu lado, meu amor. É a você que dedico este trabalho.

Eu certamente esqueci de nominar alguém nesta nota. Eu sinto muito. Espero que possamos sentar juntos e celebrar com uma taça de vinho ou cerveja para que eu me redima desta falha. A todos, muito obrigado!

This thesis exists within the cooperation among my supervisors Prof. Souza at UFSC and Prof. Alves at the University of Oulu and receives funding from various projects. Arliones was mainly supported by the Federal Institute for Education, Science, and Technology of Santa Catarina (IFSC) through IFSC Full-Time Postgraduate Leave Program. A ten-months doctoral stay/sandwich at the University of Oulu, Finland, took place between August/2019 and May/2020 supported by CNPq Grant 205166/2018-0 (Individual Doctorate Sandwich Grant - SWE). Indirectly, CAPES funds activities of the UFSC Electrical Engineering Graduate Program through UFSC PrInt Program, sub-project "Automação, Controle e Sistemas Computacionais para Indústria e Serviços 4.0". The project also received funding from the Institute of Systems Engineering and Computers Technology and Science Brazil (INESC Brasil), under the ANEEL R&D Projects PD-00405-1804/2018 and PD-00380-0027/2018, and from the Academy of Finland (Aka), projects 6Genesis Flagship (Grant 318927), Energy-Efficiency for the Internet of Things (EE-IoT) (Grant 319008), and Aka Prof (Grant 307492).

“Thoroughly conscious ignorance is the prelude to every real advance in science.”
(MAXWELL, 19th century)

RESUMO

As tecnologias de Redes de Baixa Potência e Longo Alcance – Low-Power Wide-Area Network (LPWAN) – capturaram a atenção do mercado da Internet das Coisas – Internet-of-Things (IoT) –, o que trouxe à tona a demanda por conhecimento confiável acerca do desempenho destas redes. Neste contexto, o objetivo desta tese é modelar e avaliar o desempenho de LPWANs em cenários realísticos para explorar potenciais melhorias de desempenho. Os desenvolvimentos apresentados aqui focam em Long-Range WAN (LoRaWAN), uma tecnologia líder em LPWAN. Além de modelar o canal LoRaWAN com desvanecimento, os modelos propostos se valem da Geometria Estocástica para modelar interferência tanto interna, quanto externa. Inicialmente são propostos modelos a partir dos quais são obtidas expressões fechadas do comportamento da LoRaWAN. Estes modelos são utilizados para explorar diversidade temporal e espacial para aumentar a taxa de entrega de pacotes nestas redes. Os resultados obtidos mostram que o emprego de replicação de mensagens para ativar a diversidade temporal é benéfica para redes com baixa densidade, e que existe um número ótimo de cópias para uso em cada Spreading Factor (SF). Também conclui-se que o emprego de múltiplas antenas de recepção omni-direcionais no gateway aumenta significativamente a taxa de sucesso de entrega de pacotes, independentemente da densidade da rede. Além disso, os modelos propostos são utilizados para otimizar os parâmetros da rede ao considerar interferência interna e entre tecnologias. Os modelos são estendidos para considerar a interferência que LoRaWAN recebe de redes IEEE 802.15.4g, que formam as camadas inferiores de sistemas Wireless Smart Utility Network (Wi-SUN). Também são derivadas equações fechadas para a disponibilidade esperada de redes LoRaWAN nestes cenários. A avaliação realizada parametriza os modelos com dados obtidos em medições da interação entre as tecnologias. Também são propostos dois algoritmos para determinar as melhores configurações LoRaWAN nestes cenários para atender a um nível mínimo de confiabilidade da rede. Os algoritmos maximizam alcance de comunicação ou número de usuários a partir de restrições de número mínimo de usuários, alcance mínimo, e confiabilidade mínima. Os métodos propostos se mostram ferramentas úteis ao planejamento de redes limitadas por interferência com requisitos de confiabilidade. Finalmente, é considerado o desempenho de LoRaWAN quando o mecanismo Adaptive Data Rate (ADR) é ativado. Este mecanismo ajusta dinamicamente o SF e a potência de transmissão dos nós da rede com base no estado do canal. Uma extensão do modelo desta tese é proposto para considerar o desempenho de redes LoRaWAN com ADR em regime, ou seja, após a convergência das configurações de SF e potência. Este modelo produz expressões fechadas do desempenho das redes que são utilizadas em procedimentos de otimização que maximizam o número de usuários em uma rede sob restrições de confiabilidade. Os resultados mostram que a alocação de potência reduz a interferência no gateway e aumenta a capacidade da rede, reduzindo o consumo médio de energia. Todos os modelos e algoritmos propostos nesta tese são validados através de análise numérica e simulações.

Palavras-chave: Sistemas de Comunicação Sem Fios. Machine-Type Communications. Internet das Coisas.

RESUMO EXPANDIDO

Introdução

Nos anos recentes se viu a proliferação da IoT, impulsionada pela ampla disponibilidade de dispositivos de baixo custo e conectáveis à Internet. O crescimento na quantidade de dispositivos conectados, contudo, chamou a atenção para os limites de conectividade das tecnologias como WiFi, Bluetooth, ZigBee, e redes móveis 3G/4G, não apenas a respeito de seus custos e dimensões, mas também à sua capacidade, alcance e consumo de energia. Neste contexto, as tecnologias LPWAN emergiram para atender ao mercado da chamada *Massive IoT* (mIoT), *i.e.*, aplicações não-críticas, de baixa potência e baixo custo que são tolerantes a baixas taxas de transmissão e latências altas. Dentre as tecnologias LPWAN mais proeminentes no mercado estão LoRaWAN, SigFox e Narrow-Band IoT (NB-IoT).

Embora a adoção destas tecnologias esteja acelerada, ainda não há informação publicada sobre o desempenho de redes LPWAN com grande quantidade de estações, o que torna atrativo o desenvolvimento de modelos de desempenho e capacidade. Como resultado, estudos recentes têm explorado os limites das tecnologias e proposto técnicas para melhorar seu desempenho. Esta tese aborda este problema sob uma perspectiva analítica. São estudados, modelados, e analisados o desempenho do *uplink* da tecnologia LoRa, que forma a camada física da LoRaWAN, uma das tecnologias LPWAN mais difundidas. Este trabalho permite entender e explorar algumas características da LoRaWAN e, por extrapolação, outras LPWANs.

Objetivos

O objetivo principal desta tese é modelar e analisar o desempenho de LPWANs em configurações realísticas para explorar potenciais melhorias de desempenho. Os objetivos específicos são: (1) Consolidar um arcabouço de modelos de desempenho confiável para LoRaWANs com um único gateway, permitindo a variação de parâmetros como cenários, densidade de nós, ciclo de trabalho, intensidade do desvanecimento e interferência; (2) Projetar e analisar o desempenho de LoRaWAN com técnicas que exploram as diversidades temporal e espacial; (3) Analisar o desempenho da LoRaWAN sob interferência de outras redes não-LoRa; (4) Analisar o desempenho de LoRaWAN empregando um mecanismo de alocação de potência; e (5) Propôr métodos de otimização de LoRaWANs baseados nos modelos propostos.

Metodologia

Esta tese inclui desenvolvimentos analíticos e de simulações que buscam validar modelos de desempenho de redes LoRaWAN. Os modelos apresentados descrevem o canal LoRa e se baseiam na geometria estocástica, uma ferramenta matemática para estudar padrões espaciais, para modelar a interferência nestas redes sem fios. Diversos trabalhos modelam o desempenho da LoRaWAN sob diferentes condições ou avaliam os limites da tecnologia em campanhas de medição. Estes resultados mostram que, para suportar uma taxa de erro de pacotes razoável, a maioria dos nós LoRaWAN tendem a estar perto dos gateways devido ao mecanismo de espalhamento espectral, limitando o alcance da tecnologia. Outros trabalhos exploraram diversidade espacial com múltiplos gateways espalhados geograficamente, e diversidade temporal em outras tecnologias. Neste trabalho, utilizamos uma abordagem analítica para explorar

ganhos de desempenho em LoRaWAN através do aumento da diversidade temporal por replicação de mensagens, e da diversidade espacial através de múltiplas antenas de recepção em um mesmo gateway.

Como um dos objetivos desta tese é construir um modelo de desempenho de LoRaWAN, é necessário considerar múltiplas fontes de interferência. Os trabalhos relacionados a esta tese consideram basicamente interferência interna à rede. Contudo, em um cenário real os gateways LoRaWAN estão sujeitos a interferência de outras tecnologias nas faixas de frequência ISM. Nesta tese nós investigamos, analiticamente e por simulação, a interferência entre tecnologias. Também são propostos algoritmos de otimização de desempenho com base nos modelos apresentados.

LoRaWAN explora a taxa de espalhamento espectral para estender a cobertura alocando diferentes taxas e potências de transmissão aos nós com base na qualidade de seus enlaces. Este mecanismo é chamado de Adaptive Data Rate (ADR). Este trabalho integra os mecanismos de alocação de taxa e potência aos modelos propostos, permitindo a análise e otimização do desempenho da rede.

Resultados e Discussão

A análise de desempenho das redes LoRaWAN com diversidade temporal e espacial mostrou ganhos importantes de desempenho. Foi concluído que há um número ótimo de replicações de mensagens que maximiza a taxa de entrega de pacotes para cada fator de espalhamento espectral. Além disso, replicação é útil em redes pouco densas, enquanto o emprego de gateways com múltiplas antenas de recepção é benéfico em qualquer cenário, e a combinação adequada de ambas as técnicas pode melhorar significativamente o desempenho da rede.

Foram apresentados dois algoritmos para otimizar a configuração das redes LoRaWAN sob um modelo mais amplo de interferência interna e externa. Os algoritmos propostos buscam por configurações ótimas das redes que atingem um nível alvo de confiabilidade dados valores mínimos de densidade de nós ou raio de cobertura. Com respeito à interferência externa, embora LoRaWAN com SFs mais altos sejam mais robustos a este tipo de interferência, eles acabam sofrendo mais deste problema devido a seu tempo-no-ar mais longo, o que torna a sobreposição dos sinais mais provável. Ainda com respeito aos algoritmos propostos, eles fornecem uma ferramenta para explorar trocas entre carga da rede e raio de cobertura, permitindo definir uma região de soluções com configurações LoRaWAN viáveis.

Por fim, o modelo de LoRaWAN com ADR mostra que a alocação de taxa e potência permite equalizar o desempenho dos nós em diferentes posições na região de cobertura. Com estes modelos, foi ainda possível empregar algoritmos de otimização para maximizar o número de usuários garantindo um limiar máximo da taxa de erros. Os resultados mostram como o ADR aumenta a confiabilidade da rede devido à redução da interferência, enquanto sendo mais eficiente energeticamente que uma configuração com potência fixa.

Considerações Finais

Sistemas LPWAN evoluíram rapidamente durante este projeto de tese de doutorado, e estão agora presentes em praticamente todos os países do mundo. Exemplos claros são iniciativas globais como SigFox e The Things Network (TTN). Outras iniciativas privadas implantam LoRaWAN, Wi-SUN e outras redes ISM, geralmente explorando a infraestrutura já disponível dos operadores de telefonia móvel. Além disso, a implanta-

ção das tecnologias de telecomunicações 5G está tornando o NB-IoT cada vez mais disponível nas bandas licenciadas.

Com redes cada vez maiores, a habilidade de planejar implantações considerando parâmetros tanto de cobertura quanto de co-existência é muito importante, e esta é uma das questões principais às quais esta tese buscou contribuições. Devido à alta complexidade e altos custos envolvidos para avaliar experimentalmente o desempenho de LPWANs, este projeto tomou o rumo analítico, onde modelos são adaptados ou concebidos para descrever o desempenho esperado nestes sistemas.

Os resultados obtidos incluem modelos para descrever o desempenho de LoRaWAN considerando diversidade temporal, espacial, sujeito a diferentes fontes de interferência e com técnicas de alocação de potência e taxa de transmissão, o que inclui um número razoável de características reais da tecnologia. Esta lista não é, contudo, completa. Outras técnicas de replicação e codificação de mensagens podem ser consideradas, além de ser interessante buscar modelos analíticos para descrever o desempenho de LoRaWAN com múltiplos gateways. Além disso, outras técnicas para alocação de taxa e potência podem ser estudadas, inclusive sujeitas a diferentes fontes e tipos de interferência. Finalmente, esta tese se preocupou sempre com o desempenho *médio* dos nós da rede. Embora este seja um resultado analítico importante, trabalhos futuros poderiam também considerar a meta-distribuição da SINR destas redes, permitindo obter outras métricas como a variância e o intervalo de confiança destas médias.

Palavras-chave: Sistemas de Comunicação Sem Fios. Machine-Type Communications. Internet das Coisas.

ABSTRACT

LPWAN technologies have caught the IoT market's attention, which has brought the need for reliable knowledge about such networks' performance. Within this context, the goal of this thesis is to model and analyze the performance of LPWANs in realistic set-ups to exploit potential performance enhancements. We focus our developments on LoRaWAN, a leading LPWAN technology. Besides modeling the LoRaWAN fading channel, our models also rely on Stochastic Geometry to model internal and external interference. We model and obtain closed-form expressions of the behavior of LoRaWAN, exploiting time and spatial signal diversity to enhance the delivery rate. We show that the use of message replication to enable time diversity is beneficial for low-density networks and that there is an optimum number of message copies to be used by each SF. We also show that the use of multiple, omnidirectional receive antennas at the gateway significantly enhances the rate of successful packet delivery, regardless of network density. Besides that, we build over our network model to optimize network parameters while accounting for inter-technology interference. Our analytic model accounts for the interference LoRaWAN receives from IEEE 802.15.4g networks, which forms the bottom layers of Wi-SUN systems. We derive closed-form equations for the expected reliability of LoRaWAN in such scenarios. We set the model parameters with data from real measurements of the technologies' interplay and propose two optimization algorithms to determine the best LoRaWAN configurations, given a targeted minimum reliability level. The algorithms maximize either communication range or the number of users given constraints on the minimum number of users, minimum communication range, and minimum reliability. The proposed methods are useful tools for planning interference-limited networks with requirements of minimum reliability. Finally, we consider the performance modeling of LoRaWAN using the ADR mechanism, which dynamically adjusts SF and transmit power of nodes based on channel state. We do that by extending our analytical LoRaWAN model to consider the performance of steady-state ADR-enabled LoRaWAN. We derive outage expressions and an optimization procedure to maximize the number of users under reliability constraints. Results show that power allocation reduces interference and improves network capacity while reducing average power. We validate all models and algorithms through numerical analysis and simulations.

Keywords: Wireless Communication Systems. Machine-Type Communications. Internet of Things.

LIST OF FIGURES

Figure 1 – Sample from a stochastic geometry model of a network cell with $\bar{N} = 1000$ nodes and $R = 1000m$	31
Figure 2 – $\bar{N} = 500$ nodes uniformly distributed in a circular area of radius $R = 12$ km around the gateway, with SF increasing every 2 km.	39
Figure 3 – Performance of Long-Range (LoRa) uplink baseline model ($M = 1$ and $A = 1$), with average number of nodes $\bar{N} = 500$ and $p = \{0.1, 0.5\}\%$	47
Figure 4 – Impact of message replication in LoRa uplink, with average number of nodes $\bar{N} = 500$, duty cycle $p = 0.5\%$, a single antenna ($A = 1$), and a varying number of message copies M	47
Figure 5 – Coverage probabilities of LoRa network with average number of nodes $\bar{N} = 500$ and duty cycle $p = 0.5\%$ for each SF.	48
Figure 6 – Impact of multiple receive antennas at the LoRa gateway, considering an average number of nodes $\bar{N} = 500$, a duty cycle of $p = 0.5\%$, a single message copy ($M = 1$), and different numbers of receive antennas A	49
Figure 7 – $\bar{N} = 500$ nodes uniformly distributed in a circular area of radius $R = 12000$ m around the gateway and with increasing SF every 2000m. The Time-on-Air (ToA), as in Table 1, is illustrated in the lower-left corner.	53
Figure 8 – Success probabilities of all outage sources. LoRa: $\bar{N} = 4000$, $p = 0.1\%$, $\eta = 2.75$, $\mathcal{P}_t = 14\text{dBm}$, $R = 4000m$. IEEE 802.15.4g: $\bar{N}_z = 1000$, $p_z = 0.1\%$, $\eta = 2.75$, $\mathcal{P}_t = 14\text{dBm}$, $R_z = 4000m$	64
Figure 9 – Comparison of Q_1 and Q_1^* probabilities. $\bar{N} = \{500, 2000, 4000\}$, $p = 0.1\%$, $\eta = 2.75$, $\mathcal{P}_t = 14\text{dBm}$, $R = 4000m$	65
Figure 10 – Optimization between coverage radius and number of nodes given a minimum reliability constraint when maximizing R with Algorithm 1.	66
Figure 11 – Convergence of Algorithm 1 and success probability for the scenario marked in Figure 10a.	67
Figure 12 – Optimization between the number of nodes and coverage radius (in meters) given a minimum reliability constraint when maximizing \bar{N} with Algorithm 2.	69
Figure 13 – Average outage expectation for the marked scenario in Figure 12a.	70
Figure 14 – Sample of $\bar{N} = 250$ nodes uniformly distributed in an area of radius 1200m and with SF allocation for 1% maximum disconnection probability.	73
Figure 15 – Power allocation as a function of distance.	78
Figure 16 – System performance with power allocation. $\bar{N} = 247$	78

Figure 17 – System performance with fixed power. $\bar{N} = 225$ 79

LIST OF TABLES

Table 1 – LoRaWAN Uplink characteristics for packets of 19 bytes (13-bytes header, 6-bytes payload), at $B = 125\text{kHz}$, FEC rate $\frac{4}{5}$, and CRC and Header Mode enabled (SX1276/77/78/79..., 2019).	28
Table 2 – Optimum values of M and average coverage probability $\bar{C}_{1,j}$ for each SF and the whole network ($\rho = 0.5\%$ and $\bar{N} = 500$).	48
Table 3 – Optimum M^* for different configurations of network density and number of antennas.	50
Table 4 – Detailed optimization results for the marked scenario in Figure 10a.	68
Table 5 – Detailed optimization results for the marked scenario in Figure 12a.	70
Table 6 – Model and simulation parameters.	77

LIST OF ABBREVIATIONS AND ACRONYMS

5G	Fifth Generation Communication Technologies
6LoWPAN	IPv6 for Low-Power Wireless Personal Area Networks
ADR	Adaptive Data Rate
ARQ	Automatic Repeat reQuest
AWGN	Additive White Gaussian Noise
CDF	Cumulative Distribution Function
CSL	Coordinated Sampled Listening
CSMA	Carrier-Sense Multiple-Access
CSS	Chirp Spread Spectrum
FAN	Field Area Network
FEC	Forward Error Correction
FHSS	Frequency Hopping Spread Spectrum
FSK	Frequency Shift Keying
GFSK	Gaussian Frequency Shift Keying
ILP	Integer Linear Programming
IoT	Internet-of-Things
IPv6	Internet Protocol version 6
ISM	Industrial, Scientific, and Medical
LoRa	Long-Range
LoRaWAN	Long-Range WAN
LPWAN	Low-Power Wide-Area Network
LT	Laplace Transform
MAC	Medium Access and Control
mIoT	Massive IoT
MR-FSK	Multi-Rate Frequency Shift Keying
MR-OFDM	Multi-Rate Orthogonal Frequency Division Multiplexing
MR-OQPSK	Multi-Rate Offset Quadrature Phase Shift Keying
NB-IoT	Narrow-Band IoT
PDF	Probability Density Function
PER	Packet Error Rate
PGF	Probability Generating Function
PHY	Physical Layer
PMF	Probability Mass Function
PPP	Poisson Point Process
QoS	Quality-of-Service
RF	Radio Frequency
RPL	IPv6 Routing Protocol for Low-Power and Lossy Networks
RSSI	Received Signal Strength Indicator

SF	Spreading Factor
SINR	Signal-to-Interference-and-Noise Ratio
SIR	Signal-to-Interference Ratio
SNR	Signal-to-Noise Ratio
SUN	Smart Utility Network
ToA	Time-on-Air
TTN	The Things Network
UDP	User Datagram Protocol
UNB	Ultra-Narrow Band
Wi-SUN	Wireless Smart Utility Network

LIST OF SYMBOLS

\bar{N}	Average number of nodes in the LoRaWAN.
R	Radius of LoRaWAN network.
M	Number of message replicas.
A	Number of receive antennas.
ρ	Duty cycle for LoRaWAN.
η	Path loss exponent.
\mathcal{P}_t	Transmit power.
\bar{N}_z	Average number of nodes in the IEEE 802.15.4g network.
ρ_z	Duty cycle for the IEEE 802.15.4g network.
R_z	Radius of the IEEE 802.15.4g network.
Q_1	Capture probability.
Q_1^*	Capture probability with intra-SF interference only.
$\bar{C}_{1,i}$	Average coverage probability in SF ring i .
M^*	Optimum number of message replicas.
\mathcal{V}	Region of LoRaWAN.
V	Area of LoRaWAN.
ρ	Spatial density of nodes in LoRaWAN.
Φ	PPP of LoRaWAN.
Φ_t	Thinned PPP of LoRaWAN.
α	Intensity of LoRaWAN PPP.
d_k	Euclidean distance between the k -th node and the gateway.
d_1	Euclidean distance between the node of interest and the gateway.
\mathcal{P}_1	Transmit power of the node of interest.
\mathcal{P}_k	Transmit power of node k .
s_1	Signal transmitted by the node of interest.
s_k	Signal transmitted by device k .
g_k	Path loss observed at distance d_k .
h_k	Fading for device k .
λ	Wavelength.
k	Index used to enumerate devices.
r_1	Signal received from the node of interest.
h_1	Fading for the node of interest.
g_1	Path loss observed at distance d_1 .
\mathcal{I}	Generic interference.
w	Additive White Gaussian Noise (AWGN).
σ_w^2	Variance of the AWGN.
SINR	Signal-to-Interference-plus-Noise Ratio.
γ	SINR threshold.

C_1	Coverage probability.
H_1	Connection probability.
\bar{C}_1	Average network-wide coverage probability.
S	Set of SF rings.
$\Phi_{t,i}$	Thinned PPP of LoRaWAN SF ring i .
i	Index used to enumerate LoRaWAN SFs.
ψ	Elements of Ψ – the SNR threshold for nodes in an LoRaWAN SF ring.
SNR	Signal-to-Noise Ratio.
k^*	Index used to indicate the strongest interfering device.
l_j	Outer radius of SF ring i .
l_{i-1}	Inner radius of SF ring i .
$H_{i,M}$	Connection probability with M replicas in the i -th ring.
$Q_{i,M}$	Capture probability with M replicas in the i -th ring.
$C_{i,M}$	Coverage probability with M replicas in the i -th ring.
M_i^*	Optimum number of message replicas.
$H_{i,A}$	Connection probability with A antennas in the i -th ring.
a	Index used to enumerate antennas.
k_a^*	Index used to indicate the strongest interfering device in the a -th antenna.
$h_{a,k}$	Fading for device k in antenna a .
$Q_{i,A}$	Capture probability with A antennas in the i -th ring.
SIR	Signal-to-Interference Ratio.
$h_{a,1}$	Fading for device of interest in antenna a .
\mathcal{I}_a	Internal interference received from LoRaWAN SF ring j at antenna a .
z	Subscript identifying variables related to the IEEE 802.15.4g.
F	Receiver noise figure.
B	Channel Bandwidth.
c	Speed of the light.
f	Channel central frequency.
L	Vector of distance limits for each SF ring ($l_0 \rightarrow 0$).
T	Message generation period.
p_i	Duty cycle for LoRaWAN ring i .
t_j	ToA of a message in SF ring i .
Φ_j	PPP of LoRaWAN SF ring i .
α_j	Intensity of LoRaWAN PPP i .
ρ_i	Spatial density of nodes in LoRaWAN SF ring i .
V_i	Area of LoRaWAN SF ring i .
\bar{N}_i	Average number of nodes in LoRaWAN SF ring i .
V_z	Area of the IEEE 802.15.4g network.
Φ_z	PPP of the IEEE 802.15.4g network.

α_z	Intensity of the IEEE 802.15.4g PPP.
ρ_z	Spatial density of nodes in the IEEE 802.15.4g network.
\mathcal{I}_L	Internal (LoRaWAN) interference.
\mathcal{I}_Z	External (IEEE 802.15.4g) interference.
$\Phi_{t,z}$	Thinned PPP of the IEEE 802.15.4g network.
Z_1	Capture probability under \mathcal{I}_Z
Ψ	Vector of LoRaWAN SNR thresholds.
Δ	Vector of LoRaWAN SIR thresholds under internal interference.
$\delta_{i,j}$	SIR threshold for nodes in SF ring i under \mathcal{I}_j .
j	Index used to enumerate LoRaWAN SFs.
\mathcal{I}_j	Internal interference received from nodes in LoRaWAN SF ring j .
Φ_j	PPP of LoRaWAN SF ring j .
P_{SIR_j}	Probability of successful reception under \mathcal{I}_j .
s	Laplace variable.
$\Phi_{t,j}$	Thinned PPP of LoRaWAN SF ring j .
α_j	Intensity of LoRaWAN PPP j .
l_j	Outer radius of SF ring j .
l_{j-1}	Inner radius of SF ring j .
Θ	Vector of LoRaWAN SIR thresholds under external interference.
θ_i	SIR threshold for nodes in SF ring i under \mathcal{I}_Z .
P_{SIR_z}	Probability of successful reception under \mathcal{I}_Z .
N	Number of nodes in the LoRaWAN.
H_0	Disconnection probability.
δ	SIR threshold.
Q_0	Collision probability.
\mathcal{O}	Outage probability.

CONTENTS

1	INTRODUCTION	23
1.1	OBJECTIVES	25
1.2	DOCUMENT STRUCTURE	26
2	RESEARCH CONTEXT	27
2.1	LPWAN	27
2.1.1	LoRaWAN	27
2.1.2	Wi-SUN	28
2.2	BASIC SYSTEM MODEL	29
2.2.1	Stochastic Geometry	30
2.2.2	Channel model	30
2.2.3	Success Probabilities	31
2.3	TOOLS	33
2.4	RELATED WORK	34
2.5	CLOSING	37
3	ANALYSIS AND PERFORMANCE OPTIMIZATION OF LORAWAN NETWORKS WITH TIME AND ANTENNA DIVERSITY	38
3.1	SYSTEM MODEL	38
3.1.1	Outage Condition 1: Disconnection	40
3.1.2	Outage Condition 2: Collision	40
3.1.3	Coverage Probability	41
3.2	MESSAGE REPLICATIONS – TIME DIVERSITY	42
3.3	MULTIPLE RECEIVE ANTENNAS – SPATIAL DIVERSITY	43
3.4	NUMERICAL RESULTS	46
3.4.1	Baseline Model – Without Diversity	46
3.4.2	Message Replication	47
3.4.3	Multiple Receive Antennas	49
3.5	CLOSING	50
4	OPTIMUM LORAWAN CONFIGURATION UNDER WI-SUN INTERFERENCE	51
4.1	SYSTEM MODEL	52
4.1.1	Coverage Probability	54
4.1.2	Outage Condition 1: Disconnection	54
4.1.3	Outage Condition 2: Intra-Network Interference	55
4.1.4	Outage Condition 3: External Interference	57
4.2	OPTIMUM LORAWAN CONFIGURATION	58
4.2.1	Guaranteeing the Reliability Target	58
4.2.2	Maximization of Communication Range	59

4.2.3	Maximization of Number of Nodes	62
4.3	NUMERICAL RESULTS	63
4.3.1	Model Validation	64
4.3.2	Algorithm 1: Maximization of Range	65
4.3.3	Algorithm 2: Maximization of Nodes	69
4.4	CLOSING	71
5	PERFORMANCE ANALYSIS OF SINGLE-CELL ADAPTIVE DATA RATE-ENABLED LORAWAN	72
5.1	SYSTEM MODEL	73
5.1.1	Outage Probability	74
5.2	TRANSMIT POWER ALLOCATION FOR LORAWAN	75
5.2.1	Outage Probability with Transmit Power Allocation	75
5.3	NETWORK PLANNING	76
5.4	NUMERICAL RESULTS	77
5.5	CLOSING	79
6	CONCLUSION	80
6.1	FUTURE WORK	81
6.2	LIST OF PUBLICATIONS	82
	References	84
	APPENDIX A – SOLUTION OF $f(d_1, \gamma, l_a, l_b)$	91

1 INTRODUCTION

“A journey of a thousand miles begins with a single step.” Laozi, an ancient Chinese philosopher (LAOZI, 4th century BC).

The recent years saw the proliferation of the IoT pushed by inexpensive, Internet-connected devices using off-the-shelf components. The growth in the number of connected devices, however, turned the spotlight towards the limits of connectivity technologies like WiFi, Bluetooth, ZigBee, and 3G/4G mobile networks, not only regarding cost and size but also network capacity, communication range, and energy consumption (CENTENARO et al., 2016). Within this context, the LPWAN technologies emerged to serve the market of Massive IoT (mIoT) (ERICSSON AB, 2016), i.e., non-critical, low-power, and low-cost applications tolerant to small data rates and high latency. Among the most prominent LPWAN technologies in the market, today, are LoRaWAN, SigFox, and Narrow-Band IoT (NB-IoT) (BUURMAN et al., 2020).

Although LPWAN technologies are in fast-paced adoption, performance reports on deployments with large numbers of stations are scarce, making their performance and capacity models still an open problem. As a result, recent studies have explored the technologies' capacity limits and proposed techniques to enhance their performance. This thesis tackles this problem from an analytic perspective. We study, model, and analyze the performance of the uplink of the LoRa technology (AN120. . . , 2015), which is the physical layer of LoRaWAN (LORA ALLIANCE, 2020), one of the most widely used LPWAN. The work herein allows for understanding and exploiting some characteristics of LoRaWAN and, through extrapolation, other LPWAN.

There are several LPWAN technologies. Nevertheless, LoRaWAN is the most widely used LPWAN in the scientific community, probably because it is an open standard operating in the sub-GHz Industrial, Scientific, and Medical (ISM) radio bands; LoRa end-devices and gateways are available for acquisition in several countries; and it is possible to install and operate a LoRaWAN virtually anywhere without the need to contract network management service providers, as long as one respects local telecommunications regulations, which vary considerably across countries. Among the other most known technologies, SigFox did not release its protocols specifications before the beginning of this project and, so far, has a single service provider, and NB-IoT is not yet available to the general market. Besides that, these LPWAN technologies feature similar characteristics, and, due to that, several models and conclusions drawn for one technology can be extrapolated to others. In this work, we consider LoRaWAN because of the easier access to its technical specification.

LoRaWAN is the specification of a communication protocol stack that uses Semtech LoRa technology as the Physical Layer (PHY). Its Chirp Spread Spectrum (CSS) modulation technique uses higher SF rates to allow for an increased communi-

cation range at the cost of lower bitrate and longer ToA. Moreover, different SF builds *quasi*-orthogonal transmissions, meaning that a LoRaWAN gateway can decode concurrently received messages coded with different SF rates.

Several works have considered the modeling of LoRaWAN performance under different communication phenomena. Most works consider stochastic geometry to model interference (HAENGGI, 2012b). Georgiou and Raza (GEORGIU; RAZA, 2017) model a single-gateway LoRaWAN cell's performance under Rayleigh fading and co-SF interference¹. Mahmood *et al.* (MAHMOOD *et al.*, 2019) expand this model to consider inter-SF interference². Bankov *et al.* (BANKOV *et al.*, 2017) model a LoRaWAN cell using the Okumura-Hata model (GOLDSMITH, 2005) but disregarding small-scale fading. These and other works are explored again in Section 2.4 to consolidate a modeling framework for LoRaWAN.

Although LoRa links' performance has been assessed (PETÄJÄJÄRVI *et al.*, 2017), some recent works point to limitations to the scalability of LoRaWAN, especially due to interference arriving from medium multiple access. Mikhaylov *et al.* (MIKHAYLOV *et al.*, 2016) consider the European regulations for the sub-GHz ISM band and derive the maximum theoretical capacity of a LoRaWAN cell. Their results show that to support a reasonable Packet Error Rate (PER), most nodes tend to stay close to the gateway due to the spreading mechanism, limiting the technology communication range. In a similar direction, Bor *et al.* (BOR *et al.*, 2016) used simulations to show that network performance worsens as the number of nodes increase, but there are significant performance gains if multiple gateways are deployed, probably due to gains in spatial diversity. Mo *et al.* (MO *et al.*, 2016) present an analysis of performance gains due to time diversity arising from message replication techniques in Ultra-Narrow Band (UNB)/SigFox networks. They show an optimum number of message copies that minimize PER without compromising network performance due to increased network activity. In this work, we exploit the time and spatial diversities of LoRaWAN to investigate possible performance gains.

Since one of the goals of this thesis is to build a realistic LoRaWAN model, one must consider several sources of interference. Related work has mostly only considered intra-network interference, *i.e.*, the interference generated by other LoRa devices in the same network. In order to achieve a realistic model, one should take into account that LoRa devices in the ISM radio bands are subject to interference generated by other networks sharing the same spectrum (*e.g.*, around 868 MHz in Europe and 915 MHz in the USA and Brazil). Preliminary analysis of the interaction of LoRa with other communication technologies has been carried out by different authors considering Wi-SUN (ORFANIDIS *et al.*, 2017), SigFox (KRUPKA *et al.*, 2016; POORTER *et al.*,

¹ Co-SF interference assumes that only transmissions using the same SF rate interfere with each other.

² Inter-SF interference assumes imperfect SF orthogonality, *i.e.*, transmissions can receive interference from signals coded with different SF.

2017), and IEEE 802.11ah (POORTER et al., 2017). The results in those papers suggest that LoRa susceptibility to interference arriving from other technologies depends on the configuration of the LoRa signal, especially the SF in use. Here, we integrate these results into our models to account for inter-network interference. In addition to what has been done in related work, our model enables the fine-grain modeling of the interference signals, allowing for a more accurate deployment scenarios analysis.

LoRaWAN exploits the SF parameter of the CSS to extend network coverage by allocating different data rates and transmit power to nodes according to their link quality. This mechanism is called ADR. According to Cuomo *et al.* (CUOMO et al., 2017), the traditional ADR fails to optimize network performance in some scenarios because it does not take network density/usage into account, eventually generating too many packet losses to collisions. Besides that, ADR is a dynamic reactive method, *i.e.*, ADR will adjust the nodes' configuration only when some packets have already been lost, increasing error rate and latency. In their work, Cuomo *et al.* proposed alternative data rate allocation algorithms that take network density and ToA into account. Although their methods increase network data extraction rate and throughput in some scenarios, they did not derive analytical models for their system, limiting the study possibilities to simulated applications. Here, we integrate the data rate allocation mechanisms to our analytic models, thus enabling performance analysis and optimizations.

Results of performance analysis of LPWAN networks have shown that it is possible to increase packet delivery rate to some extent (CUOMO et al., 2017; BOR; ROEDIG, 2017; MO et al., 2016; MAHMOOD et al., 2019). However, achieving a delivery rate close to 100% is either unlikely or very costly, as we show for LoRaWAN in Chapter 3. Non-critical IoT applications, however, do not require such high delivery rates. For instance, Tomé *et al.* (CASTRO TOMÉ et al., 2019) analyze sampling strategies for electricity metering applications that recover, with reasonably small error rates, the energy consumption profiles of residential consumers when the smart meters suffer from up to 20% connection outage. Also, Yasmin *et al.* (YASMIN et al., 2018) showed a functioning indoor LoRaWAN network with several sensors where packet losses were tolerable. In this work, we use the proposed modeling framework to evaluate the possible performance optimization by adequately configuring the underlying LoRaWAN sensor network.

1.1 OBJECTIVES

This thesis's main objective is **to model and analyze the performance of low-power wide-area networks in realistic set-ups to exploit potential performance enhancements**. As stated before, we focus our developments on LoRaWAN as an important representative of LPWAN technology and propose the following intermediate, specific goals to achieve the proposed objective:

- G.1. To consolidate a reliable performance modeling framework of a single-gateway LoRaWAN allowing the variation of model parameters such as deployment scenarios, node density, duty-cycle, fading, and interference;
- G.2. To design and analyze the performance of LoRaWAN using techniques to exploit time and spatial communication diversity;
- G.3. To analyze the performance of LoRaWAN under the interference of other, non-LoRa networks;
- G.4. To analyze the performance of LoRaWAN using a power allocation mechanism;
- G.5. To propose model-based LoRaWAN optimization methods.

1.2 DOCUMENT STRUCTURE

This document is a compilation of the results published in three journal papers addressing the thesis's goals. Therefore, the chapters of this document are organized as follows:

1. **Introduction.** Introduces the work, motivates the research and lists the goals of the thesis.
2. **Research Context.** Contextualizes the project by describing the LPWAN technologies, the modeling tools, and presenting third-party works related to this thesis.
3. **Analysis and Performance Optimization of LoRaWAN With Time and Antenna Diversity.** Presents the first set of contributions in this thesis. The chapter is based on a paper published in the IEEE Access Journal (HOELLER et al., 2018).
4. **Optimum LoRaWAN Configuration Under Wi-SUN Interference.** Presents the second set of contributions to the thesis, based on a paper published in the IEEE Access Journal (HOELLER et al., 2019).
5. **Performance Analysis of Single-Cell Adaptive Data Rate-Enabled LoRaWAN** Presents the final set of contributions in the thesis and is based on a letter published in the IEEE Wireless Communications Letters (HOELLER et al., 2020).
6. **Conclusion.** Summarizes the thesis' achievements and considers possible paths for continuing the research.

2 RESEARCH CONTEXT

“He pointed out that we see more and farther than our predecessors, not because we have keener vision or greater height, but because we are lifted up and borne aloft on their gigantic stature.” John of Salisbury, about the teachings of Bernard of Chartres (SALISBURY, 1159).

This chapter presents the basic concepts used in the remainder of the thesis, including the technological and theoretical aspects. We first introduce the LPWAN paradigm and then describe the LoRaWAN and Wi-SUN technologies. Afterward, we describe the Stochastic Geometry tools to model interference and introduce a basic interference model to build the following chapters. Finally, we present and discuss related work.

2.1 LPWAN

LPWAN employ low-power communication technologies that enable the connection of thousands of IoT devices. Most of these technologies work in frequencies below 1GHz and employ modulation techniques that enable link budgets of 150 ± 10 dB, resulting in robust communication channels with low energy consumption reaching distances in the order of kilometers (RAZA et al., 2017; GOURSAUD; GORCE, 2015). The most prominent LPWAN technologies are LoRaWAN, SigFox, and NB-IoT (BURMAN et al., 2020). Additionally, for reducing complexity and energy consumption, LPWAN technologies use simple Medium Access and Control (MAC) protocols that decrease channel efficiency. For instance, both LoRaWAN and SigFox transmit data using unslotted ALOHA, which presents high collision probability when many stations are connected (ABRAMSON, 1970).

2.1.1 LoRaWAN

LoRa is a proprietary sub-GHz CSS modulation technique optimized for long-range applications and low power consumption at a low transmission rate (LORA ALLIANCE, 2020). The technology enables variable transmission rates with constant bandwidth by varying the *quasi*-orthogonal SF codes. The variable data rate characteristic allows for application optimizations according to the range, robustness, or energy consumption. The use of different SF also makes it possible for the base station to decode simultaneous transmissions from several devices at the same channel frequency without relevant degradation of the received signal.

The LoRa modulation depends, basically, on three parameters (AN120. . . , 2015): bandwidth (B), usually set to 125kHz or 250kHz for uplink and 500kHz for downlink; SF, which assumes values from 7 up to 12; and the Forward Error Correction (FEC) rate, varying from $\frac{4}{8}$ to $\frac{4}{5}$. These parameters allow computing, as in Table 1, the bit

rate, the packet ToA, the receiver sensitivity, and the required Signal-to-Noise Ratio (SNR) for successful detection in the absence of interference. It is possible to observe that ToA grows exponentially with SF, reducing the bit rate while improving the receiver sensitivity, thus enhancing coverage.

Table 1 – LoRaWAN Uplink characteristics for packets of 19 bytes (13-bytes header, 6-bytes payload), at $B = 125\text{kHz}$, FEC rate $\frac{4}{5}$, and CRC and Header Mode enabled (SX1276/77/78/79... , 2019).

SF i	ToA t_i (ms)	Bitrate Rb_i (kbps)	Receiver Sensitivity S_i (dBm)	SNR threshold ψ_i (dB)
7	51.46	5.46	-123	-6
8	102.91	3.12	-126	-9
9	185.34	1.75	-129	-12
10	329.73	0.97	-132	-15
11	741.38	0.53	-134.5	-17.5
12	1318.91	0.29	-137	-20

Source: the author.

The implementation of LoRa PHY is agnostic of higher layers. LoRaWAN is the most widely used protocol stack for LoRa networks. It implements a star topology and defines three types of devices: the *end-devices* (nodes) connect through a single-hop to one or more *gateways*, which in turn connect to a *network server* via an IP network. LoRaWAN MAC uses the unslotted ALOHA (ABRAMSON, 1970). Moreover, a LoRaWAN gateway's hardware can process up to nine channels in parallel, combining different sub-bands¹ and SF (CENTENARO et al., 2016). Besides, LoRa features the capture effect, making it possible to recover a LoRa signal when two or more signals are received simultaneously, in the same frequency and SF, provided that the desired signal is sufficiently stronger than any other (BOR et al., 2016).

2.1.2 Wi-SUN

Wi-SUN is a Field Area Network (FAN) technology built over the physical and link layers of the IEEE 802.15.4g standard. IEEE 802.15.4g is an amendment to IEEE 802.15.4 with a focus on Smart Utility Network (SUN) that has been playing an important role in smart grid deployments (IEEE... , 2012). It operates in different ISM bands, including the same sub-GHz bands used by LoRaWAN. Besides the bottom layers, Wi-SUN also defines network- and application-level services, including profiles for specific utility applications (e.g., energy, gas, water). The Wi-SUN ALLIANCE – supported by Cisco, Analog Devices, Toshiba, and others – maintains the Wi-SUN specification (WI-SUN ALLIANCE, 2020; CHANG; MASON, 2012).

¹ A LoRaWAN sub-band is a set of frequency channels that devices in a network are configured to use.

The IEEE 802.15.4g standard specifies different PHY interfaces able to operate in different frequency bands, including the Sub-GHz ISM. Data rates range from 20kbps to 1000kbps, depending on the modulation technique and bandwidth in use (CHANG; MASON, 2012). The PHY can be Multi-Rate Frequency Shift Keying (MR-FSK), Multi-Rate Orthogonal Frequency Division Multiplexing (MR-OFDM), or Multi-Rate Offset Quadrature Phase Shift Keying (MR-OQPSK). The mandatory configuration for all regions is 2-FSK at 50kbps, which implies a channel spacing of 200kHz. MR-FSK, with either 2-FSK or 4-FSK, is the predominant modulation version in SUN applications due to its increased communication range (OH et al., 2014). In this configuration, the transceiver combines Frequency Shift Keying (FSK) modulation with Frequency Hopping Spread Spectrum (FHSS) to increase communication robustness (HARADA et al., 2017). The data rate may vary from 50kbps to 400kbps, depending on the region and frequency (HARADA et al., 2017). The receiver sensitivity for a PER of 10% must be better than -85dBm or -91dBm at, respectively, 200kbps and 50kbps, without FEC. If FEC is enabled, the sensitivity must drop to -91dBm and -97dBm for the same data rates. Transmit power depends on regional regulations but must be at least -3dBm (CHANG; MASON, 2012). Most typical configurations include $+14\text{dBm}$ transmit power and a 1% maximum duty cycle (MUÑOZ et al., 2018).

IEEE 802.15.4g includes extensions to the MAC mechanisms defined by the amendment IEEE 802.15.4e (IEEE. . . , 2012). It makes extensive use of the low-energy modes defined in the 4e document. The IEEE 802.15.4g networks are expected to form multi-hop mesh networks. The MAC layer performs either Carrier-Sense Multiple-Access (CSMA) or a simplified version of channel monitoring named Coordinated Sampled Listening (CSL) (DESHPANDE et al., 2007) before sending data. Higher layers tend to use IPv6 for Low-Power Wireless Personal Area Networks (6LoWPAN)/Internet Protocol version 6 (IPv6) at the network layer, User Datagram Protocol (UDP) at the transport layer, and IPv6 Routing Protocol for Low-Power and Lossy Networks (RPL) as routing protocol (SHELBY; BORMANN, 2009).

2.2 BASIC SYSTEM MODEL

According to Haenggi (HAENGGI, 2012b), classical methods of communication theory are not sufficient to perform a comprehensive analysis of wireless networks for three main reasons:

- i. The performance-limiting metric is the Signal-to-Interference-and-Noise Ratio (SINR) and not only the SNR;
- ii. The interference depends on path loss and fading characteristics of the interferers' channels, which are functions of the interferers' positions;

- iii. The uncertainty in large wireless networks can be greater than in point-to-point systems – one node seldom knows all other nodes' locations and channels.

However, stochastic geometry allows the study of the average behavior of wireless networks and is an important tool to complement such systems' performance analysis. This section presents the basic stochastic geometry model for a wireless network adapted or extended in the following chapters to address the specifics of LoRaWAN.

2.2.1 Stochastic Geometry

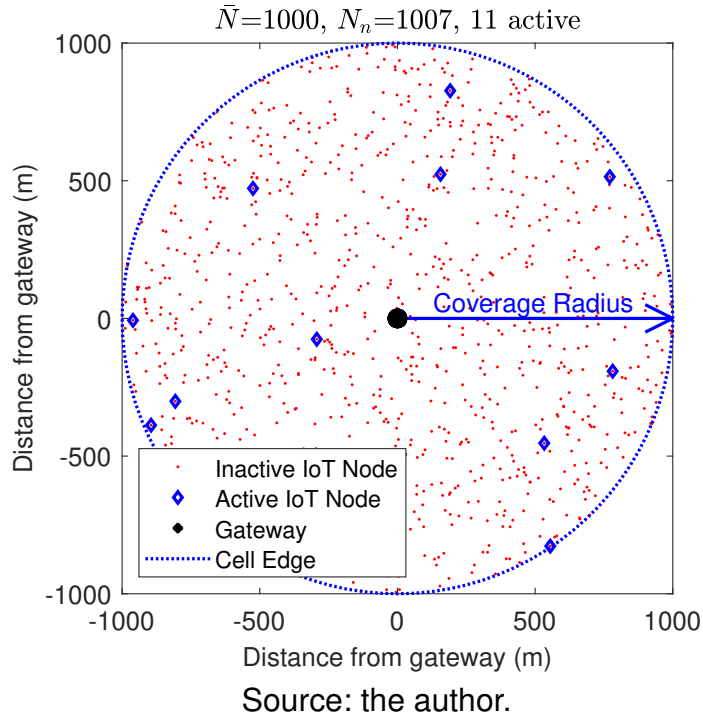
Stochastic geometry is a mathematical tool for studying random spatial patterns, being the *point processes* its most important sub-field (HAENGGI, 2012b). It allows the study of the average behavior of several spatial realizations of a wireless network, provided that node placement follows some probability distribution. When modeling wireless networks, point processes produce random collections of points representing wireless nodes' locations in a region (MILLER; CHILDERS, 2012). In this thesis, we are concerned with the modeling of interference and, therefore, we study the distribution and the activity of the transmitters in a given scenario and not necessarily all nodes in the network. In this case, the channel access (MAC) scheme performs a *thinning* procedure over the point process, reducing the set of all nodes to the set of transmitting nodes at a given instant (HAENGGI, 2012b). In ALOHA-like networks, like the ones studied in this thesis, the MAC produces a Poisson Point Process (PPP), whose intensity depends on the network's spatial density and the ALOHA transmission probability.

Figure 1 illustrates the stochastic geometry model of a hypothetical IoT network with coverage region $\mathcal{V} \subset \mathbb{R}^2$ defined by a circle of radius $R = 1\text{km}$. Let us assume that, on average, this network has $\bar{N} = 1000$ nodes, which are uniformly distributed within \mathcal{V} . If $V = \pi R^2 \approx 3.14\text{km}^2$ is the area of \mathcal{V} , then $\rho = \frac{\bar{N}}{V} \approx 0.318 \times 10^{-3}$ nodes/m² is the spatial density of the network. In the figure, a snapshot of a PPP Φ of intensity ρ describing the location of all nodes results in $N_n = 1007$ sampled nodes. If p defines the transmission probability of the ALOHA MAC, then the PPP Φ_t of intensity $\alpha = p\rho$ is the thinned PPP (HAENGGI, 2012b) of Φ describing the active nodes at a given moment.

2.2.2 Channel model

Following the definitions in (GEORGIU; RAZA, 2017), we assume that d_k is the Euclidean distance between the k -th wireless node in a network and the gateway at the origin, d_1 denotes the distance of the node of interest, \mathcal{P}_1 and \mathcal{P}_k are, respectively, the transmit power used to send signals s_1 and s_k , and both path loss (g_k) and fading (h_k) affect the received signals. Path loss follows the Friis equation $g_k = \left(\frac{\lambda}{4\pi d_k}\right)^\eta$, with wavelength λ , path loss exponent $\eta \geq 2$, while k indexes a device in the network. Finally, h_k denotes the Rayleigh fading. The choice of this fading model is justified by the easier

Figure 1 – Sample from a stochastic geometry model of a network cell with $\bar{N} = 1000$ nodes and $R = 1000\text{m}$.



analysis yielded by it and because it is accepted as a worst-case model. Therefore, a LoRaWAN signal r_1 received at the gateway is the sum of the attenuated transmitted signal s_1 , interference, and noise,

$$r_1 = s_1 h_1 \sqrt{\mathcal{P}_1 g_1} + \mathcal{I} + w, \quad (1)$$

where w is the Additive White Gaussian Noise (AWGN) with zero mean and variance σ_w^2 , and

$$\mathcal{I} = \sum_{k \in \Phi_t} s_k h_k \sqrt{\mathcal{P}_k g_k} \quad (2)$$

accounts for the interference with Φ_t as the thinned PPP of the network, *i.e.*, the set of the active nodes at a given instant. From this model, it follows that the SINR of the node of interest is observed at the gateway as

$$\text{SINR} = \frac{|h_1|^2 \mathcal{P}_1 g_1}{\sigma_w^2 + \sum_{k \in \Phi_t} |h_k|^2 \mathcal{P}_k g_k}. \quad (3)$$

2.2.3 Success Probabilities

According to Haenggi (HAENGGI, 2012b), “for a fixed modulation and coding scheme and with interference treated as noise, [...], a well-accepted model for packetized transmissions is that they succeed if the SINR exceeds a certain threshold γ ,” *i.e.*,

the coverage probability is $C_1 \triangleq \mathbb{P}(\text{SINR} \geq \gamma)$. By replacing the SINR from (3) we have that

$$C_1 \triangleq \mathbb{P}\left(\frac{\mathcal{P}_1 g_1 |h_1|^2}{\sigma_w^2 + \sum_{k \in \Phi_t} \mathcal{P}_k g_k |h_k|^2} \geq \gamma\right). \quad (4)$$

We then condition this probability on the fading power of the node of interest ($|h_1|^2$). Note that $|h_1|^2 \sim \exp(1)$, *i.e.*, the distribution of $|h_1|^2$ is exponential with rate $\lambda = 1$, with Probability Density Function (PDF) $f(x) = \lambda e^{-\lambda x} = e^{-x}$ and Cumulative Distribution Function (CDF) $F(x) = 1 - e^{-\lambda x} = 1 - e^{-x}$. From this, we obtain

$$\begin{aligned} C_1 &\triangleq \mathbb{P}\left[|h_1|^2 \geq \gamma \left(\frac{\sigma_w^2 + \sum_{k \in \Phi_t} \mathcal{P}_k g_k |h_k|^2}{\mathcal{P}_1 g_1}\right)\right] \\ &= \mathbb{E}_{|h_k|^2, \Phi_t} \left\{ \exp\left[-\gamma \left(\frac{\sigma_w^2 + \sum_{k \in \Phi_t} \mathcal{P}_k g_k |h_k|^2}{\mathcal{P}_1 g_1}\right)\right] \right\}, \end{aligned} \quad (5)$$

where C_1 is conditioned on the fading distribution of the interfering nodes and the PPP. Note that, because of the exponential, it is possible to rewrite (5) as a product of two distinct expressions, one deterministic noise-dependent part (H_1) and another stochastic interference-dependent part, *i.e.*,

$$C_1 \triangleq H_1 Q_1, \quad (6)$$

$$H_1 = \exp\left(-\frac{\gamma \sigma_w^2}{\mathcal{P}_1 g_1}\right) = \exp\left[-\frac{\gamma \sigma_w^2}{\mathcal{P}_1 d_1^{-\eta}} \left(\frac{4\pi}{\lambda}\right)^\eta\right], \quad (7)$$

$$Q_1 = \mathbb{E}_{|h_k|^2, \Phi_t} \left[\exp\left(-\frac{\gamma}{\mathcal{P}_1 g_1} \sum_{k \in \Phi_t} \mathcal{P}_k g_k |h_k|^2\right) \right]. \quad (8)$$

To obtain a closed-form representation of this success probability, we continue the analysis of (8). First, we consider that all nodes use the same transmit power, *i.e.*, $\mathcal{P}_1 = \mathcal{P}_k$ and replace the path loss function to average over the fading of the interference sources. Since we also assume that interference is subject to Rayleigh fading, the fading power also has an exponential distribution $|h_k|^2 \sim \exp(1)$, and therefore

$$Q_1 = \mathbb{E}_{\Phi_t} \left[\prod_{k \in \Phi_t} \int_0^\infty \exp\left(-\frac{\gamma d_k^\eta x}{d_k^\eta}\right) \exp(-x) dx \right] = \mathbb{E}_{\Phi_t} \left(\prod_{k \in \Phi_t} \frac{d_k^\eta}{d_k^\eta + \gamma d_1^\eta} \right). \quad (9)$$

Now, we rely on the Probability Generating Function (PGF) (MILLER; CHILDERS, 2012) of the product over PPPs where

$$\mathbb{E} \left[\prod_{x \in \Phi} f(x) \right] = \exp \left[-\alpha \int_{\mathbb{R}^2} (1 - f(x)) dx \right], \quad (10)$$

with α as the intensity of Φ , to solve the expectation in (9) as

$$Q_1 = \exp \left(-\alpha \int_{\mathbb{R}^2} 1 - \frac{d_k^\eta}{d_k^\eta + \gamma d_1^\eta} dd_k \right). \quad (11)$$

Since d_k is the Euclidean distance of the k -th node to the gateway at the origin of the coverage region, it is expressed in the Cartesian plane as $d_k = \sqrt{x^2 + y^2}$. To solve the integral in (11), we transform d_k into Polar coordinates, where $x = z \cos \theta$ and $y = z \sin \theta$, so that $d_k = \sqrt{z^2(\cos^2 \theta + \sin^2 \theta)} = z$, and

$$Q_1 = \exp \left(-\alpha \int_0^R \int_0^{2\pi} 1 - \frac{z^\eta}{z^\eta + \gamma d_1^\eta} z d\theta dz \right). \quad (12)$$

Solving the integrals, we then obtain the final expression

$$\begin{aligned} Q_1 &= \exp \left(-2\pi\alpha \int_0^R 1 - \frac{z^\eta}{z^\eta + \gamma d_1^\eta} z dz \right) \\ &= \exp \left[-\pi\alpha R^2 {}_2F_1 \left(1, \frac{2}{\eta}, 1 + \frac{2}{\eta}, -\frac{R^\eta}{\gamma d_1^\eta} \right) \right], \end{aligned} \quad (13)$$

where ${}_2F_1(\cdot)$ is the Gauss Hypergeometric function (OLVER et al., 2010).

It is also possible to obtain the mean performance by averaging C_1 over the deployment area, obtaining

$$\bar{C}_1 = \frac{2}{R^2} \int_0^R C_1 d_1 dd_1. \quad (14)$$

2.3 TOOLS

Two main tools were used to develop this thesis: Wolfram Mathematica (WOLFRAM RESEARCH, 2021) and MathWorks MATLAB (MATHWORKS, 2021). The tools supported, respectively, the two main employed methods: mathematical analysis and Monte Carlo simulation.

Wolfram Mathematica provides technical computing tools for several applications, including machine learning, image processing, geometry, data science, and more. This work mostly used the tool to analyze and solve integrals, especially to map the integrals' results into other mathematical functions such as the Hypergeometric or the Gamma Functions (OLVER et al., 2010). However, it is important to note that the tool was not able to solve by itself most of the integrals, thus requiring some manipulations and transformations, which are presented in this document.

MathWorks MATLAB is a numeric computing language and environment that supports matrix manipulations, function and data plotting, and programming for a wide range of scientific and engineering applications. This work relied on MATLAB to produce both analytic and simulated data, including the thesis's plots. Specifically, the

tool's numeric integration methods allowed to approximate the solution of integrals without closed forms. The tool's probability functions also allowed the straightforward development of the simulations that validated the proposed models.

2.4 RELATED WORK

Several recent related works sought to evaluate the performance of LoRaWAN using analytic modeling, simulation, and real measurements. Additionally, a few techniques have been proposed to enhance the performance of LPWAN in general, with potential modifications to the current technologies.

Analytic models have been proposed for a variety of scenarios and communication phenomena. Bor *et al.* (BOR *et al.*, 2016) experimentally investigate the capture effect of LoRa and model the network capacity, concluding that a LoRaWAN with only one gateway typically does not scale well, while networks with a dynamic adaptation of operating parameters or multiple gateways scale better. Georgiou and Raza (GEORGIU; RAZA, 2017) propose an analytic model that considers Rayleigh fading and equates the coverage probability considering both disconnection and collision. Their work shows that LoRaWAN is sensitive to the node density because of the increased collision probability. Mahmood *et al.* (MAHMOOD *et al.*, 2019) and Georgiou and Raza (GEORGIU; RAZA, 2017) use stochastic geometry and PPP to derive an analytic model of the coverage probability of LoRaWAN nodes in fading channels. Contrasting with (GEORGIU; RAZA, 2017), the work in (MAHMOOD *et al.*, 2019) considers the effect of interference related to the imperfect orthogonality of LoRa signals using different SF codes. Croce *et al.* (CROCE *et al.*, 2018) show that LoRa SF separation is not perfect, so besides receiving interference from nodes using the same SF (co-SF interference), LoRa nodes are also subject to some interference generated by nodes using other SF (inter-SF interference). Croce *et al.* report that the Signal-to-Interference Ratio (SIR) thresholds for Semtech's SX1272 LoRa transceiver are lower regarding co-SF interference ($\approx +1\text{dB}$) and significantly higher for inter-SF interference when compared to previously published results, including the manufacturer datasheet.

Sørensen *et al.* (SØRENSEN *et al.*, 2017) propose analytic models to investigate the LoRaWAN performance regarding uplink latency, collision rate, and throughput. They also explore the network resource allocation for given QoS requirements and traffic models. Gupta *et al.* (GUPTA *et al.*, 2017) model the IoT traffic considering periodic and event-generated messages and analyze the impact of traffic variations in LoRaWAN networks. They find that LoRaWAN gateways do not handle well bursty events, which generate a significant amount of messages in a short period, especially when there is a spatial or temporal correlation in the transmission behavior of the devices. Pop *et al.* (POP *et al.*, 2017) evaluate how the LoRaWAN downlink impacts LoRaWAN uplink goodput and coverage probability. They consider the MAC layer and,

through simulations, verify that if too many end-devices request delivery confirmation, the downlink becomes unstable and unable to deliver several acknowledgment packets, forcing nodes to retry, ultimately flooding the network. Bankov *et al.* (BANKOV *et al.*, 2017) proposed a mathematical model for LoRaWAN channel access considering the capture effect and using the Okumura-Hata model, but without fading. Concerning the modeling of communication fading, among the considered related work only Georgiou and Raza (GEORGIU; RAZA, 2017), Pop *et al.* (POP *et al.*, 2017), and Mahmood *et al.* (MAHMOOD *et al.*, 2019) consider this impairment.

Several works use measurements to evaluate the performance of LoRaWAN. Petäjälä *et al.* (PETÄJÄLÄ *et al.*, 2017) analyze Doppler robustness, scalability, and coverage of LoRaWAN and report the experimental validation of such metrics in terrestrial and water environments for static and mobile nodes. They communicate to static nodes ranging up to 30km over the water and up to 10km on the ground with a delivery ratio above 60% and LoRaWAN's most conservative configurations. Regarding Doppler robustness, they observed that communication degrades significantly when the node's speed is above 40 km/h. Yasmin *et al.* (YASMIN *et al.*, 2018) analyze the performance of a LoRaWAN deployment reporting indoor sensor data inside a university campus. There are similar reports of LoRaWAN measurements in different environments, including industry (ANGRISANI *et al.*, 2017), dense cities downtown (JÖRKE *et al.*, 2017; RADCLIFFE *et al.*, 2017), smart metering (RIZZI *et al.*, 2017), and rural areas (OLIVEIRA *et al.*, 2017). Orfanidis *et al.* (ORFANIDIS *et al.*, 2017) report an experimental evaluation of the interference between IEEE 802.15.4g and LoRaWAN by evaluating the PER in different SINR scenarios inside an anechoic chamber. The measurements consider a single IEEE 802.15.4g interferer over one LoRa link. Their results show that lower SF are more susceptible to interference than higher SF. Although all these works' measurements show interesting results, it is important to note that they consider a limited number of nodes, making it very hard to extrapolate any conclusions for dense networks.

A few recently published work also propose enhancements to LoRaWAN. Cuomo *et al.* (CUOMO *et al.*, 2017) propose algorithms to replace LoRaWAN adaptive data rate strategy. The proposed algorithms do not base the SF configuration on distance and received power measurements but on the number of connected devices, allowing the equalization of channel usage in each SF. Bor and Roedig (BOR; ROEDIG, 2017) explore LoRaWAN configuration parameters such as SF, bandwidth, coding rate, and transmission power, which result in 6720 possible settings, and propose an optimization problem that minimizes energy spent on data transmission while meeting required communication performance. Qin and McCann (QIN; MCCANN, 2017) approach the optimization of LPWAN from a resource allocation perspective. They use game theory to derive an algorithm that allows network nodes to decide which channel and SF

to use and, for each channel/SF group, the optimal transmit power that maximizes the data extraction rate. Voigt *et al.* (VOIGT *et al.*, 2017) consider the inter-network interference that is likely to occur when several independent LoRaWAN get deployed too close. Authors consider using directional antennas in network nodes and using multiple gateways in the network. Results show that directional antennas enhance the data extraction rate, although multiple gateways in the coverage area tend to perform better.

Besides the above works, some authors have explored techniques similar to those proposed in this thesis for LoRaWAN, UNB/SigFox, or LPWAN in general. Mo *et al.* (MO *et al.*, 2016) investigated the optimal number of message replications for UNB/SigFox networks. Song *et al.* (SONG *et al.*, 2017) consider the macro reception diversity of long-range ALOHA networks, where augmented spatial diversity arises from allowing several base stations to receive the same packet. Magrin *et al.* (MAGRIN *et al.*, 2017) developed a simulation model for the NS-3 network simulator with which they showed that LoRaWAN supports a large number of nodes and maintains good network quality if several gateways are carefully placed.

In this thesis, Chapter 3 models and validates the behavior of LoRaWAN using message replication to exploit time diversity and using a single gateway with multiple receive antennas to exploit spatial diversity, striving to maximize network performance. To do that, we take the work of (GEORGIU; RAZA, 2017) as a baseline model and extend it to incorporate the proposed techniques. Our work on message replication differs from (MO *et al.*, 2016) because that work considers UNB networks where each transmission uses a random central frequency – an assumption that changes the collision model. Moreover, our work considers fading, while (MO *et al.*, 2016) does not. Our approach using multiple receive antennas differs from (SONG *et al.*, 2017) and (MAGRIN *et al.*, 2017) because they consider spatial diversity generated by multiple gateways. Our work examines the case where multiple receive antennas in a single gateway create signal diversity able to enhance signal quality, an approach that can be naturally extended to the case of multiple gateways in the future. To the best of our knowledge, no work investigated the use of multiple receive antennas and message replications in LoRaWAN before (HOELLER *et al.*, 2018). In Chapter 4, we adapt our model to include the modeling of inter-SF interference of Mahmood *et al.* (MAHMOOD *et al.*, 2019). Besides that, we build over the resulting model to consider the inter-technology interference reported by Orfanidis *et al.* (ORFANIDIS *et al.*, 2017). To the best of our knowledge, no other work than that of Orfanidis *et al.* studied the susceptibility of LoRaWAN to external IEEE 802.15.4g interference, and there was no published work investigating this relationship in a network-scale scenario with several active links in both IEEE 802.15.4g and LoRaWAN before us in (HOELLER *et al.*, 2019).

2.5 CLOSING

This section presented the technical specifications and the theoretical framework that support the remaining chapters of this thesis. The use of stochastic geometry to model interference in LoRaWAN systems is the most relevant excerpt of this chapter to the following ones. To start with that, the next chapter will use a stochastic geometry model to analyze the performance of LoRaWAN with message replication and multiple receive antennas.

3 ANALYSIS AND PERFORMANCE OPTIMIZATION OF LORAWAN NETWORKS WITH TIME AND ANTENNA DIVERSITY

“Our greatest weakness lies in giving up. The most certain way to succeed is always to try just one more time.” Thomas Alva Edison.

This chapter focuses on the uplink of the LoRa technology – the underlying proprietary PHY of LoRaWAN (LORA ALLIANCE, 2020). It describes this thesis project’s contributions originally published in the *IEEE Access Journal* in 2018 (HOELLER et al., 2018). The problem under investigation in this chapter is increasing the coverage probability of LoRaWAN exploiting time and antenna diversity (GOLDSMITH, 2005). More specifically, we analyze the impact that message replication and gateways with multiple receive antennas have on the outage probability. We accomplished that by extending the outage models previously published by Georgiou and Raza (GEORGIU; RAZA, 2017) to account for the proposed diversity techniques. Simulations validate the theoretical models. The analysis of the results yields the formulation of an optimization problem that finds the optimum number of message replications for a set of network configuration parameters and different network density (number of nodes and their duty cycles).

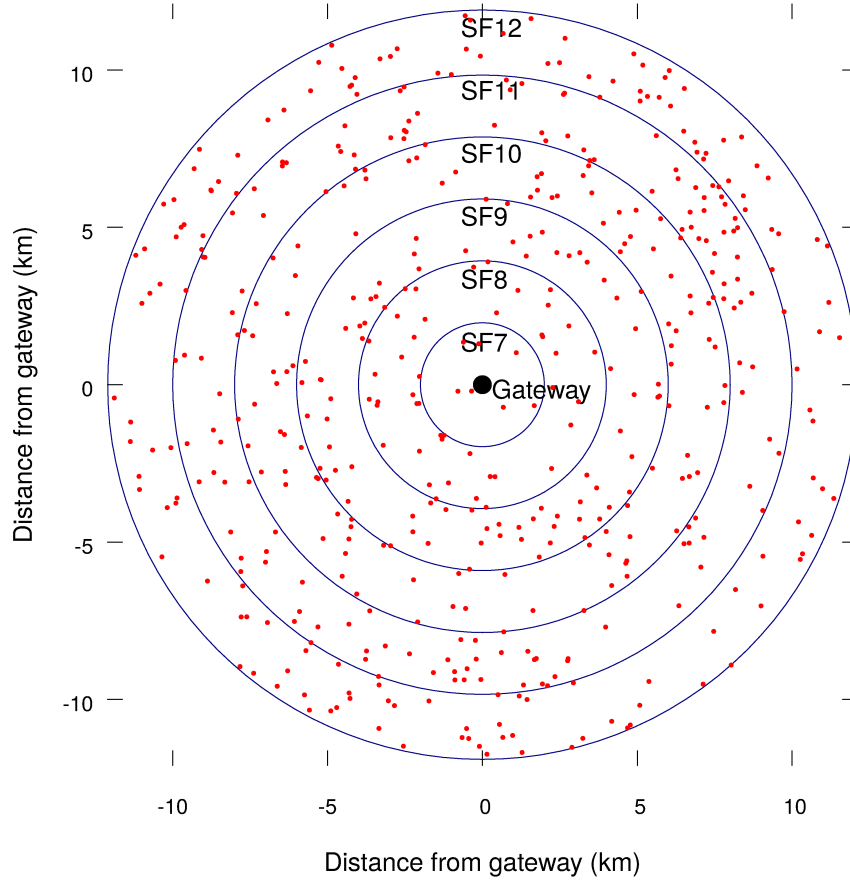
The contributions enclosed in this chapter are summarized as:

- The optimization of the number of message copies for each SF configuration that maximizes LoRaWAN coverage probability;
- The formulation of a tight closed-form bound for the collision probability considering a gateway with multiple receive antennas;
- The analysis of the interaction between message replication and multiple receive antennas in LoRaWAN, showing that message replication brings benefits only for low-density networks, while multiple receive antennas are always beneficial.

3.1 SYSTEM MODEL

Using the stochastic geometry model presented in Section 2.2, and following its application to LoRaWAN in (GEORGIU; RAZA, 2017), we consider that, on average, \bar{N} nodes are uniformly distributed around a gateway in a circular region $\mathcal{V} \subseteq \mathbb{R}^2$ of radius R and area $V = \pi R^2$. The coordinate system in Figure 2 exemplifies the considered deployment with the gateway at the origin and uniformly deployed nodes. This distribution is described by a PPP Φ with density $\rho > 0$ in \mathcal{V} and 0 otherwise. In this scenario, d_k is the Euclidean distance between the gateway and the k -th node. Devices transmit in the uplink at random using the ALOHA protocol, obeying a duty cycle p . Finally, the network area is divided into six SF rings denoted by $S = \{1, \dots, 6\}$, where

Figure 2 – $\bar{N} = 500$ nodes uniformly distributed in a circular area of radius $R = 12$ km around the gateway, with SF increasing every 2 km.



Source: the author.

rings use the SF rate in $\{7, \dots, 12\}$, respectively. In this chapter, all rings have the same width, *i.e.*, $\frac{R}{6}$. Also, all nodes transmit with the same power \mathcal{P}_t .

The uplink model considers that both path loss attenuation g_k and Rayleigh fading h_k affect the received signal, as in (GEORGIU; RAZA, 2017). Path loss follows the Friis transmission equation $g_k = \left(\frac{\lambda}{4\pi d_k}\right)^\eta$, where λ is the wavelength, and $\eta \geq 2$ is the path loss exponent. Rayleigh fading is modeled as a zero-mean, independent, circularly-symmetric complex Gaussian random variable with unit variance. Given a signal transmitted by a LoRa node s_1 , the received signal at the gateway, r_1 , is the sum of the attenuated transmitted signal, interference and noise. It can be expressed as

$$r_1 = s_1 h_1 \sqrt{\mathcal{P}_1 g_1} + \sum_{k \in \Phi_{t,i}} s_k h_k \sqrt{\mathcal{P}_k g_k} + w, \quad (15)$$

where the subscript “1” denotes the desired node, *i.e.*, the node under analysis, $\Phi_{t,i}$ is the thinned PPP of the desired node’s SF ring (SF i), and w is the AWGN with zero mean and variance σ_w^2 .

The outage probability model follows (GEORGIU; RAZA, 2017), which considers that LoRa uplink outages occur if there is no connection between a node and the

gateway or if there is a collision. This section briefly presents these probability models, which are the basis for the extensions that include time and antenna diversity presented in the next sections.

3.1.1 Outage Condition 1: Disconnection

First, we consider the connection probability, which depends on the communication distance. A node is assumed as *not* connected to the gateway if the received signal's SNR is below the reception threshold that allows successful detection in the absence of interference. Different SFs result in different receiver sensitivities, which, in turn, result in different SNR reception thresholds (ψ_i), as shown in Table 1. Thus, the *connection probability* is

$$H_1 = \mathbb{P}[\text{SNR} \geq \psi_i \mid g_1], \quad (16)$$

where ψ_i is the SNR reception threshold of SF i , and g_1 is the path loss of the node located d_1 meters from the gateway, with

$$\text{SNR} = \frac{\mathcal{P}_1 g_1 |h_1|^2}{\sigma_w^2}. \quad (17)$$

Since we consider that the fading in h_1 follows a Rayleigh distribution, $|h_1|^2$ is exponentially distributed (GOLDSMITH, 2005), and therefore

$$H_1 = \mathbb{P} \left[|h_1|^2 \geq \frac{\sigma_w^2 \psi_i}{\mathcal{P}_1 g_1} \right] = \exp \left(-\frac{\sigma_w^2 \psi_i}{\mathcal{P}_1 g_1} \right) = \exp \left[-\frac{\sigma_w^2 \psi_i}{\mathcal{P}_1 d_1^{-\eta}} \left(\frac{4\pi}{\lambda} \right)^\eta \right]. \quad (18)$$

Note that the model depends on g_1 , which can either be known or obtained from the Friis equation if d_1 is known.

3.1.2 Outage Condition 2: Collision

Since LoRa is a form of frequency modulation, it exhibits the capture effect (BOR et al., 2016), allowing stronger signals to suppress simultaneously received weaker signals. In LoRa, a collision only occurs if the power difference between the desired signal and any other simultaneously received signal using the same SF and frequency channel is less than 6dB. To evaluate this condition, one must consider the strongest interfering node k^* defined as

$$k^* = \arg \max_{k \in \Phi_{t,i}} \{\mathcal{P}_t |h_k|^2 g_k\}. \quad (19)$$

Once k^* is found, the probability that no collision occurs or that the strongest interfering signal is at least 6dB (4 times) below the desired one, termed here as *capture*

probability, is

$$\begin{aligned}
 Q_1 &= \mathbb{P} \left[\frac{|h_1|^2 g_1}{|h_{k^*}|^2 g_{k^*}} \geq 4 \mid g_1 \right] \\
 &= \mathbb{E}_{|h_1|^2} \left[\mathbb{P} \left[X_{k^*} < \frac{|h_1|^2 g_1}{4} \mid |h_1|^2, g_1 \right] \right]. \tag{20}
 \end{aligned}$$

The above probability depends on the probability distribution of the random variable $X_{k^*} = |h_{k^*}|^2 g_{k^*}$. The CDF of X_{k^*} is derived in (GEORGIU; RAZA, 2017) and is denoted as $F_{X_{k^*}}$. Thus

$$\begin{aligned}
 Q_1 &= \mathbb{E}_{|h_1|^2} \left[F_{X_{k^*}} \left(\frac{|h_1|^2 g_1}{4} \right) \right] \\
 &= \int_0^\infty e^{-z} F_{X_{k^*}} \left(\frac{z g_1}{4} \right) dz. \tag{21}
 \end{aligned}$$

Moreover, in (GEORGIU; RAZA, 2017), the authors present an approximation for (21) that is only accurate at the edges of each SF ring in Figure 2. Here, we consider only the exact probability in (21).

3.1.3 Coverage Probability

As presented in Section 2.2.3, the *coverage probability* is the probability that the selected node is in coverage, *i.e.*, it can successfully communicate, considering both the connection and collision outage conditions. However, in Section 2.2.3, (6) is a function of the SINR threshold since that generic model assumes that the SNR and SIR thresholds are close, and that subtle difference is often irrelevant. This thesis considers a specific technology for which the exact thresholds are known, so that difference becomes quite relevant. In LoRa, this difference of at least 8 dB between the SIR and the SNR thresholds delivers the spreading factor gain. This assumes that the coverage equation of the LoRaWAN model is the approximation

$$C_1 \approx H_1 Q_1, \tag{22}$$

because we now solve H_1 and Q_1 as independent variables in, respectively, (18) and (21) when in reality both depend on the same realization of the fading h_1 . The different thresholds for LoRaWAN have been considered by other publications (GEORGIU; RAZA, 2017; MAHMOOD et al., 2019; HOELLER et al., 2019; SOUZA SANT'ANA et al., 2020), and the numeric results in those works, as well as the ones presented here, suggest that our LoRaWAN model delivers a good approximation, besides being more convenient because of the independence assumption.

Moreover, we obtain the average coverage probability \bar{C}_1 by de-conditioning on the desired node position, achieved by averaging in the network area,

$$\bar{C}_1 = \frac{2}{R^2} \int_0^R C_1(d_1) d_1 dd_1. \quad (23)$$

This chapter builds on the model above by including the required changes to consider the effects of time and antenna diversity. Additionally, different than (GEOR-GIOU; RAZA, 2017), we also consider the average coverage probability per SF ring. The coverage probability of a node in the SF ring i is

$$\bar{C}_{1,i} = \frac{2}{l_i^2 - l_{i-1}^2} \int_{l_{i-1}}^{l_i} C_1(d_1) (d_1 - l_{i-1}) dd_1, \quad (24)$$

where l_{i-1} and l_i are, respectively, the inner and outer radii of the i -th ring, with $i \in \{1, \dots, 7\}$, as illustrated in Figure 2.

3.2 MESSAGE REPLICATIONS – TIME DIVERSITY

Many systems increase network reliability by using Automatic Repeat reQuest (ARQ) techniques, in which receivers automatically request the retransmission of lost packets. Although LoRa systems can use such techniques, a recent study (POP et al., 2017) has shown that LoRa downlink cannot support the high demand for acknowledgment packets generated when all nodes in a dense network request such confirmations, making delivery confirmation an unreliable feature. However, other techniques can be applied to increase network reliability, being message replication one of them.

The first contribution in this chapter is to analyze the effects of message replication in LoRa networks, where each information message is transmitted M times within the same time interval when message replication is not used. Therefore, with message replication, there is an M -fold increase in the network usage. Such technique increases the desired signal's temporal diversity, thus making it much more likely that at least one message copy arrives at the gateway. The increase in connectivity success probability is dependent on the number of replications M .

First, consider the extension of the connection probability to the case of message replications, denoted by $H_{i,M}$. In this case, a connection outage only occurs if all M message copies are lost, therefore

$$H_{i,M} = 1 - (1 - H_1)^M, \quad (25)$$

where $|h_1|^2$ is assumed independent among replications. In a real deployment, one must consider that fading independence only occurs if the time separation between message copies is greater than the channel coherence time. In our work, we assume that this condition is always met (GOLDSMITH, 2005), as this is very likely in LoRaWAN.

Similar changes need to be made to the analysis of the capture probability. In this case, (20) can be rewritten to consider the probability that at least one of the M message copies is received without interference or 6dB above the stronger interferer,

$$Q_{i,M} = 1 - (1 - Q_1)^M. \quad (26)$$

It is important to highlight that the derivation of $F_{X_{k^*}}$ in (GEORGIU; RAZA, 2017), required for evaluating Q_1 , defines the number of interfering nodes as a Poisson distribution with mean $\nu = \rho p V$, where V is the area of the SF ring of the desired node at d_1 . In the case of message replication, once the transmission of message copies increases the channel usage, it is necessary to proportionally increase the mean of the Poisson distribution by making $\nu = M \rho p V$ when evaluating (26).

Finally, the coverage probability using M message copies is

$$C_{i,M} \approx H_{i,M} Q_{i,M}. \quad (27)$$

Note that average coverage probability with message replication for the entire network or a specific SF can be derived from, respectively, (23) or (24) by replacing C_1 with $C_{i,M}$.

We observed that the response of the average coverage probability ($\bar{C}_{1,i}$) to variations in M shows an optimum point for each SF ring, within the bounds of reasonable values of M . Thus, it is possible to define the following optimization problem in the form of an Integer Linear Programming (ILP) to find the optimum integer number of message copies M^* for each SF in a given network configuration. The ILP is

$$\begin{aligned} M_i^* &= \arg \max_{M \in \mathbb{Z}} \bar{C}_{1,i} \\ &= \arg \max_{M \in \mathbb{Z}} \left[\frac{2}{l_i^2 - l_{i-1}^2} \int_{l_{i-1}}^{l_i} C_{i,M}(d_1) (d_1 - l_{i-1}) dd_1 \right] \\ &\text{subject to: } 1 \leq M \leq M_{\max}, \end{aligned} \quad (28)$$

where i is the SF ring under consideration, and M_{\max} is the maximum value for M^* . In this work, we solved this ILP by exhaustively enumerating $\bar{C}_{1,i}$ for all possible values of M . This is a viable option since the set of reasonable values of M is small, as will be shown in Section 3.4.

3.3 MULTIPLE RECEIVE ANTENNAS – SPATIAL DIVERSITY

This chapter's second contribution is to analyze the gain in coverage probability of LoRa networks when using multiple receive antennas at the gateway to build spatial diversity. Note that applying a technique such as maximum ratio combining (GOLD-SMITH, 2005) is not feasible in this case, as we consider the use of commercial LoRa radios, implying that each antenna has a complete Radio Frequency (RF) receiver

chain. As the gateway can only tune to a particular user if the SIR is at least 6dB (considering nodes with the same SF), it would not be possible to combine several branches with SIR below 6dB to achieve a combined signal with an SIR of at least 6dB. The alternative, thus, is to consider an approach based on the selection combining technique (GOLDSMITH, 2005).

In this case, the adaptation of the connection probability from (16) is straightforward. It is assumed that A receive antennas are sufficiently spaced apart so that the fading is independent among them. Therefore, a successful connection in the absence of interference is achieved if the SNR of at least one antenna is above the detection threshold

$$H_{i,A} = 1 - (1 - H_1)^A. \quad (29)$$

By its turn, the capture probability is concerned with collisions from interfering signals and demands a more intricate mathematical development. Here, the strongest interfering signal seen by the a -th antenna is denoted by k_a^* and defined as

$$k_a^* = \arg \max_{k \in \Phi_{t,i}} \{\mathcal{P}_t |h_{a,k}|^2 g_k\}, \quad (30)$$

where $h_{a,k}$ is the channel fading of the k -th node seen by the a -th antenna. Thus, the probability that there is no collision in at least one of the antennas is

$$Q_{i,A} = \mathbb{P} \left[\max_{a=1, \dots, A} \text{SIR}_a^* < 4 \mid g_1 \right], \quad (31)$$

$$\text{SIR}_a^* = \frac{|h_{a,1}|^2 g_1}{|h_{a,k_a^*}|^2 g_{k_a^*}}, \quad (32)$$

where $h_{a,1}$ is the channel fading of the desired node seen by antenna a , and SIR_a^* is the signal to interference ratio in the a -th antenna considering only the highest interferer.

Note that the distribution of $X_{k_a^*} = |h_{a,k_a^*}|^2 g_{k_a^*}$ is correlated among antennas, as $g_{k_a^*}$ is the same for all antennas. Thus, it seems intractable to make analytic progress from (31). However, a lower bound on the capture probability can be obtained as

$$Q_{i,A} \geq \mathbb{P} \left[\max_{a=1, \dots, A} \text{SIR}_a < 4 \mid g_1 \right] = Q_{1,A}^{\text{lo}}, \quad (33)$$

where

$$\text{SIR}_a = \frac{|h_{a,1}|^2 g_1}{\sum_{k \in \Phi_{t,i}} |h_{a,k}|^2 g_k} = \frac{|h_{a,1}|^2 d_1^{-\eta}}{\mathcal{I}_a}, \quad (34)$$

with

$$\mathcal{I}_a = \sum_{k \in \Phi_{t,i}} |h_{a,k}|^2 d_k^{-\eta}. \quad (35)$$

Compared with (31), (33) considers the sum of all interfering signals instead of the stronger interfering signal only. Since $SIR_a < SIR_a^*$, (33) is a lower bound. As we shall see in Section 3.4, the bound can be very tight if concurrent transmissions from more than two devices are not frequent, which is expected in most LoRa scenarios since the duty cycle is typically very low (GUPTA et al., 2017).

To evolve on the mathematical analysis of (33), we consider the development presented by Haenggi (HAENGGI, 2012a). Let us define the events $E_a \triangleq \{SIR_a > 4\}$. We focus first on the probability of the joint occurrence of z of these events,

$$P_Z \triangleq \mathbb{P} \left[\bigcap_{a=1, \dots, z} E_a \right], \quad (36)$$

i.e., the probability that the SIR exceeds 6dB at z antennas simultaneously. Thus,

$$P_Z = \mathbb{P} \left[|h_{1,1}|^2 > 4d_1^\eta \mathcal{I}_1, \dots, |h_{z,1}|^2 > 4d_1^\eta \mathcal{I}_z \right]. \quad (37)$$

Since \mathcal{I}_a , $a \in \{1, \dots, z\}$, are correlated through the common randomness Φ (the point process of the nodes), and $|h_{a,1}|^2$ is exponentially distributed, we have that

$$\begin{aligned} P_Z &= \mathbb{E} \left[e^{-4d_1^\eta \mathcal{I}_1}, \dots, e^{-4d_1^\eta \mathcal{I}_z} \right] \\ &= \mathbb{E} \left[\prod_{a=1}^z e^{-4d_1^\eta \mathcal{I}_a} \right]. \end{aligned}$$

By replacing \mathcal{I}_a ,

$$P_Z = \mathbb{E}_{|h_{a,k}|^2, \Phi_{t,i}} \left[\prod_{a=1}^z \prod_{k \in \Phi_{t,i}} e^{-4d_1^\eta |h_{a,k}|^2 d_k^{-\eta}} \right].$$

Then, since $|h_{a,k}|^2 \sim \exp(1)$,

$$P_Z = \mathbb{E}_{\Phi_{t,i}} \left[\prod_{k \in \Phi_{t,i}} \left(\frac{1}{1 + 4d_1^\eta d_k^{-\eta}} \right)^z \right].$$

Solving the expectancy of the PPP $\Phi_{t,i}$,

$$P_Z = \exp \left\{ -2\pi\rho p \int_{l_{i-1}}^{l_i} d_k \left[1 - \left(\frac{1}{1 + 4d_1^\eta d_k^{-\eta}} \right)^z \right] dd_k \right\}.$$

Solving the integral yields

$$\begin{aligned} P_Z &= \exp \left\{ -\frac{\pi\rho p d_k^2}{2 + z\eta} \left[2 + z\eta - 2 \left(\frac{d_k^\eta}{4d_1^\eta} \right)^z \dots \right. \right. \\ &\quad \left. \left. {}_2F_1 \left(z, z + \frac{2}{\eta}; 1 + z + \frac{2}{\eta}; -\frac{d_k^\eta}{4d_1^\eta} \right) \right] \Big|_{d_k=l_{i-1}}^{d_k=l_i} \right\}, \quad (38) \end{aligned}$$

where ${}_2F_1(\cdot)$ is the hypergeometric function (OLVER et al., 2010).

Finally, a transmission is successful if the SIR in at least one of the A antennas is higher than the threshold, thus

$$Q_{1,A}^{lo} \triangleq \mathbb{P} \left(\bigcup_{a=1}^A E_a \right) = \sum_{a=1}^A (-1)^{a+1} \binom{A}{a} P_a, \quad (39)$$

where P_a comes from (38) with $z = a$.

3.4 NUMERICAL RESULTS

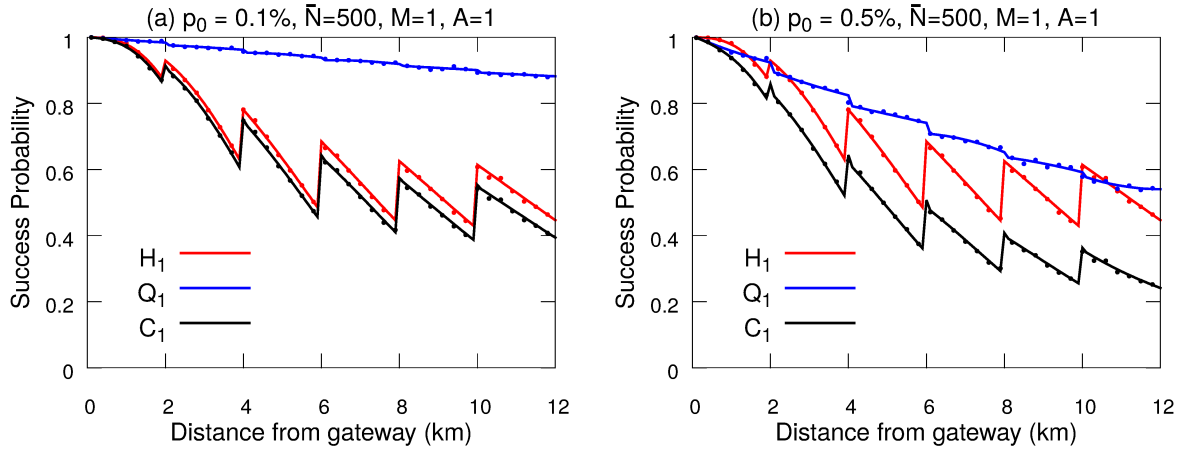
This section evaluates the proposed models using numerical simulations. In the figures, solid lines represent theoretical probabilities, while points of the same color represent the Monte Carlo simulation results. Each simulation point is the averaged result of 10^5 random deployment scenarios. Results are shown for $p = \{0.1, 0.5\}\%$, which is equivalent to $\{3.6, 18.1\}$ messages in an hour with SF₁₂, or $\{87.3, 436.7\}$ messages per hour with SF₇. These are worst-case considerations of the LoRa reality. In practice, typical LoRa applications are expected to operate with duty cycles below 0.1% and rarely above 0.5% (GUPTA et al., 2017). Moreover, following (GEORGIU; RAZA, 2017), all results presented in this chapter consider AWGN variance $\sigma_w^2 = -174 + F + 10 \log_{10} B$ dBm, where $F = 6$ dBm is the receiver noise figure, $B = 125$ kHz is the channel bandwidth, $\eta = 2.75$, $\lambda = c/f$ meters, and $f = 868$ MHz, which are typical configurations for sub-urban scenarios following European regulations.

3.4.1 Baseline Model – Without Diversity

Figure 3 shows the performance of the baseline model of Section 3.1, with varying duty cycle and an average number of nodes $\bar{N} = 500$, without any time or antenna diversity, *i.e.*, $M = 1$, $A = 1$. There is no need to vary both duty cycle and the average number of nodes in the analysis because the model is sensitive to the medium usage, *i.e.*, the product $p\bar{N}$, rather than on these parameters separately. The figure shows the connection probability H_1 , capture probability Q_1 , and coverage probability C_1 in separated curves. As expected, results for H_1 are not dependent on the duty cycle or the average number of nodes because H_1 models the connection probability, which depends only on the distance. It makes Q_1 primarily responsible for network quality degradation. That happens because Q_1 takes interference into account, which is substantially affected by increasing medium usage.

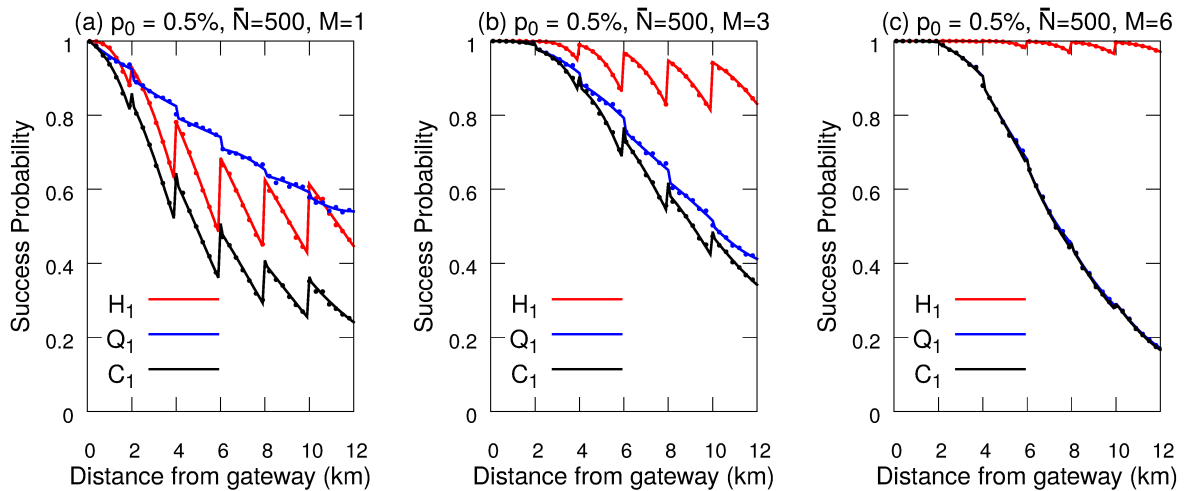
It is also possible to note that Q_1 decreases with SF, which is expected due to two factors. The first one is that ToA increases with SF (see Table 1). The second one is that, because outer rings have a larger area than inner rings, and nodes are distributed uniformly in the circular region around the gateway, more nodes use higher SF.

Figure 3 – Performance of LoRa uplink baseline model ($M = 1$ and $A = 1$), with average number of nodes $\bar{N} = 500$ and $p = \{0.1, 0.5\}\%$.



Source: the author.

Figure 4 – Impact of message replication in LoRa uplink, with average number of nodes $\bar{N} = 500$, duty cycle $p = 0.5\%$, a single antenna ($A = 1$), and a varying number of message copies M .



Source: the author.

3.4.2 Message Replication

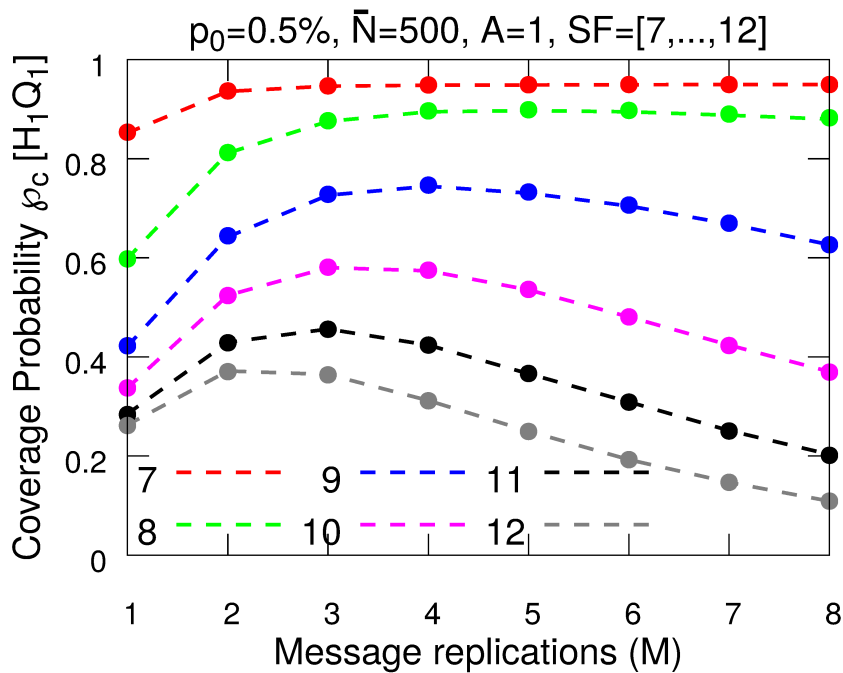
Figure 4 shows the impact of the message replication approach for $M = \{3, 6\}$ message copies using the same network configuration of the results presented in Figure 3(b), except for the value of M . As expected, message replication has a substantial positive impact on $H_{i,M}$ because M decreases this outage condition exponentially. For $Q_{i,M}$, however, the positive impact only exists as long as the message copies do not flood the network, reaching a point where the number of collisions is too high. Moreover, message replication performs better in lower SF, which happens because ToA

Table 2 – Optimum values of M and average coverage probability $\bar{C}_{1,i}$ for each SF and the whole network ($p = 0.5\%$ and $\bar{N} = 500$).

SF	M^*	$\bar{C}_{1,i}$	$\bar{C}_{1,i}$ with $M = 1$
7	8	94.9%	85.2%
8	5	89.7%	59.9%
9	4	74.4%	42.2%
10	3	58.0%	33.7%
11	3	45.6%	28.5%
12	2	37.2%	26.3%
All	2,3,4,5,8	$\bar{C}_1 = 59.7\%$	$\bar{C}_1 = 39.4\%$

Source: the author.

Figure 5 – Coverage probabilities of LoRa network with average number of nodes $\bar{N} = 500$ and duty cycle $p = 0.5\%$ for each SF.

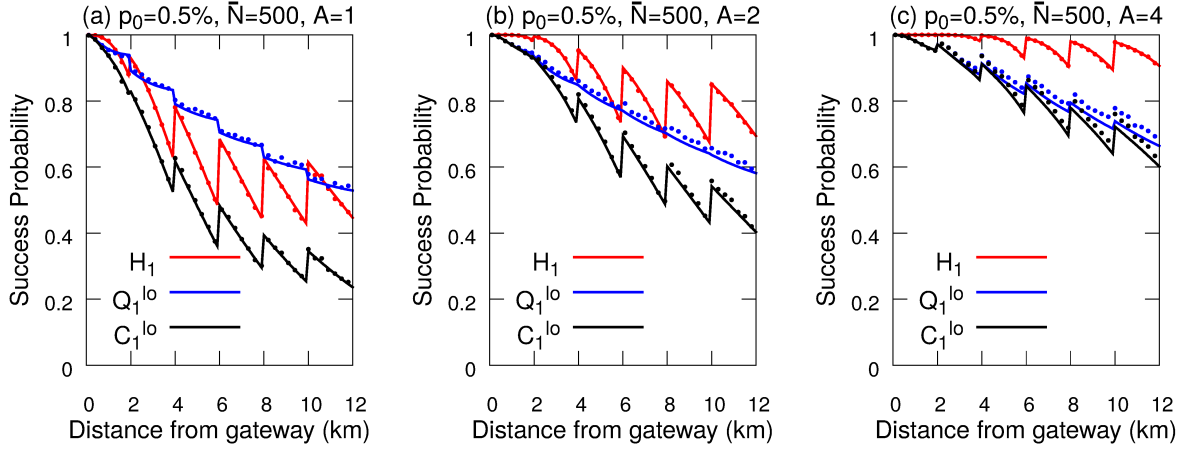


Source: the author.

nearly doubles for each SF increase, making it faster to flood the network with message replications when using higher SF.

Figure 5 shows the average coverage probability $\bar{C}_{1,i}$ of each SF, for a varying number of message copies M , considering the same network configuration of Figure 4. It is possible to observe that the optimum number of message replications is different for each SF. Table 2 summarizes, for each SF and the entire network, the optimum number of message copies (M^*) and the corresponding average coverage probability for the ring that is using that SF. The last line of the table shows the network's average

Figure 6 – Impact of multiple receive antennas at the LoRa gateway, considering an average number of nodes $\bar{N} = 500$, a duty cycle of $\rho = 0.5\%$, a single message copy ($M = 1$), and different numbers of receive antennas A .



Source: the author.

coverage probability if each node uses the M^* computed for its SF. To allow comparison, the last column of the table shows the coverage probability without message replication. Note that the optimum number of message copies is a decreasing function of the SF, which makes sense since message replications increase the network density.

3.4.3 Multiple Receive Antennas

Figure 6 shows the performance for $A = \{1, 2, 4\}$ receive antennas at the gateway, in a scenario with $\rho = 0.5\%$, $\bar{N} = 500$ and $M = 1$. It is evident the tightness of the lower bound given in (39). Unlike what happens with message replication, the packet delivery probability growth in LoRa networks with multiple receive antennas is a monotonic function of the number of antennas A . The more receive antennas a gateway has, the better. Figures 6(b) and 6(c) show that multiple receive antennas bring an average gain in C_1 probability of 50.2% and 96.9% for, respectively, $A = 2$ and $A = 4$. This gain results in the average coverage \bar{C}_1 going from 39.44% to 59.27% and 77.69%, respectively.

Table 3 presents the performance for the integration of both time and antenna diversity. It shows the average coverage probability \bar{C}_1 in the deployment area for the different duty cycles (ρ), average number of nodes (\bar{N}), and numbers of receive antennas (A). Results consider the optimum number of message copies (M^*) for each configuration. It is possible to conclude that low-density networks like those with $\rho = 0.1\%$ and $\bar{N} = 500$ achieve performance gains with message replication alone. Networks slightly denser like those with $\rho = 0.1\%$ and $\bar{N} = \{1000, 1500\}$ achieve reasonably high-performance gains by combining both techniques. Performance gains for dense networks, on the other hand, depend much more on antenna diversity to achieve larger

Table 3 – Optimum M^* for different configurations of network density and number of antennas.

		$\bar{N} = 500$		$\bar{N} = 1000$		$\bar{N} = 1500$	
p	A	M^*	\bar{C}_1	M^*	\bar{C}_1	M^*	\bar{C}_1
0.1%	1	8	99.7%	5	91.0%	4	79.1%
	2	4	100.0%	5	96.6%	4	89.2%
	4	3	100.0%	5	99.5%	3	95.8%
	8	2	100.0%	3	100.0%	4	99.4%
0.5%	1	3	59.2%	2	33.0%	2	20.5%
	2	3	73.3%	2	47.1%	1	33.3%
	4	2	85.6%	1	61.6%	1	49.1%
	8	2	94.0%	1	76.5%	1	64.2%

Source: the author.

benefits since message replications contribute to an excessive increase in collision probability. The denser cases shown in Table 3, $p = 0.5\%$, $\bar{N} = \{1000, 1500\}$, demonstrate that message replication may not be an option for similar cases. Regardless of the network density, the results show that the careful use of both techniques can achieve significant gains.

3.5 CLOSING

The main contributions in this chapter were the modeling of an optimal number of message copies for replication in LoRaWAN's uplink, the definition of closed formulas for the collision probability at a gateway with multiple antennas, and the performance analysis of a hybrid system, using both message replication and multiple antennas at the gateway. The next chapter complements these contributions by analyzing the effect that inter-SF and external interference have on LoRaWAN's uplink, and providing optimization algorithms that seek to adapt LoRaWAN networks to deal with these problems.

4 OPTIMUM LORAWAN CONFIGURATION UNDER WI-SUN INTERFERENCE

“The most important thing to do in your life is to not interfere with somebody else’s life.” Frank Vincent Zappa.

This chapter describes the contributions of this thesis project originally published in the *IEEE Access Journal* in 2019 (HOELLER et al., 2019). It focuses on the optimization of LoRaWAN networks under external interference from SUN, which has gained increased attention in recent years as key enablers of Smart Cities (CENTENARO et al., 2016). In such smart environments, the IoT will play a paramount role in connecting massive numbers of smart devices such as smart meters, smart light bulbs, and smart appliances. Besides the existence of several network technologies to connect such devices, e.g., LoRaWAN, SigFox, and Wi-SUN, the reliable and efficient connection of massive numbers of devices is still a challenge (BOCKELMANN et al., 2016).

Industry backs at least two initiatives: LORA ALLIANCE and WI-SUN ALLIANCE. LORA ALLIANCE – supported by Semtech, IBM, Cisco, Orange, among others – maintains the LoRaWAN specification (LORA ALLIANCE, 2020). WI-SUN ALLIANCE – supported by Cisco, Analog Devices, Toshiba, and others – maintains the Wi-SUN specification (WI-SUN ALLIANCE, 2020; CHANG; MASON, 2012). Wi-SUN is a FAN technology built upon the physical and link layers defined by the IEEE 802.15.4g standard. IEEE 802.15.4g operates in different ISM bands, including the same sub-GHz bands used by LoRaWAN, where it employs a Gaussian Frequency Shift Keying (GFSK) modulation over narrow-band channels. Wi-SUN also defines network- and application-level services and profiles for different utility applications (e.g., energy, gas, water).

While utility service providers modernize their systems to use smart meters, deployments can use different communication technologies in the same geographical region, thus raising the question of how inter-technology interference affects network scalability. Coordination among transmissions in different technologies is unfeasible at the network or lower layers, so it is essential to understand the impact of external interference through use cases, theoretical analysis, and design strategies (ZHANG et al., 2019). To achieve a realistic model, one should take into account that LPWAN devices in the ISM radio band are subject to interference generated by other networks sharing the same part of the spectrum. For instance, different authors report the analysis of the interaction of LoRa with other technologies considering IEEE 802.15.4g (ORFANIDIS et al., 2017), SigFox (KRUPKA et al., 2016; POORTER et al., 2017), and IEEE 802.11AH (POORTER et al., 2017). The results in those papers suggest that LoRa susceptibility to interference arriving from other technologies depends not only on the activity on those interfering networks but also on the configuration of the LoRa signal, mainly the spreading factor (SF). In this chapter, we consider LoRaWAN as our target technology and model its performance in the presence of IEEE 802.15.4g interference

sources in the sub-GHz ISM band (e.g., around 868 MHz in Europe and 915 MHz in the USA/Brazil). Please note that the model's restriction to IEEE 802.15.4g interference comes without loss of generality since one can extend it to other network technologies provided that appropriate isolation thresholds between the technologies are available.

In our work, we evolve from previous developments in (HOELLER et al., 2018) and (MAHMOOD et al., 2019) to approach the problem from an analytic perspective. We derive two optimization algorithms that explore the configuration space of LoRaWAN in the presence of internal and external interference. The algorithms are network planning tools for massive IoT applications, guiding the trading-off between reliability, the number of users, and coverage area/range. We validate our analytic findings with simulations configured according to experimental results on the interplay of these networks published in (ORFANIDIS et al., 2017). We do not consider latency here because our methods do not impact latency. A good third-party work that analyzes the latency of Class A LoRaWAN is (SØRENSEN et al., 2017).

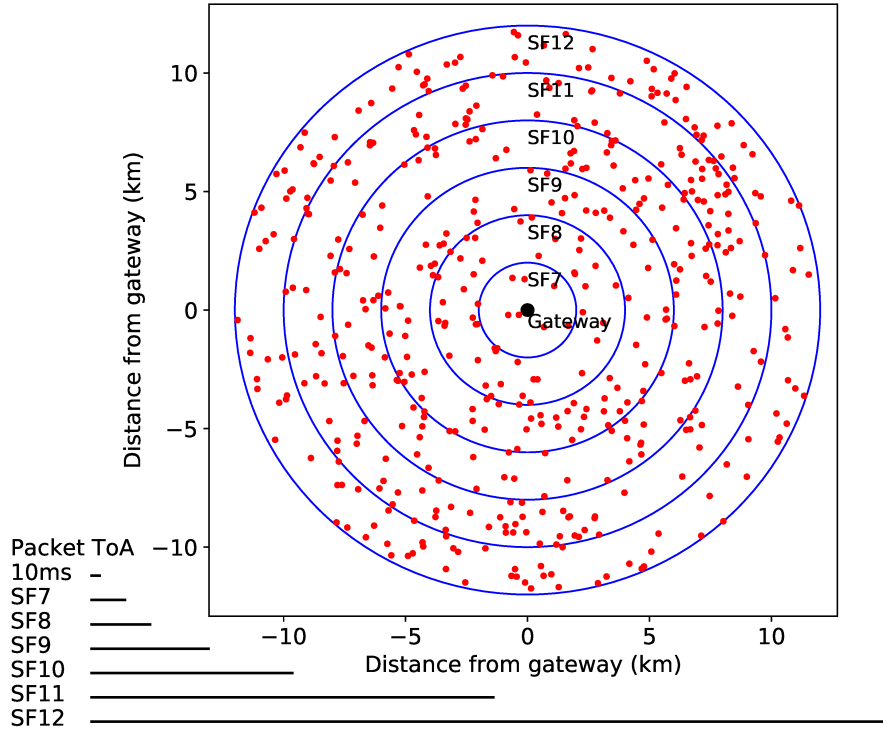
The main contributions in this chapter can be summarized as:

- A closed-form expression for the inter-SF LoRaWAN interference model of (MAHMOOD et al., 2019);
- The extension of the analytic models of (HOELLER et al., 2018) and (MAHMOOD et al., 2019) to consider external interference;
- The performance analysis of LoRaWAN, considering the experimental results on inter-technology interference from (ORFANIDIS et al., 2017);
- Two algorithms to optimize LoRaWAN configuration, either in terms of network load or communication range, under reliability constraints.

4.1 SYSTEM MODEL

Following the developments in (HOELLER et al., 2018) and (MAHMOOD et al., 2019), we use a set of PPP (HAENGGI, 2012b). Our model considers nodes deployed uniformly in a circular region around a gateway. Figure 7 illustrates a *possible* setup where SF increases according to the distance from the gateway. The figure, as in previous related work, uses fixed-width SF rings which are sub-optimal, an issue that is addressed by us in Section 4.2. The vector $L = [l_0, \dots, l_6]$, $l_0 = 0$, defines the limits of each SF ring. Note that $R = l_6$ is the maximum network communication range, *i.e.*, the coverage radius. LoRaWAN devices transmit in the uplink at random using the ALOHA protocol and transmit once in a given period T . Considering that all nodes run the same application, the network usage is different for each SF because of different data rates (see ToA in Table 1). Figure 7 also shows the ToA difference graphically. Hence, we model the transmission probability of LoRaWAN devices as a vector $p =$

Figure 7 – $\bar{N} = 500$ nodes uniformly distributed in a circular area of radius $R = 12000$ m around the gateway and with increasing SF every 2000m. The ToA, as in Table 1, is illustrated in the lower-left corner.



Source: the author.

$[p_1, \dots, p_6], p_i \in (0, 1] \forall i \in \{1, \dots, 6\}$, and $p_i = \frac{t_i}{T}$, where t_i is the ToA for SF of ring i . Note that, for the sake of simplicity, we define the set $S = \{1, \dots, 6\}$ to denote the SF rings and that each ring uses a respective SF in $\{7, \dots, 12\}$.

Each LoRaWAN SF ring constitutes a separated PPP, denoted $\Phi_i, i \in S$, making it possible to attribute different densities to each SF. Φ_i has density $\alpha_i = p_i \rho_i$ in its area $V_i = \pi(l_i^2 - l_{i-1}^2)$, where l_{i-1} and l_i are, respectively, the inner and outer radii of SF ring i (from L), and ρ_i is the spatial density of nodes in V_i . The average number of nodes in Φ_i is $\bar{N}_i = \rho_i V_i$. The average number of nodes in the LoRaWAN network is $\bar{N} = \sum_{i \in S} \rho_i V_i$. For instance, take the ring $i = 2$ in Figure 7, defined by two circles of radii $l_1 = 2$ km and $l_2 = 4$ km. Nodes in this ring use SF_8 . The ring area is $V_2 = \pi(l_2^2 - l_1^2) = 37.7$ km². If there are, on average, $\bar{N}_2 = V_2 \rho_2 = 100$ nodes in this ring, then its spatial density is $\rho_2 = \frac{\bar{N}_2}{V_2} = 2.65$ nodes/km². Finally, if nodes transmit probability is 1% ($p_2 = 0.01$), the intensity of Φ_2 is $\alpha_2 = p_2 \rho_2 = 0.0265$.

In addition to LoRaWAN, we consider an external IEEE 802.15.4g network operating in the same ISM bands and geographic region. Users of that network are spread across the LoRaWAN area. IEEE 802.15.4g transceivers in ISM sub-GHz bands employ bandwidth and transmit power configurations similar to LoRaWAN. So, we model the IEEE 802.15.4g network as an additional PPP where nodes transmit with probability $p_Z \in (0, 1]$ in area $V_Z = \pi R_Z^2$, where $R_Z \geq R$. The PPP Φ_Z has density $\alpha_Z = p_Z \rho_Z$,

where ρ_z is the spatial density of nodes in V_z . The average number of nodes in Φ_z is $\bar{N}_z = \rho_z V_z$.

In our analysis, d_k is the Euclidean distance between the k -th node and the gateway, and d_1 denotes the distance of the node of interest. All nodes use the same transmit power \mathcal{P}_t to send signal s_k , while both path loss and Rayleigh fading affect the received signals of LoRaWAN and IEEE 802.15.4g. Path loss follows $g_k = \left(\frac{\lambda}{4\pi d_k}\right)^\eta$, with wavelength λ , path loss exponent $\eta \geq 2$, while k represents a device in either network. Finally, h_k denotes the Rayleigh fading. Therefore, a LoRaWAN signal r_1 received at the gateway is the sum of the attenuated transmitted signal s_1 , interference, and noise,

$$r_1 = s_1 h_1 \sqrt{\mathcal{P}_1 g_1} + \mathcal{I}_L + \mathcal{I}_Z + w, \quad (40)$$

where

$$\mathcal{I}_L = \sum_{i \in \mathcal{S}} \sum_{k \in \Phi_{t,i}} s_k h_k \sqrt{\mathcal{P}_k g_k} \quad (41)$$

accounts for intra-network interference, considering both co-SF and inter-SF interference by summing all other received signals from all SFs, and

$$\mathcal{I}_Z = \sum_{k \in \Phi_{t,z}} s_k h_k \sqrt{\mathcal{P}_k g_k} \quad (42)$$

models external interference arising from all active nodes in the IEEE 802.15.4g network. Finally, w is the AWGN with zero mean and variance σ_w^2 . The remainder of this section uses this model to derive a reliability model of LoRaWAN.

4.1.1 Coverage Probability

The *coverage probability*, as presented in Section 2.2.3, is the probability that the selected node is in coverage (not in outage), *i.e.*, it can successfully communicate in the presence of noise, internal interference, and external interference. The coverage probability of the desired node located d_1 meters from the gateway is thus

$$C_1(d_1) \approx H_1(d_1) Q_1(d_1) Z_1(d_1), \quad (43)$$

where H_1 , Q_1 , and Z_1 are described in the following sections and denote the success probability with regards to, respectively, noise, internal interference, and external interference.

4.1.2 Outage Condition 1: Disconnection

Following (HOELLER et al., 2018), we consider the disconnection probability, which depends on the communication distance. A node is *not* connected to the gateway

if the SNR of the received signal is below the threshold that allows successful detection in the absence of interference. Receiver sensitivity is different for each SF, what results in different SNR reception thresholds defined in

$$\Psi_{[dB]} = \begin{matrix} SF_7 & SF_8 & SF_9 & SF_{10} & SF_{11} & SF_{12} \\ [-6 & -9 & -12 & -15 & -17.5 & -20], \end{matrix}$$

where Ψ is the SNR threshold vector, and ψ_i denotes the i -th element of Ψ , *i.e.*, the SNR threshold for SF ring i . Then, we model the *connection probability* as

$$H_1(d_1) = \mathbb{P}[\text{SNR} \geq \psi_i | d_1]. \quad (44)$$

Since we assume Rayleigh fading, the instantaneous SNR is exponentially distributed (GOLDSMITH, 2005), and therefore

$$\begin{aligned} H_1(d_1) &= \mathbb{P} \left[\frac{\mathcal{P}_t |h_1|^2 g_1}{\sigma_w^2} \geq \psi_i \right] \\ &= \exp \left(-\frac{\sigma_w^2 \psi_i}{\mathcal{P}_t g_1} \right). \end{aligned} \quad (45)$$

4.1.3 Outage Condition 2: Intra-Network Interference

Intra-network interference arises from the activity of other devices in the same network. We follow (MAHMOOD et al., 2019) to model both co-SF and inter-SF interference. To recover a packet, the SIR at the gateway must be above a given threshold. The transceiver manufacturer informs that SFs are orthogonal and that the co-SF SIR threshold is +6dB (SX1276/77/78/79. . . , 2019). Goursaud *et al.* (GOURSAUD; GORCE, 2015) propose theoretical SIR thresholds that match Semtech co-SF value but show that different SFs are not entirely orthogonal. However, Croce *et al.* (CROCE et al., 2018) showed, experimentally, that the SIR thresholds for Semtech SX1272 LoRa transceiver are lower with regards to co-SF interference ($\approx +1$ dB) but significantly higher with respect to (w.r.t.) inter-SF interference. In this paper, we assume the experimental SIR thresholds of (CROCE et al., 2018)

$$\Delta_{[dB]} = \begin{matrix} & SF_7 & SF_8 & SF_9 & SF_{10} & SF_{11} & SF_{12} \\ SF_7 & \left[\begin{array}{cccccc} +1 & -8 & -9 & -9 & -9 & -9 \end{array} \right. \\ SF_8 & \left[\begin{array}{cccccc} -11 & +1 & -11 & -12 & -13 & -13 \end{array} \right. \\ SF_9 & \left[\begin{array}{cccccc} -15 & -13 & +1 & -13 & -14 & -15 \end{array} \right. \\ SF_{10} & \left[\begin{array}{cccccc} -19 & -18 & -17 & +1 & -17 & -18 \end{array} \right. \\ SF_{11} & \left[\begin{array}{cccccc} -22 & -22 & -21 & -20 & +1 & -20 \end{array} \right. \\ SF_{12} & \left[\begin{array}{cccccc} -25 & -25 & -25 & -24 & -23 & +1 \end{array} \right. \end{matrix} ,$$

where Δ is the SIR threshold matrix, and $\delta_{i,j}$ denotes the element of Δ at the i -th line and j -th column, *i.e.*, the SIR threshold for the desired signal using SF $_i$ and interference

using SF_j . Note that $i = j$ relates to the co-SF SIR while $i \neq j$ relates to inter-SF SIR. If one takes the SF_7 column as an example, it shows how SF_7 interference affects the LoRa signals. Desired signals using higher SF are more robust to inter-SF interference, allowing for the decoding of LoRa packets even if the interference power is much higher than the signal (e.g., 25dB higher if the signal uses SF_{12}).

Following this rationale, we first use the formulations in (MAHMOOD et al., 2019) to analyze the success probability considering the interference from only one different SF_j . Let

$$SIR_j = \frac{|h_1|^2 g_1 \mathcal{P}_t}{\mathcal{I}_j}, \quad (46)$$

where the interference received from nodes using SF_j is

$$\mathcal{I}_j = \sum_{k \in \Phi_j} |h_k|^2 g_k \mathcal{P}_t. \quad (47)$$

Since the desired node at d_1 uses SF_j , the success probability is

$$\begin{aligned} P_{SIR_j}(d_1, j) &= \mathbb{P}[SIR_j \geq \delta_{i,j}] \\ &= \mathbb{E}_{\mathcal{I}_j, |h_1|^2} \left[\mathbb{P} \left[|h_1|^2 \geq \frac{\mathcal{I}_j \delta_{i,j}}{g_1 \mathcal{P}_t} \right] \right]. \end{aligned}$$

Since $|h_1|^2 \sim \exp(1)$,

$$P_{SIR_j}(d_1, j) = \mathbb{E}_{\mathcal{I}_j} \left[\exp \left(-\frac{\mathcal{I}_j \delta_{i,j}}{g_1 \mathcal{P}_t} \right) \right]. \quad (48)$$

Note that (48) has the form of the Laplace Transform (LT) w.r.t. \mathcal{I}_j , where $L_{\mathcal{I}_j}(s) = \mathbb{E}_{\mathcal{I}_j}[\exp(-s\mathcal{I}_j)]$, $s = \frac{\delta_{i,j}}{g_1 \mathcal{P}_t}$. Thus, using (47) and applying the property of the sum of exponents,

$$P_{SIR_j}(d_1, j) = \mathbb{E}_{\Phi_{t,j}, |h_k|^2} \left[\prod_{k \in \Phi_{t,j}} \exp \left(-s |h_k|^2 g_k \mathcal{P}_t \right) \right].$$

Solving the expectation over $|h_k|^2 \sim \exp(1)$ yields

$$P_{SIR_j}(d_1, j) = \mathbb{E}_{\Phi_{t,j}} \left[\prod_{k \in \Phi_{t,j}} \frac{1}{1 + s g_k \mathcal{P}_t} \right].$$

We solve the expectation over the PPP $\Phi_{t,j}$ using the probability generating functional of the product over PPPs where $\mathbb{E}[\prod_{x \in \Phi_{t,j}} f(x)] = \exp[-\alpha_j \int_{\mathbb{R}^2} (1 - f(x)) dx]$, with α_j as the density of $\Phi_{t,j}$, converting d_k to polar coordinates, and replacing s , obtaining

$$P_{SIR_j}(d_1, j) = \exp \left(-2\pi\alpha_j \int_{l_{j-1}}^{l_j} \frac{\delta_{i,j} d_1^\eta}{x^\eta + \delta_{i,j} d_1^\eta} x dx \right). \quad (49)$$

As a contribution over (MAHMOOD et al., 2019), we provide in Appendix A a closed-form solution for the integral in (49), which we represent as function $f(\cdot)$. The solution is

$$f(d_1, \delta_{i,j}, l_{j-1}, l_j) = \frac{l_j^2}{2} {}_2F_1 \left(1, \frac{2}{\eta}; 1 + \frac{2}{\eta}; -\frac{l_j^\eta}{d_1^\eta \delta_{i,j}} \right) - \frac{l_{j-1}^2}{2} {}_2F_1 \left(1, \frac{2}{\eta}; 1 + \frac{2}{\eta}; -\frac{l_{j-1}^\eta}{d_1^\eta \delta_{i,j}} \right), \quad (50)$$

and therefore,

$$P_{SIR_j}(d_1, j) = \exp \left[-2\pi\alpha_j f(d_1, \delta_{i,j}, l_{j-1}, l_j) \right]. \quad (51)$$

Now we consider interference from all SFs when

$$SIR = \frac{|h_1|^2 g_1 \mathcal{P}_t}{\sum_{j \in \mathcal{S}} \mathcal{I}_j}. \quad (52)$$

Following (MAHMOOD et al., 2019), we consider that an outage takes place if the SIR for at least one interfering SF exceeds the threshold in Δ . Conversely, the probability that a collision does not occur is

$$Q_1(d_1) = \prod_{j \in \mathcal{S}} P_{SIR_j}(d_1, j).$$

Since P_{SIR_j} , shown in (51), is an exponential function, we compute the above product by summing the exponents and reorganizing, obtaining

$$Q_1(d_1) = \exp \left(-2\pi \sum_{j \in \mathcal{S}} \alpha_j f(d_1, \delta_{i,j}, l_{j-1}, l_j) \right). \quad (53)$$

4.1.4 Outage Condition 3: External Interference

Orfanidis *et al.* (ORFANIDIS et al., 2017) report the selectivity of LoRa receivers in the presence of IEEE 802.15.4g signals. We use Orfanidis *et al.* experimentally obtained isolation thresholds to analyze the SIR in the presence of external interference generated by an IEEE 802.15.4g network. Here, we model the IEEE 802.15.4g network as PPP Φ_Z and consider (ORFANIDIS et al., 2017)

$$\Theta_{[dB]} = \begin{matrix} SF_7 & SF_8 & SF_9 & SF_{10} & SF_{11} & SF_{12} \\ [-6 & -9 & -12.5 & -16 & -16 & -16], \end{matrix}$$

where Θ denotes the LoRa vs. IEEE 802.15.4g SIR threshold vector, and θ_i denotes the i -th element of Θ , *i.e.*, the SIR threshold for the desired signal in SF ring i and interference from the IEEE 802.15.4g network.

The analysis of the LoRa capture probability in the presence of IEEE 802.15.4g interference is similar to the case for one SF (P_{SIR_j}), but taking the Θ vector and the IEEE 802.15.4g network parameters into account. For

$$SIR_z = \frac{|h_1|^2 g_1 \mathcal{P}_t}{\sum_{k \in \Phi_{t,z}} |h_k|^2 g_k \mathcal{P}_t}, \quad (54)$$

the *capture probability* w.r.t. external interference is

$$Z_1(d_1) = P_{SIR_z}(d_1) = \exp(-2\pi\alpha_z f(d_1, \theta_i, 0, R_z)). \quad (55)$$

Note that the model for external interference supports any other communication technology given that adequate SIR thresholds of Θ are provided.

4.2 OPTIMUM LORAWAN CONFIGURATION

The expressions in Section 4.1 determine the expected reliability of a single node located at a given distance from the gateway. *However, what if one wants to plan the network deployment?* In this section, we consider the use of the previous model to this end. We first consider the inversion of the expressions in the model to obtain network configurations for a targeted minimum average reliability. Afterward, we propose two algorithms that derive optimum network configurations supporting the desired minimum reliability requirement.

4.2.1 Guaranteeing the Reliability Target

To start our search for optimal LoRaWAN configurations we invert the previously described outage expressions defined in (45) and (53), so the network parameters can be extracted from them to achieve a minimum desired reliability level. Note that (55) does not depend on the LoRaWAN configuration. It is, however, taken into account in the optimization algorithm proposed in Sections 4.2.2 and 4.2.3 to consider external interference. One can assume that, in our network model, the nodes presenting the worst average reliability in each SF ring are those on the outer ring limit. It happens because the signals emitted by those nodes suffer greater path-loss and are, therefore, more susceptible to interference.

As a first step, we find the maximum distance that ensures the required minimum average reliability level w.r.t. the connection probability H_1 . We denote this threshold by \mathcal{T}_{H_1} . We rewrite (45) to perform operations over the SNR threshold ψ_i in Ψ and the outer SF ring limit l_j ,

$$\mathcal{T}_{H_1} = \exp\left(-\frac{\sigma_w^2 \psi_i}{\mathcal{P}_t g_{l_j}}\right), \quad (56)$$

and then it is straightforward to obtain

$$l_i = \frac{\lambda}{4\pi} \left[-\frac{\mathcal{P}_t \ln(\mathcal{T}_{H_1})}{\sigma_w^2 \psi_i} \right]^{\frac{1}{n}}. \quad (57)$$

Note that the radius of the overall coverage area is $R = l_6$.

Since (57) defines the network geometry, it is now possible to obtain the outage due to external interference observed by the nodes at each ring edge from $Z_1(l_i)$. After that, we compute the maximum densities of the PPPs in Q_1 that satisfy the given final reliability target \mathcal{T} , the previously assumed connection reliability target \mathcal{T}_{H_1} , and the external interference of each SF i . Thus, following (43), making $C_1(l_i) = \mathcal{T}$ and $H_1(l_i) = \mathcal{T}_{H_1}$, we have for each SF ring i that $\mathcal{T} = \mathcal{T}_{H_1} Q_1(l_i) Z_1(l_i)$, and thus

$$\frac{\mathcal{T}}{\mathcal{T}_{H_1} Z_1(l_i)} = \exp \left(-2\pi \sum_{j \in S} \alpha_j f(l_i, \delta_{i,j}, l_{j-1}, l_j) \right). \quad (58)$$

In (58), the function $f(\cdot)$ is independent of α_j if the SF limits are pre-defined. Then, let $y_{i,j} = f(l_i, \delta_{i,j}, l_{j-1}, l_j)$ and $b_i = -\frac{1}{2\pi} \ln \left(\frac{\mathcal{T}}{\mathcal{T}_{H_1} Z_1(l_i)} \right)$, yielding, for each SF ring i ,

$$y_{i,1} \alpha_1 + y_{i,2} \alpha_2 + y_{i,3} \alpha_3 + y_{i,4} \alpha_4 + y_{i,5} \alpha_5 + y_{i,6} \alpha_6 = b_i. \quad (59)$$

If we name the vectors $A = [\alpha_1, \dots, \alpha_6]$, $B = [b_1, \dots, b_6]$, and matrix $Y = [y_{i,j}], \forall i, j \in S$, from (59), we derive a system of linear equations $Y \times A = B$ and solve it for the PPPs densities A by making

$$A = Y^{-1} \times B. \quad (60)$$

Note that Y is a $|S| \times |S|$ square matrix, both A and B are row vectors of length $|S|$, and all values $y_{i,j}$ in Y are positive real numbers. To be invertible (Y^{-1}), Y must have a non-zero determinant. Considering the diagonal method to compute the determinant of Y , we observe that, due to Δ , the values at $i = j$ are significantly higher than when $i \neq j$, thus making the positive diagonal greater than the negative diagonal, yielding a determinant that is virtually never zero.

4.2.2 Maximization of Communication Range

The expressions presented above allow us to obtain twelve network parameters: six communication range limits $L = [l_1, \dots, l_6]$ from (57), and six PPP densities $A = [\alpha_1, \dots, \alpha_6]$ from (60). Note that (60) depends on (57) because of L . Combining both equations generates an incomplete linear system of six equations and twelve variables. In order to search for optimized feasible network configurations, we propose an algorithm that uses (57) and (60) in an iterative method, trying to extend the outer SF

ring limits as much as possible, while preserving the targeted final reliability level \mathcal{T} and ensuring service to a minimum quantity of nodes (N_{min}). The algorithm extends the outer SF ring limits by reducing \mathcal{T}_{H_1} . Similarly, increasing \mathcal{T}_{H_1} shortens these limits. The algorithm iteratively guesses values for \mathcal{T}_{H_1} and then, after obtaining L through (57), analyzes the maximum possible densities A . As \mathcal{T}_{H_1} gets closer to \mathcal{T} , the capture probability Q_1 increases and, with fixed L and Z_1 , higher Q_1 is possible only with lower densities. It may lead to configurations breaking the N_{min} restriction. Conversely, if \mathcal{T}_{H_1} is too close to 1, the outer limits of the SF rings will be shorter, leading to small coverage areas that are useless in practice. However, the proposed algorithm identifies feasible ranges for the network parameters, thus dealing with this parameter trade-off.

Algorithm 1 employs a bisection technique (BURDEN et al., 2016) to explore the network design space (*i.e.*, possible values of \mathcal{T}_{H_1}), seeking to maximize the width of each SF ring and, as a consequence, the network communication range (disk radius), while preserving the targeted minimum reliability \mathcal{T} and ensuring service to, at least, a given number of nodes (N_{min}). The bisection technique fits well to our problem because it accelerates convergence by reducing the design space in half in each iteration, and it is guaranteed to converge if the problem is feasible. The inputs of the algorithm are the targeted reliability \mathcal{T} , the duty-cycle vector p , N_{min} , and the density of IEEE 802.15.4g interfering nodes α_z . The algorithm outputs a *result* variable stating if the algorithm converged (1) or not (-1), the achieved number of nodes N , and the vectors L and A containing, respectively, the rings limits and densities ensuring the target reliability.

After initializing the variables (lines 1-4), the optimization loop starts and runs until the algorithm converges (line 26) or diverges (line 23). The optimization procedure “guesses” values for \mathcal{T}_{H_1} , trying to reduce it to enlarge the width of each SF ring, thus increasing the coverage area. Note that since C_1 depends on H_1 from (43), \mathcal{T}_{H_1} must be greater than \mathcal{T} ; otherwise, both Q_1 and Z_1 would have to be 1, which is impossible in practice. Thus, Algorithm 1 sets the initial search region for \mathcal{T}_{H_1} to $(\mathcal{T}, 1)$. The guessed value for \mathcal{T}_{H_1} in each iteration is at the center of this region, as expressed in line 6. At each iteration, if the selected \mathcal{T}_{H_1} generates a configuration where the number of nodes is above N_{min} , it is assumed that Q_1 can be enhanced by decreasing N , which allows for further decreasing \mathcal{T}_{H_1} in the next iteration. Conversely, if $N < N_{min}$, \mathcal{T}_{H_1} is increased so that Q_1 can be lower, allowing for more nodes in the network. This “binding” part of the algorithm is in lines 30-34.

Provided the bisection technique guesses \mathcal{T}_{H_1} in line 6, the range limits for all SF are computed using (57) in line 7. In the following, the algorithm uses the newly computed vector L to obtain vector B and matrix Y (lines 11-16), allowing for the computation of the PPPs densities in A (line 17), using (60). Following that, the number of nodes fitting the generated configuration is computed by first obtaining the area of each SF ring in lines 18-19 as $V_i = \pi(l_i^2 - l_{i-1}^2)$. The algorithm converges and

Algorithm 1 Maximization of SF rings widths given the target reliability (\mathcal{T}) and the minimum number of nodes (N_{min}).

Input: $\mathcal{T}, \rho, N_{min}, \alpha_z$

Output: result, A, L, N

```

1:  $\mathcal{T}_{H_1, max} \leftarrow 1$ 
2:  $\mathcal{T}_{H_1, min} \leftarrow \mathcal{T}$ 
3:  $R \leftarrow 0, N \leftarrow 0$ 
4: result  $\leftarrow 0$ 
5: while result = 0 do
6:    $\mathcal{T}_{H_1} \leftarrow (\mathcal{T}_{H_1, max} + \mathcal{T}_{H_1, min})/2$ 
7:    $L \leftarrow \frac{\lambda}{4\pi} \left[ -\frac{\mathcal{P}_t \ln(\mathcal{T}_{H_1})}{\sigma_w^2 \Psi} \right]^{\frac{1}{\eta}}$  {Equation (57)}
8:    $R_{last} \leftarrow R$ 
9:    $R \leftarrow L_{end}$ 
10:   $R_z \leftarrow R$ 
11:  for  $i = [1, \dots, 6]$  do
12:    for  $j = [1, \dots, 6]$  do
13:       $Y[i, j] \leftarrow f(l_j, \delta_{i,j}, l_j, l_{j-1})$ 
14:    end for
15:     $B[i] \leftarrow -\frac{1}{2\pi} \ln \frac{\mathcal{T}}{Z_1(l_i) \mathcal{T}_{H_1}}$ 
16:  end for
17:   $A \leftarrow Y^{-1} \times B$  {Equation (60)}
18:   $V \leftarrow \text{ComputeRingAreas}(L)$ 
19:   $N \leftarrow (A\rho) \times V'$ 
20:  if  $\text{abs}(R - R_{last}) < \chi$  and  $A_j \geq 0, \forall A_j$  then
21:    if  $N < N_{min}$  then
22:      if  $\mathcal{T}_{H_1, max} - \mathcal{T}_{H_1, min} < \epsilon$  then
23:        result  $\leftarrow -1$ 
24:      end if
25:    else
26:      result  $\leftarrow 1$ 
27:    end if
28:  end if
29:  if result = 0 then
30:    if  $A_j \geq 0, \forall A_j$  and  $N \geq N_{min}$  then
31:       $\mathcal{T}_{H_1, max} = \mathcal{T}_{H_1}$ 
32:    else
33:       $\mathcal{T}_{H_1, min} = \mathcal{T}_{H_1}$ 
34:    end if
35:  end if
36: end while
37: return result,  $A, L, N$ 

```

stops when the difference in the radius R of the overall coverage area between two consecutive iterations is less than χ (line 20) and $N > N_{min}$ (line 21), where χ defines the precision of R . If the variation of R , *i.e.*, $\text{abs}(R - R_{last})$, is too small and the algorithm did not achieve N_{min} yet, the algorithm keeps trying to converge until the variation in the guessed \mathcal{T}_{H_1} is below a threshold ϵ (line 22), in which case the algorithm stops and announces a divergence. After evaluating the proposed algorithm for a set of test scenarios, we concluded that good values for the stopping thresholds are $\chi = 1\text{m}$ and $\epsilon = 10^{-9}$.

Algorithm 1 always converges if there are feasible solutions to the problem. If the requirements of minimum network density (N_{min} and ρ), targeted reliability (\mathcal{T}), or both, are too high, however, the algorithm may take too long to converge. Hence, we stop the algorithm when the changes in \mathcal{T}_{H_1} get too small (line 22), thus guaranteeing that the algorithm will not run forever since $\mathcal{T}_{H_1,max} - \mathcal{T}_{H_1,min}$ decreases every iteration. It is important to note, however, that achieving higher network density is always possible by reducing the reliability requirement \mathcal{T} . Moreover, highly demanding scenarios without feasible solutions or with lengthy convergence are not typical in LoRaWAN, since the technology has been conceived to support massive rather than critical IoT applications.

The algorithm has linear complexity, *i.e.*, $\mathcal{O}(n)$. Analysis of convergence time of this method depends on the precision, which we define in Algorithm 1 as $\chi = 1\text{m}$. Therefore, the literature defines the maximum number of iterations as $n = \log_2 \left(\frac{\chi_0}{\chi} \right)$, where χ_0 is the initial error (BURDEN et al., 2016). In Algorithm 1, $\chi_0 = |R_1 - R_0|$, with $R_0 = 0$ (Algorithm 1, line 3) and R_1 computed in the first iteration (line 9) using (18) with $\mathcal{T}_{H_1} = \frac{1+\mathcal{T}}{2}$ (line 6). Note that although Algorithm 1 involves the solution of a system of linear equations with matrix inversion (line 17) and matrix multiplications (line 19), these are computed quite efficiently since it handles low-dimension matrices – the largest matrix is \mathbf{Y} , which is 6-by-6.

4.2.3 Maximization of Number of Nodes

Now we consider the case of maximizing the total number of nodes given restrictions of minimum coverage radius (R_{min}) and average reliability (\mathcal{T}). We use a more straightforward approach than in Algorithm 1. The problem of maximizing the number of nodes is equivalent to the problem of minimizing Q_1 . Thus it is straightforward to conclude, from (43), that we should maximize H_1 because higher H_1 allows for lower Q_1 . Since we assume that the worst cases are at the edge of the SFs and we have a restriction on the coverage radius, the maximum possible H_1 is that yielding $l_6 = R_{min}$. Thus, from (45), we conclude that $\mathcal{T}_{H_1} = H_1(R_{min})$. Assuming the same \mathcal{T}_{H_1} for all SFs, we use (57) to compute L and obtain the geometry of the network.

Once we obtain L , we use (60) to get the maximum allowable densities ensuring \mathcal{T} , as shown in Algorithm 2. Line 1 uses (45) to compute the maximum \mathcal{T}_{H_1} satisfying

R_{min} . Line 2 uses the computed \mathcal{T}_{H_1} to obtain the geometry of the network L . The loop in lines 5-10 computes matrix Y and vector B , so the maximum device density vector A can be computed in line 11. Finally, after computing the areas of the rings and storing them in vector V (line 12), we obtain the maximum number of nodes in line 13.

Algorithm 2 Maximization of the number of nodes given the target reliability (\mathcal{T}) and the minimum coverage radius (R_{min}).

Input: $\mathcal{T}, \rho, R_{min}, \alpha_Z$

Output: result, A, L, N_{max}

```

1:  $\mathcal{T}_{H_1} \leftarrow \exp\left(-\frac{\sigma_w^2 \psi_6}{\mathcal{P}_t g_{R_{min}}}\right)$ 
2:  $L \leftarrow \frac{\lambda}{4\pi} \left[-\frac{\mathcal{P}_t \ln(\mathcal{T}_{H_1})}{\sigma_w^2 \Psi}\right]^{\frac{1}{\eta}}$  {Equation (1)}
3:  $R \leftarrow L_{end}$ 
4:  $R_Z \leftarrow R$ 
5: for  $i = [1, \dots, 6]$  do
6:   for  $j = [1, \dots, 6]$  do
7:      $Y[i, j] \leftarrow f(l_i, \delta_{i,j}, l_j, l_{j-1})$ 
8:   end for
9:    $B[i] \leftarrow -\frac{1}{2\pi} \ln \frac{\mathcal{T}}{Z_1(l_i) \mathcal{T}_{H_1}}$ 
10: end for
11:  $A \leftarrow Y^{-1} \times B$  {Equation (2)}
12:  $V \leftarrow \text{ComputeRingAreas}(L)$ 
13:  $N_{max} \leftarrow (A\rho) \times V'$ 
14: if  $A_j \geq 0, \forall A_j$  then
15:   result  $\leftarrow 1$ 
16: else
17:   result  $\leftarrow -1$ 
18: end if
19: return result,  $A, L, N_{max}$ 

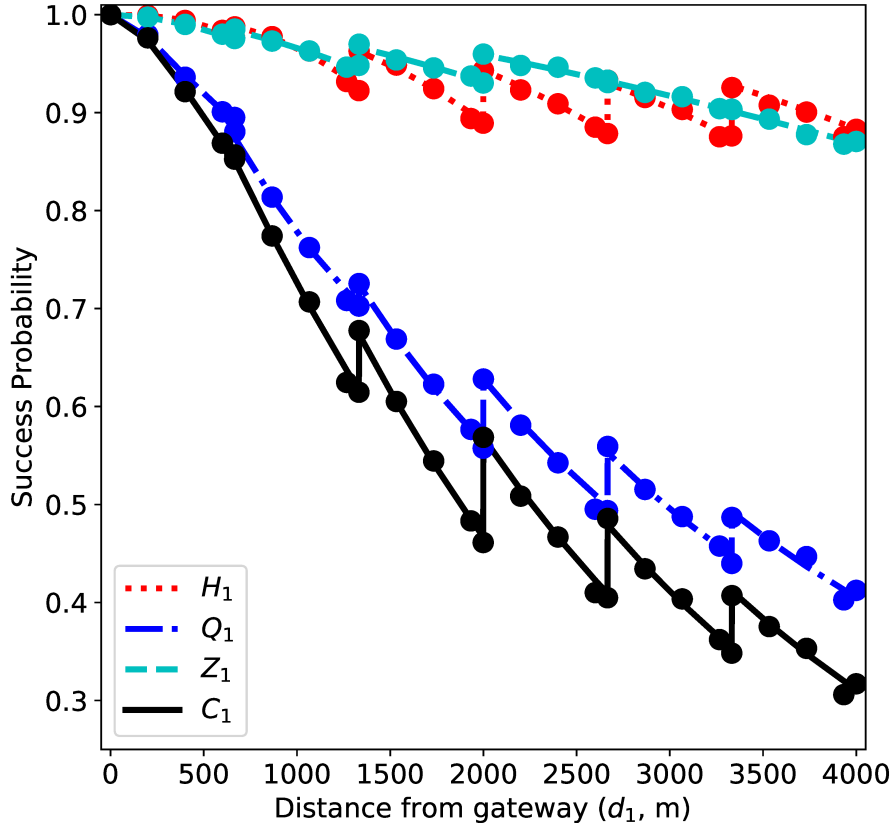
```

Note that Algorithm 2 is not iterative since there is no loop searching for the optimum solution and, therefore, it has complexity $\mathcal{O}(1)$. This algorithm merely describes how to use the proposed models to determine the optimum LoRaWAN configuration considering the restrictions. The approach produces unfeasible configurations if the restrictions are too strict. Thus, lines 14-18 check whether the method generated non-negative densities for all SFs to assess whether the results are feasible or not.

4.3 NUMERICAL RESULTS

This section evaluates the proposed model and algorithms. In all figures, lines represent theoretical probabilities (*i.e.*, H_1, Q_1, Z_1), while marks along the lines show the results of Monte Carlo simulations. Each mark in a figure is the average of 10^5 simulations considering random deployments. Moreover, we assume $\sigma_w^2 = -174 + F +$

Figure 8 – Success probabilities of all outage sources. LoRa: $\bar{N} = 4000$, $p = 0.1\%$, $\eta = 2.75$, $\mathcal{P}_t = 14\text{dBm}$, $R = 4000\text{m}$. IEEE 802.15.4g: $\bar{N}_z = 1000$, $p_z = 0.1\%$, $\eta = 2.75$, $\mathcal{P}_t = 14\text{dBm}$, $R_z = 4000\text{m}$.



Source: the author.

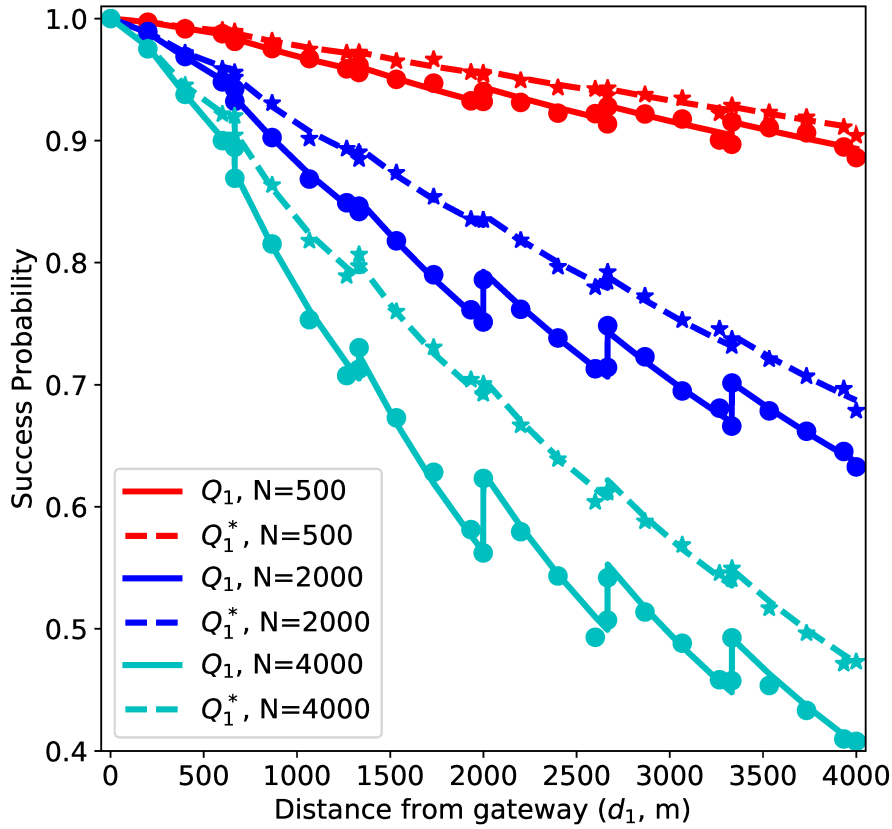
$10 \log_{10} B$ dBm, where $F = 6\text{dB}$ is the receiver noise figure, $\eta = 2.75$, $\lambda = c/f\text{m}$, $c = 3 \times 10^8\text{m/s}$ (speed of light), $f = 868\text{MHz}$ for both LoRaWAN and IEEE 802.15.4g. LoRaWAN channel bandwidth is $B_l = 125\text{kHz}$, and IEEE 802.15.4g channel bandwidth is $B_z = 200\text{kHz}$. We also assume that nodes in LoRaWAN and IEEE 802.15.4g transmit with $\mathcal{P}_t = 14\text{dBm}$. These parameters configure typical European sub-urban scenarios.

Concerning IEEE 802.15.4g interference, we evaluate the algorithms considering three scenarios. In real deployments, the designer of a LoRaWAN network may not know the operational parameters of the interfering IEEE 802.15.4g network. Thus, in a practical situation, the designer should assume worst-case configurations for the external network.

4.3.1 Model Validation

Figure 8 aims to validate the presented models by showing the success rates H_1 , Q_1 , Z_1 , and C_1 as a function of the distance from the gateway. The scenario considers an average number of nodes $\bar{N} = 4000$, transmitting with duty cycle $p = 0.1\%$ in a circular area around the gateway with radius $R = 4000\text{m}$. The IEEE 802.15.4g

Figure 9 – Comparison of Q_1 and Q_1^* probabilities. $\bar{N} = \{500, 2000, 4000\}$, $p = 0.1\%$, $\eta = 2.75$, $\mathcal{P}_t = 14\text{dBm}$, $R = 4000\text{m}$.



Source: the author.

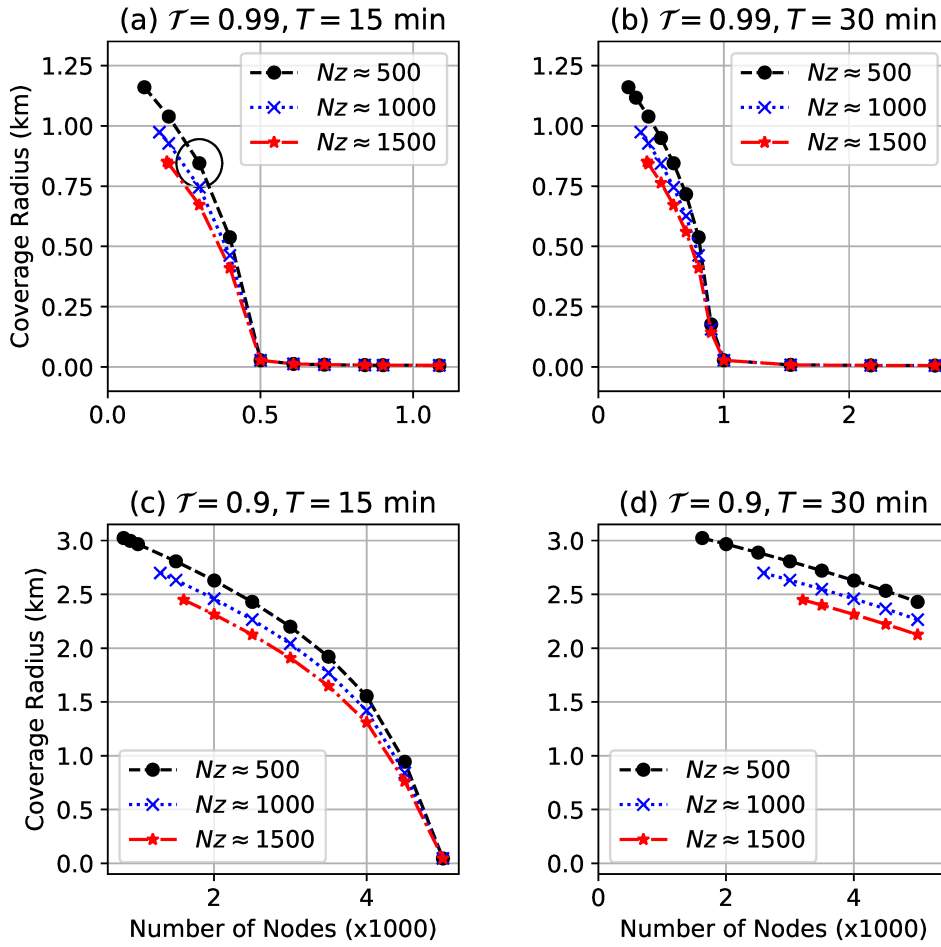
network generating external interference has $\bar{N}_z = 1000$ nodes transmitting with duty cycle $p_z = 0.1\%$, also in a circular area with radius $R_z = 4000\text{m}$. As can be seen, all theoretical expressions (lines) match the simulation results (marks). One can observe in Z_1 that a relatively light interference from IEEE 802.15.4g ($\bar{N}_z = 1000$, $p_z = 0.1\%$) has little impact in lower SFs due to the smaller ToA and reduced probability of concurrent transmissions. Higher SFs, on the other hand, have higher ToA and thus suffer more from this external interference.

In Figure 9, Q_1^* shows what the capture probability would be if we consider that LoRa signals are perfectly orthogonal. We obtain Q_1^* from (53) by considering only $j = i$. As can be seen, the gap between Q_1 and Q_1^* shows that inter-SF interference plays a vital role in link quality.

4.3.2 Algorithm 1: Maximization of Range

Now we evaluate Algorithm 1 of Section 4.2.2. These results use the same network parameters employed to validate the network model. Figure 10 presents a series of graphs for varying optimization objectives. Plots in the same row consider the same reliability target \mathcal{T} , while plots in the same column use the same packet

Figure 10 – Optimization between coverage radius and number of nodes given a minimum reliability constraint when maximizing R with Algorithm 1.



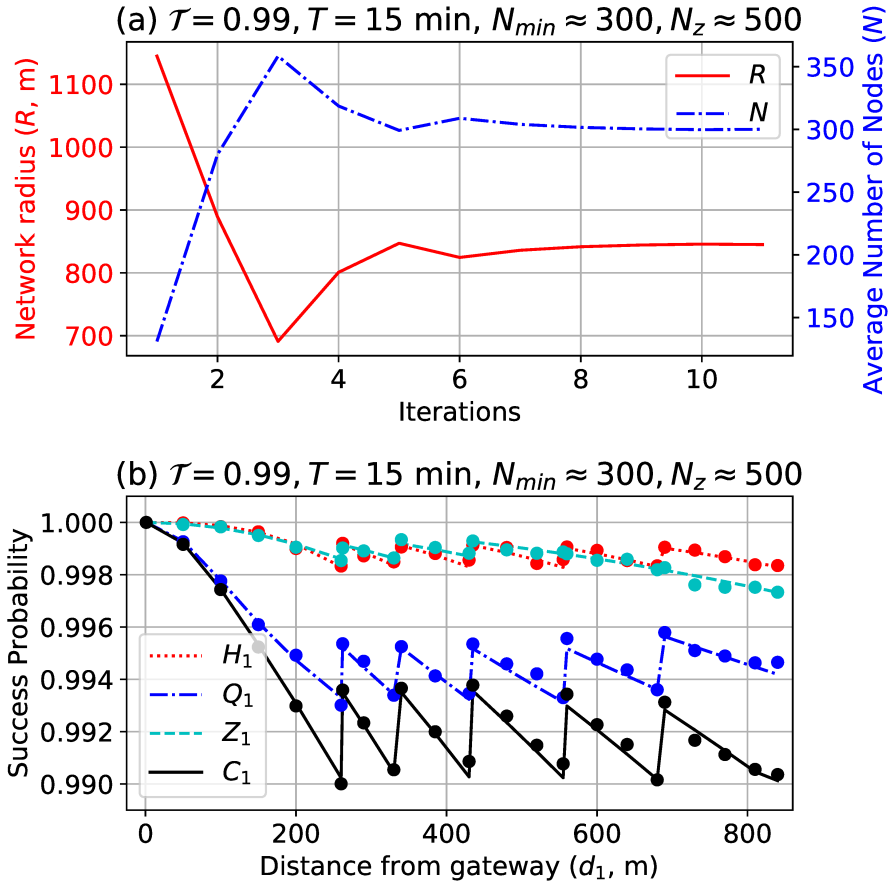
Source: the author.

generation interval T , expressed in minutes. Each graph shows three curves, each one considering a different amount of IEEE 802.15.4g interference, which varies by changing the number of IEEE 802.15.4g nodes (\bar{N}_z), always with duty cycle $p_z = 0.1\%$. Each optimization point considers different N_{min} values, evaluated every 100m.

The first conclusion, when comparing the curves in all plots, is that different IEEE 802.15.4g interference leads to shorter communication ranges when following our proposed optimization procedure. That makes sense since shorter distances feature smaller path loss, making signals less susceptible to external interference. It is also possible to observe that less stringent reliability targets lead to larger coverage areas. Again, that makes sense since smaller \mathcal{T} yields smaller \mathcal{T}_{H_1} , which in turn enables longer communication range.

Also, in Figure 10, plot (a) shows the more rigorous scenario; the configuration allowing the required reliability is only practical for $N_{min} \leq 400$ nodes, with a radius varying from 410m to 1160m, depending on N_{min} and the external interference. The coverage radius with $N_{min} \geq 500$ either converged to unpractical distances of less than

Figure 11 – Convergence of Algorithm 1 and success probability for the scenario marked in Figure 10a.



Source: the author.

10 meters or diverged, meaning that we could not place this many nodes with packet generation interval of 15 minutes while ensuring minimum reliability of $\mathcal{T} = 0.99$.

For $\mathcal{T} = 0.99$, there are more feasible scenarios if network usage decreases. Plot 10b shows that configurations with up to 900 nodes are possible if the packet transmission interval is $T = 30$ minutes. For $\mathcal{T} = 0.9$ with $T = 15$ minutes, it is possible to find reasonably good network configurations up to $N_{min} = 4500$. However, $N_{min} = 5000$ shrinks the communication range to unpractical distances.

Figure 11 illustrates the behavior of Algorithm 1 and network performance when taking the circled case in Figure 10a as an example. Figure 11a shows the convergence of R and \bar{N} for this scenario. Applying the estimate of the number of iterations presented in Section 4.2.2 to this example makes $R_1 = 1244.7\text{m}$ because of $\mathcal{T} = 0.99$. Therefore, the maximum number of iterations to reach $|R - R_{last}| < \chi$ (line 20, Algorithm 1) is $n = \log_2 \left(\frac{\chi_0}{\chi} \right) = \log_2 \left(\frac{1244.7}{1} \right) = 10.28$. We see in Figure 11a that the algorithm converges after the 11th iteration with $\bar{N} = 300.1$, thus “stretching” the network range as much as possible. Also, note that convergence time depends on χ_0 , which in turn depends on \mathcal{T} . If we consider the same case above with $\mathcal{T} = 0.9$ or $\mathcal{T} = 0.8$, we

Table 4 – Detailed optimization results for the marked scenario in Figure 10a.

Interference:		All sources			Intra-SF only		
Scenario	SF	Range (m)	\bar{N}_i	\bar{N}	Range (m)	\bar{N}_i	\bar{N}
10a	7	261.6	162.8	300.1	370.0	124.6	300.0
	8	336.4	67.5		475.7	87.1	
	9	432.4	32.5		611.6	43.5	
	10	555.9	21.8		786.2	25.3	
	11	685.4	10.6		969.3	12.9	
	12	845.0	4.7		1195.1	6.4	

Source: the author.

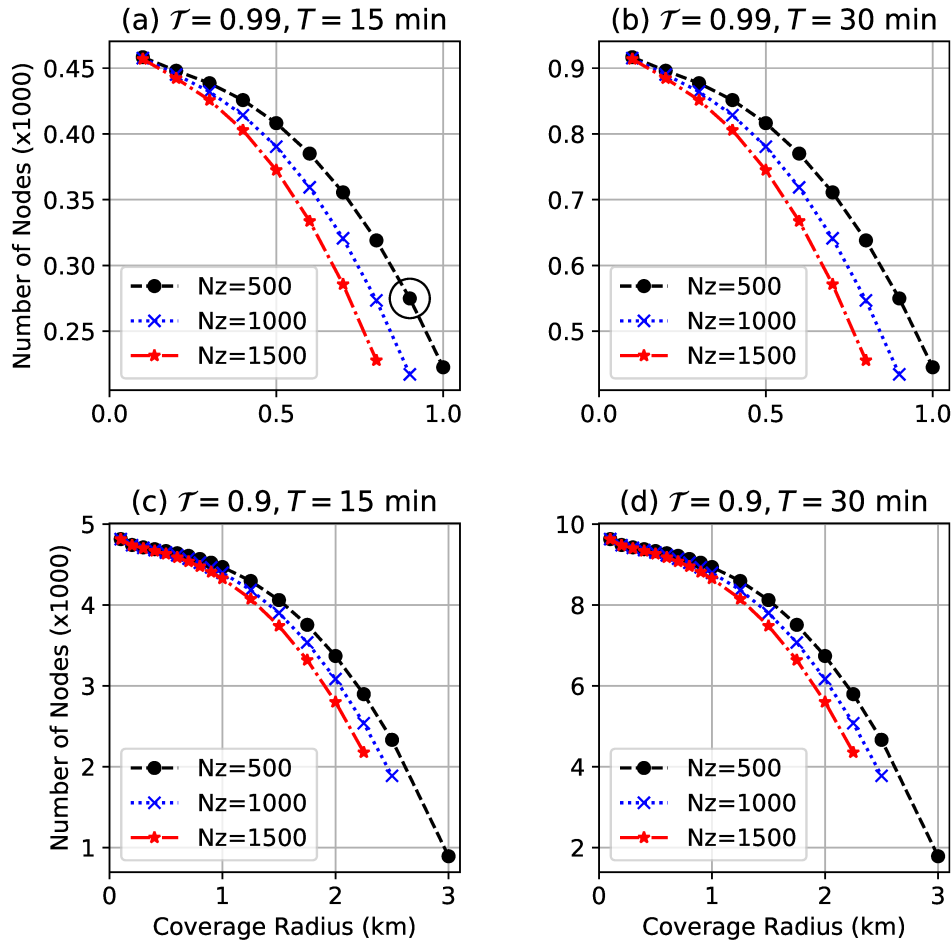
would have, respectively, $\chi_0 = 2899.7$ or $\chi_0 = 3767.3$, what would make, respectively, $n = 11.50$ or $n = 11.88$, showing that the impact of \mathcal{T} in convergence time is small.

Table 4 shows numerical results of the same scenario in two columns: “All sources” with the results for our complete model; and “Intra-SF only” disregarding both inter-SF and external interference sources. We get the results in the “Intra-SF only” column using the same models, but setting $\theta_i = -\infty, \forall i \in S$ in Θ , and $\delta_{i,j} = 1$ for $i = j$ and $\delta_{i,j} = -\infty$ otherwise. When considering all sources of interference, as expected, the fact that ToA impacts the duty cycle induces the optimization procedure to allocate most of the nodes with lower SF. That happens because signal attenuation increases with distance, making more distant nodes more vulnerable to both internal and external interference. Recall that a shorter ToA reduces the collision probability. Moreover, longer ToA generates more internal interference to other SFs.

In some cases, higher SFs may not be used to ensure minimum reliability. However, note that (57), (60), and Algorithm 1 can be extended to change the restriction N_{min} to represent a vector with the minimum number of nodes using each SF. One can achieve that by revisiting the computation of the densities in (60) to consider such a minimum number of nodes when computing the spatial density. Since doing that will possibly result in more nodes using higher SFs, it is expected that fewer nodes use lower SF, resulting in a smaller total number of nodes, as well as a shorter network radius, since the algorithm will converge to a higher H_1 to compensate the increased Q_1 . When disregarding inter-SF and external interference, we observe that higher SFs are profoundly affected by inter-SF and external interference, mainly due to their extended ToA. In particular, we observe that interference, rather than path loss, is the main factor for which our method disfavors the use of higher SF. Moreover, it is clear that interference considerably affects coverage.

Finally, Figure 11b shows the success probabilities of the example scenario, where the optimized configurations consider the minimum average reliability target \mathcal{T} for all distances from the gateway. As expected, the success probability approaches the

Figure 12 – Optimization between the number of nodes and coverage radius (in meters) given a minimum reliability constraint when maximizing \bar{N} with Algorithm 2.



Source: the author.

desired minimum $\mathcal{T} = 0.99$ at the edge of each SF. We can see that collisions (Q_1) are kept almost constant or increase slightly with SF. That happens because the algorithm reduces the number of nodes using each SF to keep Q_1 in pace with H_1 and Z_1 , to ensure the minimum \mathcal{T} .

4.3.3 Algorithm 2: Maximization of Nodes

Now we evaluate Algorithm 2 of Section 4.2.3. The plots in Figure 12 show the results for different scenarios of required minimum reliability (\mathcal{T}) and message generation period (T). For all plots, the x-axis represents the R_{min} input to the algorithm, while the y-axis shows the achieved maximized number of nodes. In each plot, the x-axis grows up to the value for which the requirements yield practical results.

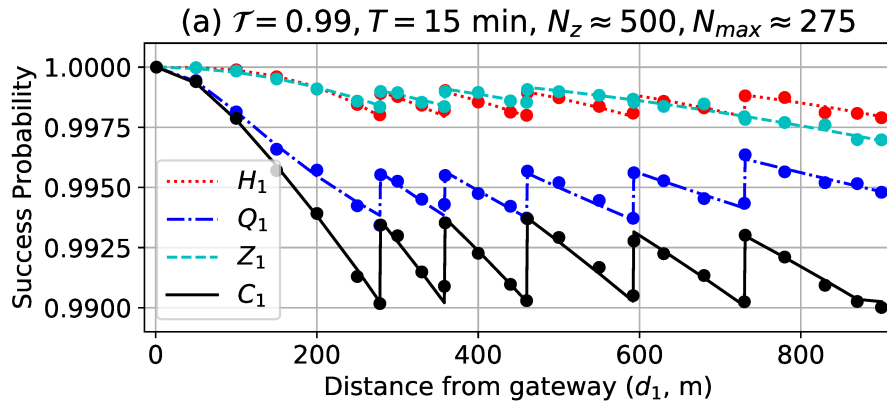
In Figure 12, if we analyze each row of plots independently, we see that the maximum number of nodes is a linear function of the transmission period T . For instance, considering $R_{min} = 500\text{m}$ and $\bar{N}_Z = 500$, N_{max} in plots 12a and 12b are, respectively, 408.18 and 816.36, *i.e.*, N_{max} doubles when T doubles. That is expected

Table 5 – Detailed optimization results for the marked scenario in Figure 12a.

Interference:		All sources			Intra-SF only		
Scenario	SF	Range (m)	\bar{N}_i	\bar{N}	Range (m)	\bar{N}_i	\bar{N}
12a	7	278.7	149.2	274.9	278.7	211.1	508.2
	8	358.3	61.8		358.3	147.6	
	9	460.6	29.9		460.6	73.7	
	10	592.1	20.2		592.1	42.9	
	11	730.0	9.5		730.0	21.8	
	12	900.0	4.0		900.0	10.9	

Source: the author.

Figure 13 – Average outage expectation for the marked scenario in Figure 12a.



Source: the author.

since these variations ensure the same network load in all scenarios. We also observe, in all plots, that increased external interference reduces both the number of nodes and the achievable coverage radius.

Table 5 shows the achieved geometry and number of nodes of the marked scenario of Figure 12a. Again, the “All sources” column presents the results of our complete model, while the “Intra-SF only” column disregards inter-SF and external interference. Since the method assumes that the maximum number of nodes is achieved with the shortest possible distances, the maximum range of a node using SF₁₂ has to be R_{min} (900m for this case). As for Algorithm 1, Algorithm 2 also favors lower SFs. Moreover, Table 5 shows that the maximum number of nodes almost doubles when disregarding inter-SF and external interference, emphasizing the importance of taking such impairments into account to avoid overestimating the network performance. Finally, Figure 13 shows success probabilities for the example scenario, which approach $\mathcal{T} = 0.99$ at SF edges but stay above the required minimum \mathcal{T} for all distances shorter than R_{min} .

4.4 CLOSING

The main contributions in this chapter were the extension of the interference models to consider external and inter-SF interference sources, considering experimental results on inter-technology interference. The chapter also presented two algorithms to optimize LoRaWAN configuration under reliability constraints. In the next chapter, we build over our models to analyze the performance of LoRaWAN under the power and rate allocation mechanism known as ADR.

5 PERFORMANCE ANALYSIS OF SINGLE-CELL ADAPTIVE DATA RATE-ENABLED LORAWAN

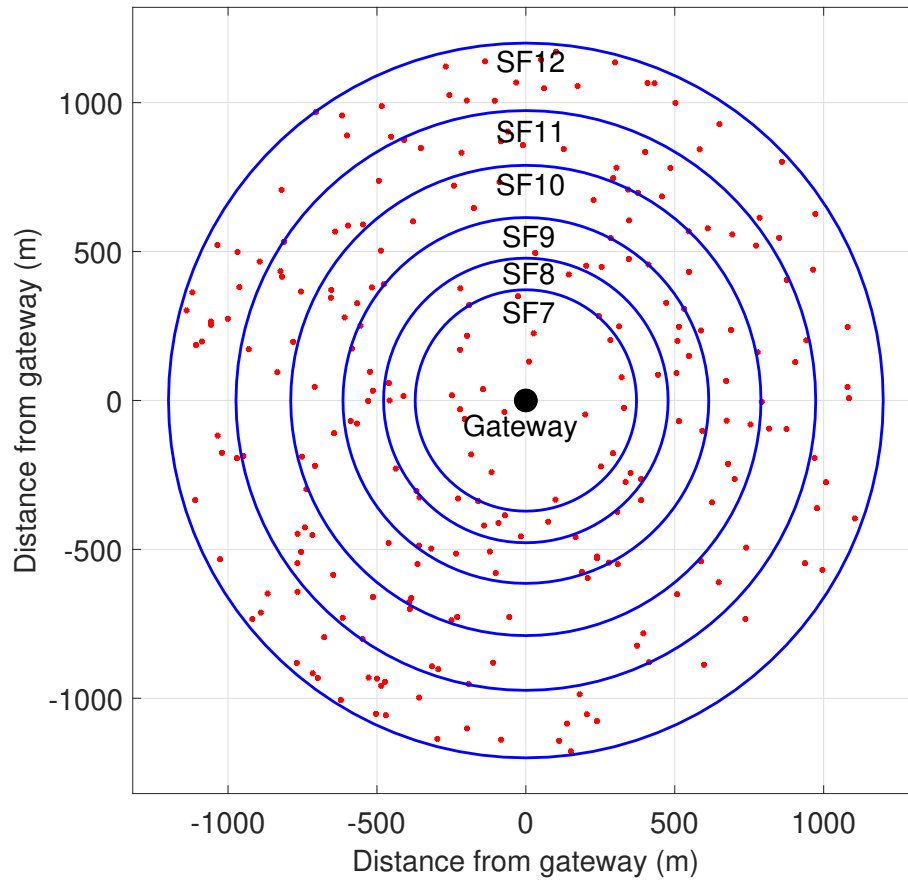
“The balance of power is the scale of peace.” Thomas Paine.

This chapter presents this thesis project’s contributions originally published in the *IEEE Wireless Communication Letters* in 2020 (HOELLER et al., 2020). It focuses on modeling LoRaWAN performance when the ADR feature is enabled. Recent research on LoRaWAN shows that it may embrace the massive IoT applications’ requirements, and the ADR mechanism plays an important role in this achievement. Aligned to the problem we address here, Abdelfadeel *et al.* (ABDELFADEEL et al., 2018) assess the performance of ADR-enabled LoRaWAN, achieving results similar to our theoretical analysis, and Li *et al.* (LI et al., 2018) study ADR convergence, both through simulations.

In this chapter, we revise the analytic models for single-cell LoRaWAN and propose an adaptation to include the ADR feature. Although multi-cell systems are likely to shape the topology of LoRaWAN networks in dense urban deployments, single-cell systems are still of interest for deployments in small town or villages, industrial plants, and in the agribusiness sector, where a dedicated single-cell LoRaWAN system may support a known number of users and applications. Analytic models allow for faster evaluation and insights that are hard to obtain from simulations. We validate our analytic model through Monte Carlo simulations. Following the algorithms we propose in Chapter 4, we use our model to plan the network deployment to respect a maximum outage probability under ADR. We show that power control considerably reduces interference, increasing network capacity by up to 50% and reducing average transmit power by roughly 25%.

This chapter’s main contributions are the performance analysis of steady-state, single-cell, ADR-enabled LoRaWAN and a simple closed expression for its outage probability in steady-state operation. We assume the network reaches a steady-state when ADR converges for all nodes, and their SF and transmit power configuration remain unchanged, as defined in (LI et al., 2018). The performance analysis shows that ADR is an important feature of the technology and must be considered. The closed-form expression assumes, as in (LI et al., 2018), that a network with static nodes converges to Received Signal Strength Indicator (RSSI)-based SF and transmit power figures, implementing, in practice, a truncated channel inversion scheme (ELSAWY; HOSSAIN, 2014). Also, transient periods occur when channel or network conditions change, and the time to return to steady-state depends on application and deployment scenario (LI et al., 2018). Therefore, it is important to emphasize that our work’s assumptions configure an ideal scenario, meaning that this model does not fit well to highly dynamic networks because we do not model the so-called transient periods, which may dominate the network operation in such dynamic environments.

Figure 14 – Sample of $\bar{N} = 250$ nodes uniformly distributed in an area of radius 1200m and with SF allocation for 1% maximum disconnection probability.



Source: the author.

5.1 SYSTEM MODEL

We model the spatial distribution and activity of LoRaWAN nodes with stochastic geometry. We divide the network into rings according to the distance from the node to the gateway. The vector $L = [l_0, \dots, l_6]$, $l_0 = 0$, defines the SF ring edges, with $R = l_6$ as the coverage radius. For simplicity, $S = \{1, \dots, 6\}$ is the set of SF rings, and each ring uses a respective SF in the set $\{7, \dots, 12\}$. We consider that all nodes run the same application. Thus network usage differs for each SF because of different data rates (see ToA in Table 1). We also assume that devices generate a packet for transmission once every T seconds and that the packet is transmitted with a given probability according to the pure ALOHA protocol. The transmission probability is a vector $p = [p_1, \dots, p_6]$, $p_i \in (0, 1] \forall i \in S$, and $p_i = t_i/T$, where t_i is the ToA of the packet with the SF of ring i . For example, Figure 14 presents a network configuration with $\bar{N} = 250$ nodes and network geometry (L), obtained to ensure 0.99 connection probability according to the method we describe in Section 5.3.

Each SF ring constitutes a separate PPP Φ_i with intensity $\alpha_i = p_i \rho_i$ in its area $V_i = \pi(l_i^2 - l_{i-1}^2)$, where l_{i-1} and l_i form its inner and outer edges. $\rho_i = \bar{N}_i/V_i$ is the

spatial density of nodes in ring i . The average number of nodes in Φ_i is $\bar{N}_i = \rho_i V_i$. The average total number of nodes is $\bar{N} = \sum_{i \in \mathcal{S}} \bar{N}_i$. The coverage area is $V = \pi R^2$. For instance, take ring $i = 5$ (SF_{11}) in Figure 14, defined by two circles of radii $l_4 = 789.5\text{m}$ and $l_5 = 973.4\text{m}$. The ring area is $V_5 = \pi(l_5^2 - l_4^2) = 1.02\text{km}^2$. With $\bar{N}_5 = \rho_5 V_5 = 50$ nodes in the ring, the spatial density is $\rho_5 = \bar{N}_5/V_5 = 49.1$ nodes/ km^2 . If the transmit probability is $p_5 = 0.01$, then the intensity of Φ_5 is $\alpha_5 = p_5 \rho_5 = 0.49$.

In our analysis, d_k is the Euclidean distance between the k -th node and the gateway, and d_1 denotes the distance of the node of interest to the gateway. We use the subscript “1” whenever a variable refers to the node under analysis. Nodes use a transmit power \mathcal{P}_k to send signal s_k , and both path loss and Rayleigh fading h_k affect the signal r_1 received at the gateway. Path loss follows $g_k = \left(\frac{\lambda}{4\pi d_k}\right)^\eta$, with wavelength λ , and path loss exponent $\eta > 2$. Therefore¹

$$r_1 = s_1 \sqrt{\mathcal{P}_1 g_1} h_1 + \sum_{k \in \Phi_i} s_k \sqrt{\mathcal{P}_k g_k} h_k + w, \quad (61)$$

where the first term is the attenuated signal of interest, the second is interference, i is the ring of s_1 , and w is the zero-mean AWGN of variance σ_w^2 .

5.1.1 Outage Probability

We consider that communication outage occurs due to disconnection or interference, which are, respectively, conditioned on the realization of the SNR and the SIR of a transmitted packet. We base our analysis on the stochastic geometry model of the SINR of Poisson Bipolar Networks with Rayleigh fading in (HAENGGI, 2012b, Theorem 5.7). Disconnection depends on distance and happens if the SNR is below the threshold ψ_i (see Table 1). The disconnection probability is (GEORGIU; RAZA, 2017)

$$H_0(d_1, \mathcal{P}_1) = \mathbb{P}[\text{SNR} < \psi_i] = \mathbb{P}\left[\frac{\mathcal{P}_1 g_1 |h_1|^2}{\sigma_w^2} < \psi_i \mid g_1\right],$$

with i indicating the SF ring in use by the node under analysis. With known d_1 and \mathcal{P}_1 , we condition H_0 to the probability of the Rayleigh fading power in $|h_1|^2 \sim \exp(1)$, so

$$H_0(d_1, \mathcal{P}_1) = 1 - \exp\left(-\frac{\psi_i \sigma_w^2}{\mathcal{P}_1 g_1}\right). \quad (62)$$

The outage due to interference (*i.e.*, collision with other packets) considers the capture effect. Thus, the collision probability concerning the SIR threshold δ is

$$Q_0(d_1, \mathcal{P}_1) = \mathbb{P}[\text{SIR} < \delta | g_1] = \mathbb{P}\left[\frac{\mathcal{P}_1 g_1 |h_1|^2}{\sum_{k \in \Phi_{t,i}} \mathcal{P}_k g_k |h_k|^2} < \delta \mid g_1\right]. \quad (63)$$

¹ In this first model we do not consider inter-SF interference.

5.2 TRANSMIT POWER ALLOCATION FOR LORAWAN

When considering transmit power allocation, \mathcal{P}_k may be different for each node. We assume that nodes at the edge of each SF ring use the highest available transmit power (\mathcal{P}_{tmax}) to extend the coverage area. Considering a predefined target outage due to disconnection (\mathcal{T}_{H_0}), we define the network geometry by making $H_0(l_j, \mathcal{P}_{tmax}) = \mathcal{T}_{H_0}$, so that

$$l_j = \frac{\lambda}{4\pi} \left(-\frac{\mathcal{P}_{tmax} \ln(1 - \mathcal{T}_{H_0})}{\sigma_w^2 \psi_j} \right)^{\frac{1}{\eta}}. \quad (64)$$

We also use (62) to define the minimum transmit power the k -th device must use to ensure \mathcal{T}_{H_0} as

$$\mathcal{P}_{kmin} = -\frac{\sigma_w^2 \psi_j}{\ln(1 - \mathcal{T}_{H_0}) g_k}. \quad (65)$$

In practice, \mathcal{P}_{kmin} should be rounded up to the immediately higher value available. Additionally, we obtain the network average transmit power by averaging (65) over the area, *i.e.*,

$$\begin{aligned} \mathcal{P}_{tavg} &= \frac{2\pi}{V} \sum_{i \in \mathcal{S}} \int_{l_{i-1}}^{l_i} -\frac{\sigma_w^2 \psi_j}{\ln(1 - \mathcal{T}_{H_0}) g_k} d_k \, dd_k \\ &= -\frac{2\pi \sigma_w^2}{V \ln(1 - \mathcal{T}_{H_0})} \left(\frac{4\pi}{\lambda} \right)^\eta \sum_{i \in \mathcal{S}} \frac{\psi_j}{\eta + 2} (l_i^{\eta+2} - l_{i-1}^{\eta+2}). \end{aligned} \quad (66)$$

5.2.1 Outage Probability with Transmit Power Allocation

Rewriting the disconnection probability in (62) with the power allocation method defined by (65) yields

$$H_0(d_1, \mathcal{P}_{1min}) = 1 - \exp \left(-\frac{\psi_j \sigma_w^2}{\mathcal{P}_{1min} g_1} \right) = \mathcal{T}_{H_0}, \quad (67)$$

so that transmit power control compensates for path loss, makes H_0 independent of \mathcal{P}_1 and d_1 , and ensures \mathcal{T}_{H_0} for all nodes. Similarly, rewriting (63) with (65) yields

$$Q_0(i) = \mathbb{P} \left[\frac{|h_1|^2}{\sum_{k \in \Phi_i} |h_k|^2} < \delta \right], \quad (68)$$

and therefore Q_0 becomes independent of transmit powers and distances from the gateway, being only dependent on fading.

If we define $X_i = \sum_{k \in \Phi_i} |h_k|^2$ and $Y_i = \frac{|h_1|^2}{X_i}$, then $Q_0(i) = \mathbb{P}[Y_i < \delta] = F_{Y_i}(\delta)$, with the cdf of Y_i obtained as

$$F_{Y_i}(y) = \int_0^\infty F_{|h_1|^2}(xy) f_{X_i}(x) \, dx, \quad (69)$$

where $|h_1|^2 \sim \exp(1)$, $F_{|h_1|^2}(z) = 1 - e^{-z}$, X_i is Gamma distributed, $X_i \sim \Gamma(N_{\Phi_i}, 1)$, $f_{X_i}(x) = \frac{1}{\Gamma(N_{\Phi_i})} x^{N_{\Phi_i}-1} e^{-x}$, and $\Gamma(\cdot)$ is the Gamma Function (OLVER et al., 2010). Following the duality of notation of PPPs (HAENGGI, 2012b, Box 2.3), $N_{\Phi_i} \sim \text{Poiss}(\beta_i)$ is a Poisson random variable of mean $\beta_i = \alpha_i V_i = \rho_i \bar{N}_i$ describing the average number of active interferers in the PPP Φ_i . Thus,

$$Q_0(i) = \mathbb{E}_{N_{\Phi_i}} \left[\int_0^\infty (1 - e^{-x\delta}) \frac{1}{\Gamma(N_{\Phi_i})} x^{N_{\Phi_i}-1} e^{-x} dx \right], \quad (70)$$

which is solved by distributing the multiplication, factoring out independent terms, and applying the identity $\int_0^\infty x^n e^{-ax} dx = \frac{\Gamma(n+1)}{a^{n+1}}$ (OLVER et al., 2010). Thus, the N_{Φ_i} -dependent collision probability is

$$Q_0(i) = \mathbb{E}_{N_{\Phi_i}} \left[1 - (\delta + 1)^{-N_{\Phi_i}} \right]. \quad (71)$$

Since the Probability Mass Function (PMF) of N_{Φ_i} is $f_{N_{\Phi_i}}(z) = \frac{\beta_i^z e^{-\beta_i}}{z!}$,

$$Q_0(i) = 1 - \exp\left(-\frac{\delta}{\delta + 1} \beta_i\right). \quad (72)$$

Finally, complementary to the success probability definition in Section 2.2.3, the total outage probability for each SF ring i is

$$\mathcal{O}(i) \approx H_0 + Q_0(i) - H_0 Q_0(i). \quad (73)$$

Our model preserves the PPP properties for each point as long as the fixed communication distances and transmit powers satisfy $\frac{P_1 g_1}{P_k g_k} = 1$ in (63), which is guaranteed by (65).

5.3 NETWORK PLANNING

We use the outage probability in (73) as a tool to plan the deployment of a single-cell LoRaWAN. We assume a target maximum outage \mathcal{T}_O for all nodes, $\mathcal{O}(i) \leq \mathcal{T}_O, \forall i$. We use this reliability constraint to maximize coverage radius and network usage. After a closer look at (73), we observe that, for each ring, $\mathcal{O}(i)$ depends on the outer limit l_i and the average number of active interferers β_i . Unfortunately, it is impossible to solve such optimization for both variables simultaneously, so, here, we explore the trade-off between coverage radius and network usage. Assuming that the larger coverage radius and higher network usage occur on the worst-case scenario where $\mathcal{O}(i) = \mathcal{T}_O, \forall i$, we represent the trade-off, following from (73), as $\mathcal{T}_O = \mathcal{T}_{H_0} + Q_0(i) - \mathcal{T}_{H_0} Q_0(i)$, from which we equate, either, the maximum β_i assuming a given \mathcal{T}_{H_0} as

$$\beta_i = -\frac{\delta + 1}{\delta} \ln\left(\frac{1 - \mathcal{T}_O}{1 - \mathcal{T}_{H_0}}\right), \quad (74)$$

Table 6 – Model and simulation parameters.

Parameter	Value
f	868MHz
B	125kHz
F	6dB
σ_w^2	$-174 + F + 10\log_{10}B = -117\text{dBm}$
T	15 minutes
$\rho (\times 10^{-6})$	{57.1, 114.3, 205.9, 366.3, 823.7, 1465.4}
\mathcal{P}_k	{-1, 0, ..., 14}dBm
\mathcal{P}_{tavg}	12.63dBm
\mathcal{P}_{tmax}	14dBm
δ	6dB
\mathcal{T}_O	0.01
R_{min}	1200m

Source: the author.

or the maximum \mathcal{T}_{H_0} assuming a given β_i as

$$\mathcal{T}_{H_0} = \frac{\mathcal{T}_O - Q_0(i)}{1 - Q_0(i)}. \quad (75)$$

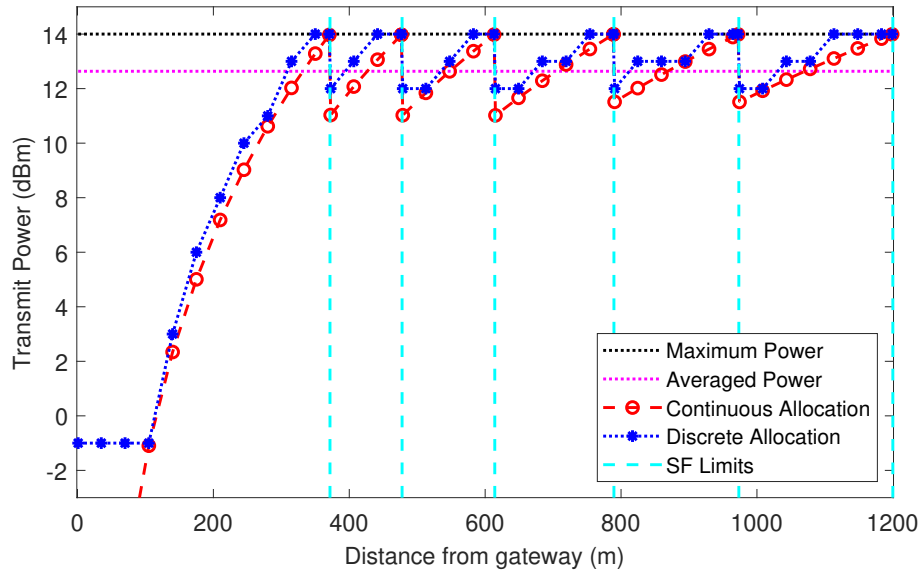
Note that $\beta_i = p_i \bar{N}_i$, so we use (74) to obtain the maximum number of nodes in each ring, assuming that all nodes in a ring use the same duty-cycle p_i . Similarly, because of (64), we obtain the SF ring range l_j with \mathcal{T}_{H_0} from (75).

5.4 NUMERICAL RESULTS

We assume the parameters in Tables 1 and 6 to mimic a suburban deployment of a single-cell LoRaWAN under European regulations. The figures show our theoretical model (solid lines) and Monte Carlo simulations (marks). Figure 15 shows the power allocation using (65) and the average power in the network. The dashed curve shows the continuous power allocation according to distance and considering different SF. It shows that SF_7 uses a wider range of transmit power because its nodes are closer to the gateway. The power variation is 3dB in SF_8 , SF_9 , and SF_{10} , and 2.5dB in SF_{11} and SF_{12} . That matches the SNR threshold variation in Table 1 (ψ_j) and is also aligned with the ADR power and SF allocation method defined by LoRaWAN. Still, in Figure 15, the dotted curve shows the discrete practical power allocation, obtained by rounding up the continuous values of (65). That mostly impacts the power of nodes closer to the gateway. Figure 15 also shows the average power in the network from (66) as 12.63dBm – an average power reduction of 27%.

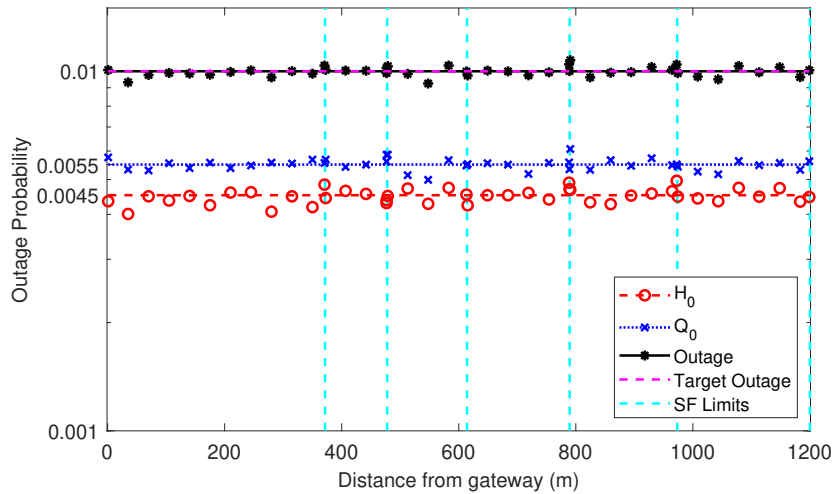
Figures 16 and 17 show results using two approaches: power allocation as in (65), and all nodes with maximum power (14dBm). The most noticeable aspect is that proper power allocation allows all nodes in the network to experience similar

Figure 15 – Power allocation as a function of distance.



Source: the author.

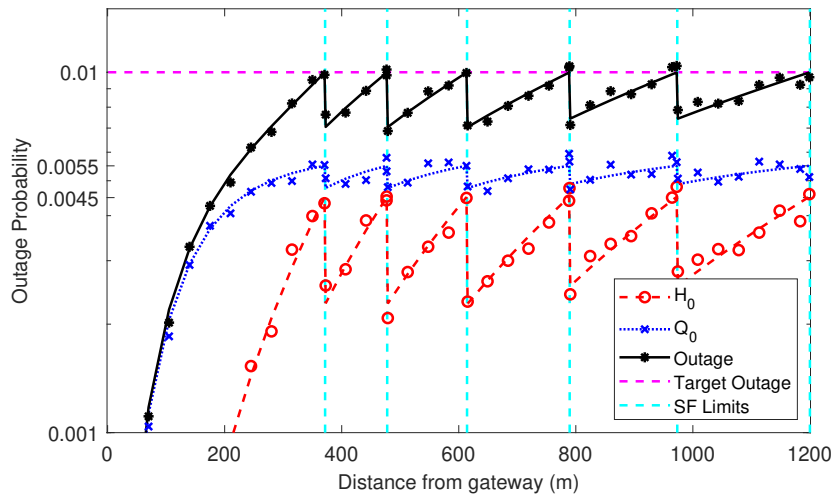
Figure 16 – System performance with power allocation. $\bar{N} = 247$.



Source: the author.

outage probabilities close to the target $\mathcal{T}_0 = 0.01$. When nodes use constant power, \mathcal{T}_0 is reached only on the edges of each SF ring. In the constant power scenario, the nodes closer to the ring inner edge use more power than needed, thus spending more energy and causing more interference.

The method in Figure 16, besides using less average power than that in Figure 17, also serves more users. We observe a gain of 9.3% in the number of supported users, on average, from 225 to 247 nodes. If we consider a scenario with fixed transmit power equal to the average power used in Figure 16, then power allocation leads to a gain of 56.7% in the number of users, from 157 to 247. Our results show that adequate power allocation in LoRaWAN contributes to the network capacity due to the

Figure 17 – System performance with fixed power. $\bar{N} = 225$.

Source: the author.

interference reduction while being more energy-efficient.

5.5 CLOSING

The main contributions in this chapter were the performance analysis of steady-state, single-cell, ADR-enabled LoRaWAN, and a closed expression for its outage probability. This closes the set of contributions in this thesis. The next chapter summarizes and discusses all contributions of the thesis and closes the document.

6 CONCLUSION

“Mysteries do not lose their poetry when solved. Quite the contrary; the solution often turns out more beautiful than the puzzle and, in any case, when you have solved one mystery you uncover others, perhaps to inspire greater poetry.”
Richard Dawkins.

LPWAN systems evolved rapidly during this thesis project and are now widely adopted in virtually every country. Clear examples of such evolution are the global initiatives SigFox, a worldwide low-power UNB network, and the open, community-supported LoRaWAN network The Things Network (TTN)¹. TTN launched in 2015 and, by 2020, operates in 150 countries with over sixteen thousand gateways deployed. Besides these, other private initiatives exist in several countries, deploying LoRaWAN, Wi-SUN, and other ISM networks, generally exploring the mobile operators' already available tower infrastructure. Together with that, the unrolling of the Fifth Generation Communication Technologies (5G) deployment is making NB-IoT increasingly available in licensed bands.

With increasingly growing networks, the ability to plan deployments for both coverage and coexistence is of paramount importance, and that is one of the key issues we sought contributions for in this work. Because of the obvious high complexity and costs involved in evaluating LPWAN performance through measurements in “real-world” scenarios, this project took the analytic path, where models were adapted or conceived to describe such systems' expected performance. Monte Carlo simulations supported the analysis process as a tool to validate the analytical findings.

Chapter 3 used time and spatial diversity to enhance the uplink performance in LoRa networks through message replication and multiple receive antennas. We concluded that there is an optimal number of copies for message replication to be employed in each network configuration and each SF. Moreover, replication is very useful in low-density networks, while multiple receive antennas are always beneficial, and the adequate combination of both techniques can improve the network performance.

Chapter 4 presented two algorithms to optimize the configuration of LoRaWAN under imperfect SF orthogonality and Wi-SUN interference. We used models of LoRaWAN networks to derive success probabilities of packet delivery under internal and external (IEEE 802.15.4g) interference. The presented algorithms search for optimum LoRaWAN configurations given minimum network density or coverage radius restrictions, meeting a target minimum reliability level. Regarding IEEE 802.15.4g interference over LoRaWAN, although higher SF should be more robust to this type of interference, they suffer more from that impairment because their increased ToA makes it more likely that transmissions overlap IEEE 802.15.4g activity. Also, regarding the proposed algo-

¹ <https://www.thethingsnetwork.org>

rithms, they provide a tool for exploring trade-offs between network load and coverage range by showing the feasible region of LoRaWAN network configurations.

Finally, in Chapter 5, we modeled the performance of LoRaWAN with power and rate (SF) allocation, considering two outage conditions: disconnection and interference. We used an algorithm similar to the ones proposed in Chapter 4 to determine the maximum number of users who ensure maximum outage probability. The results showed that power allocation increases network reliability due to reduced interference while being more energy-efficient than a setup using fixed transmit power.

6.1 FUTURE WORK

One can elaborate on several ways of extending the results in this work. Regarding the message replication issue, for instance, one can consider the optimization of message replication, taking into account energy efficiency, as well as the allocation of different numbers of message copies for different users to favor nodes that require a better Quality-of-Service (QoS). Additionally, combined message codification and replication techniques other than the ones explored in (SOUZA SANT'ANA et al., 2020) could be considered. Moreover, spatial diversity can also be exploited in a macro sense, with multiple gateways with multiple receive antennas.

Regarding the proposed network planning algorithms, a push forward to evaluate their performance would be to evaluate them on an extended simulated scenario that considers the RSSI metric instead of the theoretical path loss to maximize either the communication range or the number of nodes of each SF. Moreover, the important ISM spectrum sharing issue could be further studied and spectrum allocation methods proposed.

Also, the performance of LoRaWAN with power and rate allocation mechanisms other than ADR could be an interesting problem to investigate, although complex allocation methods may make it unfeasible to derive closed-form performance models. The performance analysis of LoRaWAN with ADR and under inter-SF and external interference could also be performed, and the adequate allocation of SF and power for each user considering message replication and multiple antennas is an interesting open problem.

Finally, one important aspect of this work is that it models the networks' *average* performance. Although it forms an important analytical result, future work may extend the model to consider the meta-distribution of the network SINR (HAENGGI, 2016) to obtain, analytically, other metrics like the variance and the confidence interval.

6.2 LIST OF PUBLICATIONS

Here we list the articles produced during this thesis project. Besides the three papers that formed the core contributions in this thesis (publications 1, 6, and 8), this thesis's work made it possible to collaborate with colleagues in other universities.

1. **A. Hoeller**, R. D. Souza, O. L. Alcaraz López, H. Alves, M. de Noronha Neto and G. Brante, "Analysis and Performance Optimization of LoRa Networks With Time and Antenna Diversity," in *IEEE Access*, vol. 6, pp. 32820-32829, 2018. ©2018 IEEE. Reprinted, with permission from authors.
2. F. Honorio, G. Brante, G. L. Moritz, M. Noronha-Neto, **A. Hoeller** and R. D. Souza, "Effect of Nakagami-m Fading on the Scalability of LoRa/LoRaWAN Networks," In: XXXIII Simpósio Sul de Microeletrônica (SIM 2018), 2018, Curitiba, Brazil.
3. **A. Hoeller**, R. D. Souza, O. L. Alcaraz López, H. Alves, M. de Noronha Neto and G. Brante, "Exploiting Time Diversity of LoRa Networks Through Optimum Message Replication," 2018 15th International Symposium on Wireless Communication Systems (ISWCS), Lisbon, 2018, pp. 1-5.
4. S. Montejo-Sánchez, C. A. Azurdia-Meza, R. D. Souza, E. M. G. Fernandez, I. Soto and **A. Hoeller**, "Coded Redundant Message Transmission Schemes for Low-Power Wide Area IoT Applications," in *IEEE Wireless Communications Letters*, vol. 8, no. 2, pp. 584-587, April 2019.
5. M. Asad-Ullah, J. Iqbal, **A. Hoeller**, R. D. Souza and H. Alves, "K-Means Spreading Factor Allocation for Large-Scale LoRa Networks," *Sensors* 2019, 19, 4723.
6. **A. Hoeller**, R. D. Souza, H. Alves, O. L. Alcaraz López, S. Montejo-Sánchez and M. E. Pellenz, "Optimum LoRaWAN Configuration Under Wi-SUN Interference," in *IEEE Access*, vol. 7, pp. 170936-170948, 2019. ©2019 IEEE. Reprinted, with permission from authors.
7. J. M. d. S. Sant'Ana, **A. Hoeller**, R. D. Souza, S. Montejo-Sánchez, H. Alves and M. d. Noronha-Neto, "Hybrid Coded Replication in LoRa Networks," in *IEEE Transactions on Industrial Informatics*, vol. 16, no. 8, pp. 5577-5585, Aug. 2020.
8. **A. Hoeller**, R. D. Souza, S. Montejo-Sánchez and H. Alves, "Performance Analysis of Single-Cell Adaptive Data Rate-Enabled LoRaWAN," in *IEEE Wireless Communications Letters*, vol. 9, no. 6, pp. 911-914, June 2020. ©2020 IEEE. Reprinted, with permission from authors.
9. **A. Hoeller**, J. Sant'Ana, J. Markkula, K. Mikhaylov, R. Souza and H. Alves, "Beyond 5G Low-Power Wide-Area Networks: A LoRaWAN Suitability Study," 2020 2nd 6G Wireless Summit (6G SUMMIT), Levi, Finland, 2020, pp. 1-5.

10. J. M. d. S. Sant'Ana, **A. Hoeller**, R. D. Souza, H. Alves and S. Montejo-Sánchez, "LORA Performance Analysis with Superposed Signal Decoding," in IEEE Wireless Communications Letters, vol. 9, no. 11, pp. 1865-1868, Nov. 2020.
11. G. G. M. de Jesus, R. D. Souza, C. Montez and **A. Hoeller**, "LoRaWAN Adaptive Data Rate with Flexible Link Margin," in IEEE Internet of Things Journal (early access).
12. W. Henrique, **A. Hoeller**, R. D. Souza, "Alocação Conjunta de Potência e SF em Redes LoRaWAN com Múltiplos Gateways," In: XXXVIII Simpósio Brasileiro de Telecomunicações e Processamento de Sinais (SBrT 2020), Florianópolis, Brazil, 2020, (to appear).
13. G. G. M. Jesus, R. D. Souza, C. Montez, **A. Hoeller**, "Improving LoRaWAN Performance Through Adaptive Data Rate Parameter Selection," In: XXXVIII Simpósio Brasileiro de Telecomunicações e Processamento de Sinais (SBrT 2020) – Scientific Initiation Track, Florianópolis, Brazil, 2020, (to appear).

REFERENCES

- ABDELFADEEL, Khaled Q.; CIONCA, Victor; PESCH, Dirk. Fair Adaptive Data Rate Allocation and Power Control in LoRaWAN. In: IEEE International Symposium on a World of Wireless, Mobile and Multimedia Networks. [S.l.: s.n.], June 2018. P. 1–9.
- ABRAMSON, Norman. THE ALOHA SYSTEM - Another alternative for computer communications. In: PROCEEDINGS of the Fall Joint Computer Conference. [S.l.: s.n.], Dec. 1970. P. 281–285.
- ANGRISANI, Leopoldo; ARPAIA, Pasquale; BONAVOLONTÀ, Francesco; CONTI, Mario; LICCARDO, Annalisa. LoRa protocol performance assessment in critical noise conditions. In: IEEE 3rd International Forum on Research and Technologies for Society and Industry (RTSI). [S.l.: s.n.], 2017.
- BANKOV, Dmitry; KHOROV, Evgeny; LYAKHOV, Andrey. Mathematical Model of LoRaWAN Channel Access with Capture Effect. In: IEEE 28th Annual International Symposium on Pervasive, Indoor, and Mobile Radio Communications (PIMRC). [S.l.: s.n.], 2017.
- BOCKELMANN, Carsten; PRATAS, Nuno; NIKOPOUR, Hosein; AU, Kelvin; SVENSSON, Tommy; STEFANOVIC, Cedomir; POPOVSKI, Petar; DEKORSY, Armin. Massive machine-type communications in 5G: physical and MAC-layer solutions. **IEEE Communications Magazine**, v. 54, n. 9, p. 59–65, Sept. 2016.
- BOR, Martin; ROEDIG, Utz. LoRa Transmission Parameter Selection. In: 13TH International Conference on Distributed Computing in Sensor Systems (DCOSS). [S.l.: s.n.], 2017. P. 27–34.
- BOR, Martin; ROEDIG, Utz; VOIGT, Thiemo; ALONSO, Juan M. Do LoRa Low-Power Wide-Area Networks Scale? In: 19TH ACM International Conference on Modeling, Analysis, and Simulation of Wireless Mobile Systems (MSWiM). Malta, Malta: [s.n.], 2016. P. 59–67.
- BURDEN, Richard L.; FAIRES, Douglas J.; BURDEN, Annette M. **Numerical Analysis**. USA: Cengage Learning, 2016.

BUURMAN, B.; KAMRUZZAMAN, J.; KARMAKAR, G.; ISLAM, S. Low-Power Wide-Area Networks: Design Goals, Architecture, Suitability to Use Cases and Research Challenges. **IEEE Access**, v. 8, p. 17179–17220, 2020.

CASTRO TOMÉ, Maurício de; NARDELLI, Pedro H. J.; ALVES, Hirley. Long-Range Low-Power Wireless Networks and Sampling Strategies in Electricity Metering. **IEEE Transactions on Industrial Electronics**, v. 66, n. 2, p. 1629–1637, 2019.

CENTENARO, Marco; VANGELISTA, Lorenzo; ZANELLA, Andrea; ZORZI, Michele. Long-range communications in unlicensed bands: the rising stars in the IoT and smart city scenarios. **IEEE Wireless Communications**, v. 23, n. 5, p. 60–67, 2016.

CHANG, Kuor-Hsin; MASON, Robert. The IEEE 802.15.4g standard for smart metering utility networks. In: 2012 IEEE Third International Conference on Smart Grid Communications (SmartGridComm). [S.l.: s.n.], Nov. 2012. P. 476–480.

CROCE, Daniele; GUCCIARDO, Michele; MANGIONE, Stefano; SANTAROMITA, Giuseppe; TINNIRELLO, Ilenia. Impact of LoRa Imperfect Orthogonality: Analysis of Link-Level Performance. **IEEE Communications Letters**, v. 22, n. 4, p. 796–799, Apr. 2018.

CUOMO, Francesca; CAMPO, Manuel; CAPONI, Alberto. EXPLoRa: Extending the performance of LoRa by suitable spreading factor allocations. In: IEEE 13th International Conference on Wireless and Mobile Computing, Networking and Communications (WiMOB). [S.l.: s.n.], 2017.

DESHPANDE, Udayan; KOTZ, David; MCDONALD, Chris. Coordinated Sampling to Improve the Efficiency of Wireless Network Monitoring. In: 2007 15th IEEE International Conference on Networks. [S.l.: s.n.], Nov. 2007. P. 353–358.

ELSAWY, Hesham; HOSSAIN, Ekram. On Stochastic Geometry Modeling of Cellular Uplink Transmission With Truncated Channel Inversion Power Control. **IEEE Transactions on Wireless Communications**, v. 13, n. 8, p. 4454–4469, Aug. 2014.

ERICSSON AB. **White paper: Cellular Networks for Massive IoT - Enabling Low Power Wide Area Applications**. [S.l.], Jan. 2016. P. 13.

GEORGIU, Orestis; RAZA, Usman. Low Power Wide Area Network Analysis: Can LoRa Scale? **IEEE Wireless Communications Letters**, v. 6, n. 2, p. 162–165, Apr. 2017.

GOLDSMITH, Andrea. **Wireless Communications**. New York, NY, USA: Cambridge University Press, 2005.

GOURSAUD, Claire; GORCE, Jean-Marie. Dedicated networks for IoT: PHY/MAC state of the art and challenges. **EAI Endorsed Transactions on Internet of Things**, EAI, v. 15, n. 1, p. 1–11, Oct. 2015.

GUPTA, Vinay; DEVAR, Sendil Kumar; KUMAR, N Hari; BAGADI, Kala Praveen. Modelling of IoT Traffic and its Impact on LoRaWAN. In: 2017 IEEE Global Communications Conference (GLOBECOM). [S.l.: s.n.], 2017.

HAENGGI, Martin. Diversity Loss Due to Interference Correlation. **IEEE Communications Letters**, v. 16, n. 10, p. 1600–1603, Oct. 2012a.

HAENGGI, Martin. **Stochastic Geometry for Wireless Networks**. Cambridge: Cambridge University Press, 2012b.

HAENGGI, Martin. The Meta Distribution of the SIR in Poisson Bipolar and Cellular Networks. **IEEE Transactions on Wireless Communications**, v. 15, n. 4, p. 2577–2589, Apr. 2016.

HARADA, Hiroshi; MIZUTANI, Keiichi; FUJIWARA, Jun; MOCHIZUKI, Kentaro; OBATA, Kentaro; OKUMURA, Ryota. IEEE 802.15.4g Based Wi-SUN Communication Systems. **IEICE Transactions on Communications**, E100.B, n. 7, p. 1032–1043, 2017.

HOELLER, Arliones; SOUZA, Richard Demo; ALVES, Hirley; LÓPEZ, Onel Luíz Alcaraz; MONTEJO-SÁNCHEZ, Samuel; PELLENZ, Marcelo Eduardo. Optimum LoRaWAN Configuration Under Wi-SUN Interference. **IEEE Access**, v. 7, p. 170936–170948, Dec. 2019. ©2019 IEEE. Reprinted, with permission from authors.

HOELLER, Arliones; SOUZA, Richard Demo; LÓPEZ, Onel Luíz Alcaraz; ALVES, Hirley; NORONHA-NETO, Mário de; OLIVEIRA BRANTE, Glauber Gomes de. Analysis and Performance Optimization of LoRa Networks With Time and Antenna

Diversity. **IEEE Access**, v. 6, p. 32820–32829, July 2018. ©2018 IEEE. Reprinted, with permission from authors.

HOELLER, Arliones; SOUZA, Richard Demo; MONTEJO-SÁNCHEZ, Samuel; ALVES, Hirley. Performance Analysis of Single-Cell Adaptive Data Rate-Enabled LoRaWAN. **IEEE Wireless Communications Letters**, v. 9, n. 6, p. 911–914, 2020. ©2020 IEEE. Reprinted, with permission from authors.

IEEE Standard for Local and metropolitan area networks—Part 15.4: Low-Rate Wireless Personal Area Networks (LR-WPANS) Amendment 1: MAC sublayer. [S.l.: s.n.], Apr. 2012.

IEEE Standard for Local and metropolitan area networks—Part 15.4: Low-Rate Wireless Personal Area Networks (LR-WPANS) Amendment 3: Physical Layer (PHY) Specifications for Low-Data-Rate, Wireless, Smart Metering Utility Networks. [S.l.: s.n.], Apr. 2012.

JÖRKE, Pascal; BÖCKER, Stefan; LIEDMANN, Florian; WIETFELD, Christian. Urban Channel Models for Smart City IoT-Networks Based on Empirical Measurements of LoRa-links at 433 and 868 MHz. In: IEEE 28th Annual International Symposium on Personal, Indoor, and Mobile Radio Communications (PIMRC). [S.l.: s.n.], 2017.

KRUPKA, Lukas; VOJTECH, Lukas; NERUDA, Marek. The issue of LPWAN technology coexistence in IoT environment. In: 2016 17th International Conference on Mechatronics - Mechatronika (ME). [S.l.: s.n.], Dec. 2016.

LAOZI. **Tao Te Ching**. China: Unknown publisher, 4th century BC.

LI, Shengyang; RAZA, Usman; KHAN, Aftab. How Agile is the Adaptive Data Rate Mechanism of LoRaWAN? In: IEEE Global Communications Conference. [S.l.: s.n.], Dec. 2018. P. 206–212.

LORA ALLIANCE. **LoRa Alliance Website**. <http://www.lora-alliance.org>. Nov. 2020.

MAGRIN, Davide; CENTENARO, Marco; VANGELISTA, Lorenzo. Performance evaluation of LoRa networks in a smart city scenario. In: IEEE International Conference on Communications. [S.l.: s.n.], 2017.

MAHMOOD, Aamir; SISINNI, Emiliano Ge; GUNTUPALLI, Lakshmikanth; RONDÓN, Raúl; HASSAN, Syed Ali; GIDLUND, Mikael. Scalability Analysis of a LoRa Networks Under Imperfect Orthogonality. **IEEE Transactions on Industrial Informatics**, v. 15, n. 3, p. 1425–1436, Mar. 2019. ISSN 1551-3203.

MATHWORKS. **MathWorks MATLAB Website**.

<https://www.mathworks.com/products/matlab.html>. Jan. 2021.

MIKHAYLOV, Konstantin; PETAJAJARVI, Juha; HANNINEN, Tuomo. Analysis of Capacity and Scalability of the LoRa Low Power Wide Area Network Technology. In: EUROPEAN Wireless 2016; 22th European Wireless Conference. [S.l.: s.n.], May 2016. P. 1–6.

MILLER, Scott L.; CHILDERS, Donald. **Probability and Random Processes With Applications to Signal Processing and Communications**. Waltham, MA, USA: Elsevier Inc., 2012.

MO, Yuqi; DO, Minh-Tien; GOURSAUD, Claire; GORCE, Jean-Marie. Optimization of the predefined number of replications in a Ultra Narrow Band based IoT network. In: WIRELESS Days (WD). [S.l.: s.n.], Mar. 2016.

MUÑOZ, Jonathan; CHANG, Tengfei; VILAJOSANA, Xavier; WATTEYNE, Thomas. Evaluation of IEEE802.15.4g for Environmental Observations. **Sensors (Basel)**, v. 18, n. 10, 2018.

OH, Mi-kyung; KIM, Jae-young; LEE, Sangjae; JEON, Youngae; CHOI, Sangsung. A fully integrated IEEE 802.15.4g MR-FSK SoC soc for smart utility network applications. **IEEE Transactions on Consumer Electronics**, v. 60, n. 4, p. 580–586, Nov. 2014.

OLIVEIRA, Ruben; GUARDALBEN, Lucas; SARGENTO, Susana. Long Range Communications in Urban and Rural Environments. In: IEEE Symposium on Computers and Communications. [S.l.: s.n.], 2017.

OLVER, Frank W. J.; LOZIER, Daniel W.; BOISVERT, Ronald F.; CLARK, Charles W. **NIST Handbook of Mathematical Functions**. Cambridge: Cambridge University Press, 2010.

ORFANIDIS, Charalampos; FEENEY, Laura Marie; JACOBSSON, Martin; GUNNINGBERG, Per. Investigating interference between LoRa and IEEE 802.15.4g

networks. In: IEEE 13th International Conference on Wireless and Mobile Computing, Networking and Communications. [S.l.: s.n.], Oct. 2017. P. 1–8.

PETÄJÄJÄRVI, Juha; MIKHAYLOV, Konstantin; PETTISSALO, Marko; JANHUNEN, Janne; IINATTI, Jari. Performance of a low-power wide-area network based on LoRa technology: Doppler robustness, scalability, and coverage. **International Journal of Distributed Sensor Networks**, v. 13, n. 3, p. 1–16, 2017.

POORTER, Eli De; HOEBEKE, Jeroen; STROBBE, Matthias; MOERMAN, Ingrid; LATRÉ, Steven; WEYN, Maarten; LANNOO, Bart; FAMAHEY, Jeroen. Sub-GHz LPWAN Network Coexistence, Management and Virtualization: An Overview and Open Research Challenges. **Wireless Personal Communications**, v. 95, n. 1, p. 187–213, July 2017.

POP, Alexandru-Ioan; RAZA, Usman; KULKARNI, Parag; SOORIYABANDARA, Mahesh. Does Bidirectional Traffic Do More Harm Than Good in LoRaWAN Based LPWA Networks? In: 2017 IEEE Global Communications Conference (GLOBECOM). [S.l.: s.n.], 2017.

QIN, Zhijin; MCCANN, Julie A. Resource Efficiency in Low-Power Wide-Area Networks for IoT Applications. In: 2017 IEEE Global Communications Conference (GLOBECOM). [S.l.: s.n.], 2017.

RADCLIFFE, Peter J.; CHAVEZ, Karina Gomez; BECKETT, Paul; SPANGARO, Justin; JAKOB, Conrad. Usability of LoRaWAN Technology in a Central Business District. In: IEEE 85th Vehicular Technology Conference (VTC-Spring). [S.l.: s.n.], 2017.

RAZA, Usman; KULKARNI, Parag; SOORIYABANDARA, Mahesh. Low Power Wide Area Networks: An Overview. **IEEE Communications Surveys Tutorials**, v. 19, n. 2, p. 855–873, Apr. 2017.

RIZZI, Mattia; FERRARI, Paolo; FLAMMINI, Alessandra; SISINNI, Emiliano. Evaluation of the IoT LoRaWAN Solution for Distributed Measurement Applications. **IEEE Transactions on Instrumentation and Measurement**, v. 66, n. 12, p. 3340–3349, 2017.

SALISBURY, John of. **Metalogicon**. [S.l.]: Unknown Publisher, 1159.

SEMTECH CORPORATION. **AN120.22 LoRa Modulation Basics**. [S.l.], Mar. 2015.

SEMTECH CORPORATION. **SX1276/77/78/79 - 137 MHz to 1020 MHz Low Power Long Range Transceiver**. [S.l.], Jan. 2019.

SHELBY, Zach; BORMANN, Carsten. **6LoWPAN: The Wireless Embedded Internet**. [S.l.]: Wiley, 2009.

SONG, Qipeng; LAGRANGE, Xavier; NUAYMI, Loutfi. Evaluation of Macro Diversity Gain in Long Range ALOHA Networks. **IEEE Communications Letters**, v. 21, n. 11, p. 2472–2475, 2017.

SØRENSEN, René Brandborg; KIM, Dong Min; NIELSEN, Jimmy Jessen; POPOVSKI, Petar. Analysis of Latency and MAC-Layer Performance for Class A LoRaWAN. **IEEE Wireless Communications Letters**, v. 6, n. 5, p. 566–569, Oct. 2017.

SOUZA SANT'ANA, Jean Michel de; HOELLER, Arliones; SOUZA, Richard Demo; MONTEJO-SÁNCHEZ, Samuel; ALVES, Hirley; NORONHA-NETO, Mario de. Hybrid Coded Replication in LoRa Networks. **IEEE Transactions on Industrial Informatics**, v. 16, n. 8, p. 5577–5585, 2020.

WI-SUN ALLIANCE. **Wi-SUN Alliance Website**. <http://www.wi-sun.org>. Nov. 2020.

VOIGT, Thiemo; BOR, Martin; ROEDIG, Utz; ALONSO, Juan M. Mitigating Inter-network Interference in LoRa Networks. In: INTERNATIONAL Conference on Embedded Wireless Systems and Networks. Uppsala, Sweden: Junction Publishing, 2017. P. 323–328.

WOLFRAM RESEARCH. **Wolfram Mathematica Website**.

<https://www.wolfram.com/mathematica>. Jan. 2021.

YASMIN, Rumana; PETÄJÄJÄRVI, Juha; MIKHAYLOV, Konstantin; POUTTU, Ari T. Large and Dense LoRaWAN Deployment to Monitor Real Estate Conditions and Utilization Rate. In: IEEE 29th Annual International Symposium on Personal, Indoor, and Mobile Radio Communications (PIMRC). Bologna, Italy: [s.n.], Sept. 2018.

ZHANG, Lin; LIANG, Ying-Chang; XIAO, Ming. Spectrum Sharing for Internet-of-Things: A Survey. **IEEE Wireless Communications**, v. 26, n. 3, p. 132–139, June 2019.

APPENDIX A – SOLUTION OF $f(d_1, \gamma, l_a, l_b)$

Here we solve the integral in (49). Let

$$f(d_1, \gamma, l_a, l_b) = \int_{l_a}^{l_b} \frac{\gamma d_1^\eta}{x^\eta + \gamma d_1^\eta} x \, dx.$$

We rearrange $f(\cdot)$ as

$$f(d_1, \gamma, l_a, l_b) = \int_{l_a}^{l_b} x \left(\frac{x^\eta}{d_1^\eta \gamma} + 1 \right)^{-1} dx$$

and use the binomial theorem $(x + 1)^{-1} = \sum_{k=0}^{\infty} (-1)^k x^k$ to obtain

$$f(d_1, \gamma, l_a, l_b) = \int_{l_a}^{l_b} \sum_{k=0}^{\infty} \left(\frac{-1}{d_1^\eta \gamma} \right)^k x^{\eta k + 1} dx.$$

Since $f(\cdot)$ is continuous in $\mathbb{R} \forall x > 0$, we interchange the sum and the integration and solve the integral, yielding

$$f(d_1, \gamma, l_a, l_b) = \sum_{k=0}^{\infty} \left(\frac{-1}{d_1^\eta \gamma} \right)^k \frac{x^{2+\eta k}}{\eta k + 2} \Big|_{l_a}^{l_b}.$$

We resort to the Pochhammer function $(a)_k = a(a+1) \cdots (a+k-1) = \frac{\Gamma(a+k)}{\Gamma(a)}$ and to $\frac{(b)_k}{(b+1)_k} = \frac{b}{b+k}$, and reorganize $f(\cdot)$ as

$$f(d_1, \gamma, l_a, l_b) = \frac{x^2}{2} \sum_{k=0}^{\infty} \frac{(1)_k}{k!} \frac{\left(\frac{2}{\eta}\right)_k}{\left(1 + \frac{2}{\eta}\right)_k} \left(-\frac{x^\eta}{d_1^\eta \gamma} \right)^k \Big|_{l_a}^{l_b},$$

which is in the form of the Gaussian Hypergeometric function (OLVER et al., 2010) ${}_2F_1(a, b; c; z) = \sum_{k=0}^{\infty} \frac{(a)_k (b)_k}{(c)_k} \frac{z^k}{k!}$, what yields

$$f(d_1, \gamma, l_a, l_b) = \frac{x^2}{2} {}_2F_1 \left(1, \frac{2}{\eta}; 1 + \frac{2}{\eta}; -\frac{x^\eta}{d_1^\eta \gamma} \right) \Big|_{l_a}^{l_b}.$$